UNIVERSITY OF BIRMINGHAM

Real Time Measurement of Oxygen by Integrating a Clark Sensor with Low Cost Printed Circuit Board Technology and Solid Electrolyte Membrane

By

Ayda Niazi

A thesis submitted to
The University of Birmingham
for the degree of

DOCTOR OF PHILOSOPHY

COLLEGE OF ENGINEERING AND PHYSICAL SCIENCE
SCHOOL OF MECHANICAL ENGINEERING
JANUARY 2016

Abstract

A prototype of a miniaturized Clark type electrochemical oxygen sensor integrated with a 3D printed in vitro cell culturing platform is designed and developed for the purpose of monitoring the cellular oxygen consumption by the solution flowing through the cultured cells on the platform. Oxygen respiration indicates a cell's metabolic activity, so by measuring a chemical's oxygen content as it passes through a cell chamber, we can measure that chemical's potential effectiveness. This miniature micro sensor is designed and fabricated on a printed circuit board for the first time and integrated with a solid electrolyte membrane and 3D printed cell culturing platform to ensure robustness and low manufacturing cost. Hence the sensor is aimed at enabling the pharmaceutical industry to rapidly test chemical products on animal and cancer cells; and has been designed to be low cost and suitable for mass production.

The cell culturing platform's prototype, which contains inlet and outlet pipes and a cell culturing chamber, was manufactured by The Eden250™ 3D Printing System using the Objet biocompatible material MED610™. The presented oxygen sensor configuration consists of two identical series of working, reference and counter microelectrodes, placed before and after the cell culturing chamber. It was manufactured by combining printed circuit board technology and laser micro machining techniques to create microscale microelectrode spacing. The usual electrolyte solution is replaced with a solid polymer electrolyte membrane, Nafion (perfluorosulfunic acid membrane, DuPont Company), which removed requirement for extra humidification and increased the shelf life of the dissolved oxygen sensing system. The solid polymer electrolyte also ensured robustness and good electrical conductivity for sensing. The sensor functions without humidification or any special condition and has a long shelf life. The sensitivity of the oxygen sensor was tested in different oxygen concentration in gas and liquid states and was calibrated with measurements

from a Portable Multi-Gas Analyser provided by Super Systems Europe and a Gold probe dissolved oxygen analyser. The prototype can detect the small changes in oxygen concentration in the range of 0 to 5 μA current and has a response time of less than 5 seconds.

I dedicate this thesis to my parents.

Acknowledgment

List of Publications

During the course of this project, the following Conference Proceedings have been published:

- Ayda Niazi, Carl Anthony, Development of oxygen sensor by integrating the low cost printed circuit board technology and solid electrolyte membrane, ICBES (International Conference on Biomedical Engineering and Systems) Prague, Czech Republic, August 2014.

- Ayda Niazi, Carl Anthony, Real time measurement of oxygen by integrating a Clark sensor with printed circuit board technology and solid electrolyte, MNE (International Conference on Micro and Nano Engineering), September 2014.

- Ayda Niazi, Carl Anthony, Modelling of the oxygen consumption of cells in the cell culturing platform, COMSOL Conference, Cambridge, UK, September 2014.

Also a journal paper is submitted and under review:

- Ayda Niazi, Carl Anthony, Comparison of six miniaturized oxygen sensors, fabricated by printed circuit board technology and solid polymer electrolyte in liquid and gas state measurements.

Contents

List of Figures

List of Tables

1. Introduction

1.1. Introduction

The Clark type oxygen sensor is extensively used among the diverse instruments to measure oxygen in many clinical researches, fermentation monitoring and biosensor developments [1]. It was invented by Leland C. Clark in 1956 to detect low levels of oxygen [2].

As an electrochemical sensor, it has a low deviation among the sensors and produces good repeatability and reproducibility. In the past two decades there have been various developments on the Clark type sensors which can now be fabricated utilizing MEMS technology. Miniaturized dissolved oxygen sensors have been frequently produced using silicon-based and poly dimethyl siloxane (PDMS) materials for their ease of applying micro fabrication processes such as lithography, spincoating and wet/dry-etching on them [3-6].

However it has been proven to be difficult to incorporate these miniaturized sensors in the environment due to their need for rehydration, sophisticated sealing systems to prevent leakage or drying of liquid electrolyte and continuous maintenance [3, 4, 6].

Usage of a solid electrolyte eliminates the need of rehydration while increasing the shelf life, as described by Glen W. McLaughlin and co-workers [5]. Solid state proton conductive matrix (PCM) as an electrolyte was coated on the oxygen sensor that was fabricated using silicon wafer and microfabrication techniques. Further it was encapsulated in a bio inert polytetrafluoroethelene (PTFE), which improved the performance of the microfabricated electrode matrix and was shown to have a linear response over 0 – 300 mmHg of dissolved oxygen concentration through cyclic voltammetry (CV) and voltage step (VS) measurements.

Though there were issues of robustness and short shelf life due to the fragile behaviour of silicon [5].

Recently printed circuit board technology has created a potential as a MEMS platform for developing microsensors due to their advantages of robustness, acknowledged commercial production methods and good connectivity to standard systems [7]. "Having the advantages of robustness, easy connectivity to standard electrical systems and firm commercial fabrication techniques, PCB (Printed circuit board) makes it easy to fabricate microelectrode features like pads and tracks with gold coating and strong connectivity, which is difficult to achieve in silicon wafer processing and standard MEMS techniques" [7].

In this thesis, the potential of using printed circuit board technology as a miniaturized biological oxygen sensor platform, having advantages of reduced price and advanced production technology has been investigated.

Prospective applications of the oxygen monitoring device include pharmacological product testing. E.g., monitoring the cellular respiration during the examination of new chemical products on the animal cells can point to specific state of metabolism of that cell, which is affected by the chemical product. Oxygen is an important regulator of normal cell behaviour. It is one of the most important indicators of biological activity during cell culture and microbial development. Theoretically, the concentration of oxygen in a solution containing live cells will demonstrate key statuses of those cells, since the living cells will consume oxygen from solution and thus reduce its concentration. The damaged cells will consume a lower amount of oxygen due to their decreased metabolic activities; dead cells won't consume any oxygen so there won't be any reduction in the oxygen concentration [8].

1.2. Aims and Objectives

The aim of this project is to design an integrated oxygen sensor with cell culturing platform to allow monitoring the cellular respiration of the cultured cells simultaneously. And to develop a system suitable for mass production that enables the pharmaceutical industry to rapidly test chemical products on animal and cancer cells and measures that chemical's potential effectiveness.

It was decided to use miniaturized Clark type oxygen sensor as a cellular respiration monitoring device. It is possible to measure the respiration of cells in a given time by utilizing two simultaneously operating oxygen sensors that measure the oxygen concentration of the fluid or gas medium, before and after being exposed to cells. By this method reduction of the oxygen concentration in the fluid or gas medium can be calculated after being exposed to cells. Consequently, the effects of different drugs and chemicals on the metabolism of the cells can be investigated by reading the oxygen level of the solution or gas under test before and after adding the drugs and toxins to the cells. The objective is to produce this miniaturized Clark type oxygen sensor using the low cost printed circuit board technology having advantages of robustness and advanced fabrication techniques, which permits easy fabrication of microelectrode features like pads and tracks with gold coating and strong connectivity on its surface with a precision of 100 microns. A Laser micromachining process is going to be used to machine sensors with dimensions smaller than 100 microns.

In addition a cell culturing platform prototype was developed utilizing a 3D printing device, which can produce complex features inside the chip with the potential for cells to grow and adhere to its chamber and can be easily integrated with a PCB based miniature oxygen sensor, allowing the measurement of oxygen concentration by the oxygen sensors as the test solution or gas is flowing through the cultured cells and pipes on the cell culturing platform.

It is considered to be designed having lighter, stronger and smaller dimensions to reduce the overall cost and lead time by integrating flow channels and fittings using the most advanced technologies. Printed circuit board technology and micro fabrication techniques such as laser micro-machining will be used to achieve the high precision to increase the accuracy of the sensor.

The usual electrolyte solution will be replaced with a solid polymer electrolyte membrane, Nafion (perfluorosulfunic acid membrane, DuPont Company), which removes requirement for extra humidification and increases the product shelf life. The prototype is aimed to detect changes in the 0-5 μAmp range, having response time of less than 5 seconds.

The cell culturing platform's prototype, which contains an inlet and outlet pipes and a cell culturing chamber, will be manufactured by The Eden250™ 3D Printing System using the Objet biocompatible material MED610™. The presented oxygen sensor configuration consists of two identical series of working, reference and counter microelectrodes, placed before and after the cell culturing chamber. The sensitivity of the PCB oxygen sensor will be tested in different oxygen concentration in gas and liquid states and calibrated with measurements from a Portable Multi-Gas Analyzer provided by Super Systems Europe and a Gold probe dissolved oxygen analyser provided by Chemical engineering, University of Birmingham.

1.3. Thesis Overview

The structure of this thesis consists of five main chapters. In first chapter a concise introduction is given about the objective of this research, highlighting the advantages and improvements.

In the second chapter a broad overview about the background theories of the electrochemical oxygen sensors is described. Microelectrodes and their electrochemical reactions are explored. Further the state of the art has been explored comparing the most recent researches in the development of electrochemical oxygen sensors in biological applications and discussing the cons and pros.

In the third chapter, the design of microelectrode based oxygen sensors will be described. Design of an electronic control circuit is explored which will be used to control the applied voltage to electrodes and record the data being measured using data acquisition modules. The cell culturing platform design will be presented and along with Finite Element Analysis. The final design of the integrated oxygen sensor platform will be demonstrated.

In the fourth chapter, different materials used in electrode design will be introduced, as well as materials used for the cell culturing platform and different fabrication processes such as PCB fabrication, Laser micromachining and 3D printing. Material preparation and fabrication processes for the control circuit will be described.

In the fifth chapter, the results of the sensor examination will be shown. It will be tested by liquid and gas medium and the experimental setups will be demonstrated. Cyclic voltammetry and voltage step measurements will be carried out. The sensitivity, linearity and reproducibility of the sensor will be investigated.

In the last chapter a general conclusion and further ideas for future work will be given.

2. Literature Review

2.1. Introduction

In this chapter a brief overview of electroanalysis and biosensors is given. Different types of oxygen biosensor is outlined and introduced. Fundamentals of electrochemistry are defined as well as diffusion process in electrochemistry and kinetics of electrochemical reactions. Microelectrodes and their electrochemical reactions are explored. Finally the state of art in electrochemical oxygen sensors in biological applications has been reviewed.

Electroanalysis is a method in analytical chemistry, which study an analyte by measuring the potential and current in an electrochemical device encompassing the analyte [9]. Improvements in the electroanalysis created the fast developments of biosensors. First of all, in the development of biosensors, appropriate bioreceptor, immobilization method and a transducer should be considered. These sensors allow the analysis with high level of sensitivity, selectivity, faster and cheaper cost in principle. Among the numerous applications of these sensors, they are being used in different areas such as clinical analysis and online control processes for industrial or environmental or in vivo studies. The detectable element in a biosensor is a biological compound which distinguishes this sensor from other physical or chemical sensors [10].

2.2. Biosensors

A biosensor is an analytical device that converts a biological reaction into an electrical signal and combines a biological element (e.g. Glucose) and a physicochemical detector.

Biological and biochemical processes have a significant function in biology and biotechnology [11]. In the past it has been problematic to convert biological data to electrical

signal directly, however in the recent years with the application of biosensing it has been easier to overcome these problems [12].

In 1962 Clark and Lyons introduced the first biosensor in order to measure glucose concentration in a specimen by immobilizing glucose oxidase (GOx) enzyme on an amperometric oxygen electrode surface and semi permeable dialysis membrane (figure 2.1) [13, 14].
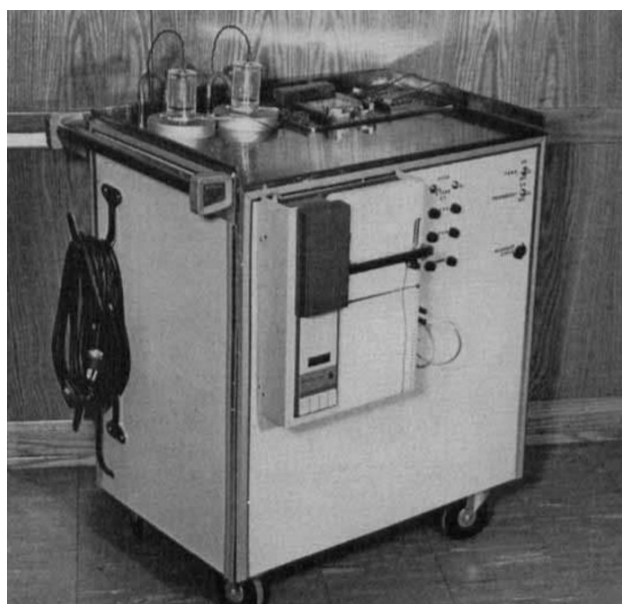
Figure 2.1 Clark and Lyons electrode system [15].

They have demonstrated by addition of enzyme transducers as membrane bounded sandwiches, it is possible to create smarter electrochemical sensors such as pH, polarographic, potentiometric or conductometric sensors.

As defined by International Union of Pure and Applied Chemistry (IUPAC), "*A biosensor is an independent unified device which is able to provide explicit quantitative or semi-quantitative analytical data using a biochemical receptor which is in direct spatial connection with a transducer element. A biosensor should be clearly distinguished from a bioanalytical system, which requires additional processing steps, such as reagent addition. Moreover, a biosensor should be distinguished from a bio probe which is either disposable after one measurement or unable to continuously monitor the analyte concentration*" [16].

A biosensor is a device of two components combination; 1) A bioreceptor is an element of a biosensor such as enzyme, DNA probe and antibody, which is immobilized and sensitive to identify the analyte, respectively enzyme substrate, complementary DNA and antigen. Enzymes are the most commonly employed type of bioreceptor in biosensors.

2) A transducer transforms the chemical fluctuation produced from the reaction of the analyte and the bioreceptor into an electronic signal. The intensity of generated signal is directly or inversely proportional to the analyte concentration [13].

However it is not always the enzyme substrate or antigen that needs to be detected in a biological assay. Another class of biosensor deals with the measurement of oxygen consumed in living organisms. As mentioned previously oxygen consumption acted as an indicator of cell metabolism is an important factor in biological analysis [8]. Oxygen sensors have a variety of biomedical and industrial applications, for example measuring the exhaust gas concentration of oxygen for internal combustion engines in automobiles or determining the partial pressure of oxygen in divers breathing gas. Scientists use oxygen sensors to measure respiration or production of oxygen in an organism [17]. Oxygen sensors are used in oxygen analysers in medical applications such as anaesthesia monitoring, respirators and oxygen concentrators.

2.3. Classification of Oxygen Biosensors

2.3.1. Optical oxygen sensors

The optical oxygen sensor measures the oxygen concentration optically with the aid of a chemical transducer, which is a chemical film with fluorescence properties (related to the oxygen concentration) attached at the tip of the optical cable. A transducer is a device that converts one form of energy to another, in here converts optical form of energy to chemical.

In the absence of oxygen the fluorescence is at maximum and at the presence of oxygen, its molecules collide with the fluorescent film, quenching the photoluminescence [18].

Figure 2.2 shows a general optical fluorescence dissolved oxygen analyzer schematic. The blue light having about 470 nm wavelength is transmitted to the sensing element causing the dye material to release a pink beam having more than 600 nm wavelength. The light detector reacts to the pink light. There is no chemical reaction between the oxygen molecules and the dye material on the chemical film, though the oxygen extinguishes the quantity of the pink beam by producing different transition states for the excited dye electrons. Measured oxygen concentration is proportional to the quantity of active fluorescence quenching detected by the light detector. The electronic analyzer processes the output of the light detector and temperature sensor and generates a readable oxygen concentration in parts per million (ppm) [19].
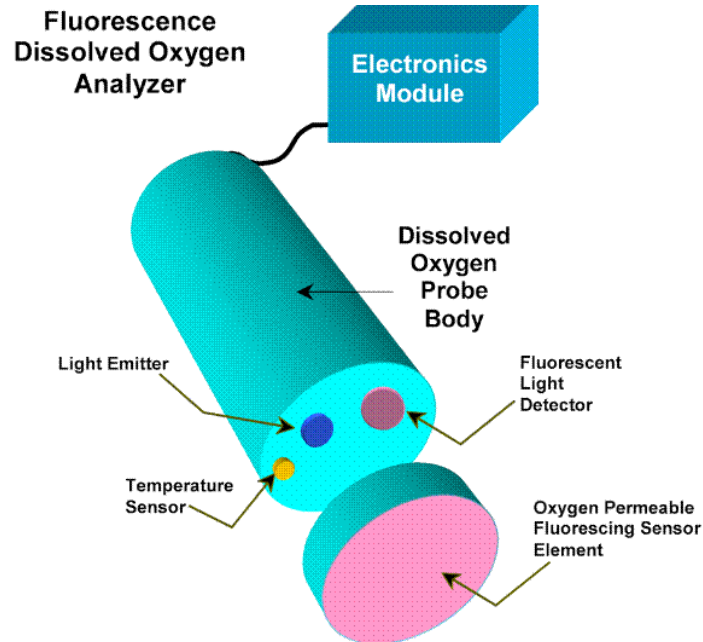
Figure 2.2 Generic Optical Fluorescence Dissolved Oxygen Analyzer Configuration [16].

The optical oxygen sensor is mainly sensitive at low oxygen concentration. Its sensitivity reduces as the dissolved oxygen increases since the fluorescence signal to oxygen ratio is

nonlinear [20]. There is no oxygen consumption and it's not sensitive to stirring. They can be utilized for instantaneous monitoring of oxygen production in water splitting reactions as described by Calzaferri and his co-workers who used this method broadly to observe the hydrogen production in water splitting research [21].

However the optical oxygen sensors have higher initial acquisition cost, slower measurement response time than traditional electrochemical sensors and consume more power than traditional electrochemical sensors.

Alternatively, electrochemical oxygen sensors are very sensitive, since they can detect electron flow from one molecule. Electrochemical systems are unique in many ways to overcome problems in optical sensors such as optimising dye loading concentration, photo bleaching, and reactive oxygen species concentration outside the limited range of detection. Moreover, electrochemical sensors are faster, simpler to use, and operate at a lower cost compared to optical systems.

2.3.2. Electrochemical oxygen sensors

The electrochemical oxygen sensor is the most common type of oxygen sensor for measuring oxygen dissolved in a liquid or gas. Among them, the Clark-type electrode is the most commonly employed electrochemical sensor and its basic principle is that there is a cathode and an anode submersed in an electrolyte. Oxygen is an electroactive element, which leads a change in current intensity. This change is proportional to the concentration of oxygen. Oxygen enters the sensor through a permeable membrane by diffusion, and is reduced at the cathode, creating a measurable electrical current [22].

The relationship between oxygen concentration and the current which is being measured is linear. Oxygen can be measured in the sample under the test considering a two-point calibration of 0% and 100% air saturation. However there are limitations in this method, such

as that oxygen is consumed while doing measurements at a rate identical to the diffusion in the electrodes. To get correct measurements, the sensor should be stirred constantly and stagnation of water should be avoided. The bigger the electrode's size, there will be more oxygen consumption and sensitivity for stirring also increases. In macro sensors since the electrolyte is being consumed quickly, over time, it causes a drift in the output signal. On the other hand it is possible to miniaturize the Clark-type sensors down to a tip size of 10 μm. The oxygen consumption in these miniaturized sensors is little and its sensitivity to stirring is insignificant and they can be utilized in stagnant samples such as sediments or inside plant tissue. Utilizing solid electrolyte eliminates the possibility of liquid electrolyte evaporation or consumption, which reduces or removes the sensor conductivity and eventually functionality [22].

The considered electrochemical reaction would generate a measurable current (amperometric detection), a measurable potential or charge accumulation (potentiometric detection) or measurable conductivity change of a medium; for example the change of the electrical conductivity of cell solution (conductometric detection) between electrodes. Amperometry is a measurement method for current, done at a constant potential. Voltammetry is another method in which the electrical current is measured while a specific variation of the potential is being exerted.

Electrochemical oxygen sensors have benefits that they can detect without harming the system. Their application in industrial and environmental analysis is vital such as the control of food manufacturing processes, evaluation of food quality and control of fermentation due to their precise detection, simple use and low cost [23, 24].

2.3.2.1.   Clark-type oxygen sensor theory of operation

In this sensor the current is measured that result from the electrochemical reduction of the oxygen, which is dissolved in the solution under the test. The current demonstrates the concentration of the oxygen.

This sensor needs to be enclosed in oxygen permeable membrane to improve the measurement accuracy by eliminating other electroactive species that produce reduction current signal. Furthermore it enables the measurement of dissolved oxygen in sensitive biological media for example blood.

The classic design of this sensor is a two electrode system being placed in an electrolyte solution and the electrodes does not reduce easily as shown in figure 2.3 [25].
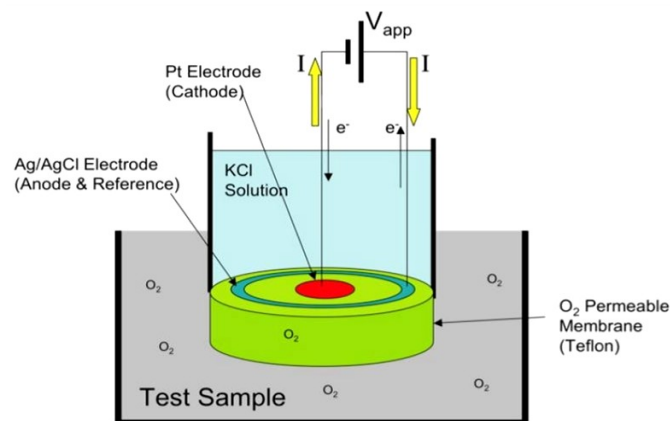
Figure 2.3 the classic two electrode (Platinum and Ag/AgCl) Clark sensor [26]

To reduce the diffusion time of the oxygen the oxygen, permeable membrane will be located close to the cathode [27]. The oxygen dissolved in the media passes through the membrane and will reduce at the cathode where a fixed potential is applied and the current flowing between the cathode and the anode will be constant under the diffusion limited current conditions. There are three regions of function in this sensor as can be seen in figure 2.4. In the first region the reaction is kinetically controlled and the nature of current is in an exponential proportion to the applied voltage. The current's behaviour is independent of the applied voltage in region two and it is called the diffusion limited region. Since the sensitivity

of the current to applied voltage is independent in this section, usually the sensor operates in this region. The current and voltage has an exponential nature in region three same as region one [25].
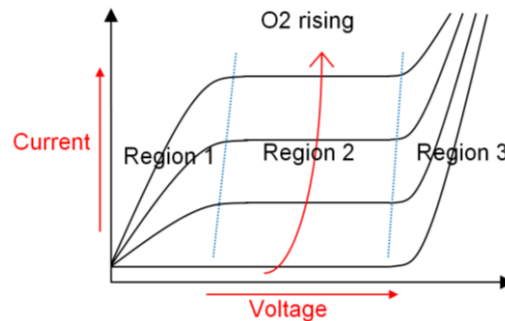
Figure 2.4 Diagram of current/voltage features of dissolved gas sensing electrode. Region 1 shows the redox reaction under kinetic control. Region 2 corresponds to the redox reaction under diffusion limited conditions. Region 3 signifies additional redox reactions occurring [25].

The behaviour in the diffusion limited condition can be defined by equation (1) and shows that in an equilibrium condition the produced current is proportional to the concentration of the oxygen as shown by equation (2). The current has a linear relationship with the dissolved oxygen concentration in the medium under diffusion limited condition.

$$i = nFAD\frac{\partial C(x, t)}{\partial x} \tag{1}$$

$$i = nFAD\frac{C_0}{x} \tag{2}$$

Where i is the current (A), n is the number of oxidised electrons (reduced), F is Faraday constant (C/mol), A is the area of electrode (cm^2) and C(x,t) is the concentration of electroactive species at distance x and time t.

According to Henry's law when a solution is equilibrated with the surrounding atmosphere, at a constant temperature, the concentration of the dissolved oxygen in the solution is in direct proportion to the partial pressure of the oxygen in the atmosphere air [28]. This relationship can be shown by equation (3) that declares as the molar fraction of oxygen dissolved in the

solution move towards the dilute values, the partial pressure of the oxygen on top of the solution is directly proportional to the amount of the oxygen dissolved in the solution.

$$P_i = y_i P = K_i x_i \tag{3}$$

In this equation the partial pressure of the specified gas, P_i (Pa), is equal to the molar fraction of that specified gas y_i (%), multiplied by the gas pressure of all the gases P (Pa). Henry states that the Pi (Pa) is equal to the amount of dissolved oxygen in a solution multiplied by an empirically measured constant K_i (Pa) for different solutions and gases. The K_i for oxygen in a solution is 4.40×10^9 (Pa) [28]. By this method we can determine the concentration of the dissolved oxygen in a solution at equilibrium state.

In a two electrode system there are drift caused by parasitics inside the sensor, to solve this issue a three electrode configuration is selected. Oxygen reduces in the cathode (working electrode) in two steps [29]. At the surface of the working electrode, oxygen first transforms to hydrogen peroxide and then reduces further to water. This process is presented in figure 2.5. Oxygen concentration in the solution is a factor to advance these processes. The equations (4 and 5) show the reactions taking place at the working electrode, the equation (6) is the net of first two reactions. The equation (7) shows that the product from the working electrode is converted back to reactants at the anode or counter electrode [22].

$$O_2 + 2H^+ + 2e^- \rightarrow H_2O_2 \tag{4}$$

$$H_2O_2 + 2H^+ + 2e^- \rightarrow 2H_2O \tag{5}$$

$$O_2 + 4H^+ + 4e^- \rightarrow 2H_2O_2 \tag{6}$$

$$2H_2O \rightarrow O_2 + 4H^+ + 4e^- \tag{7}$$
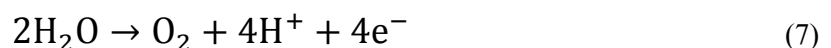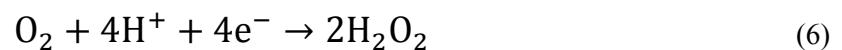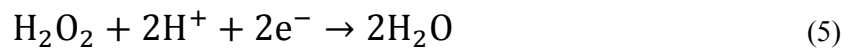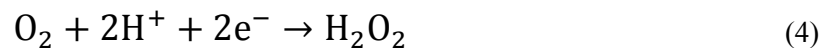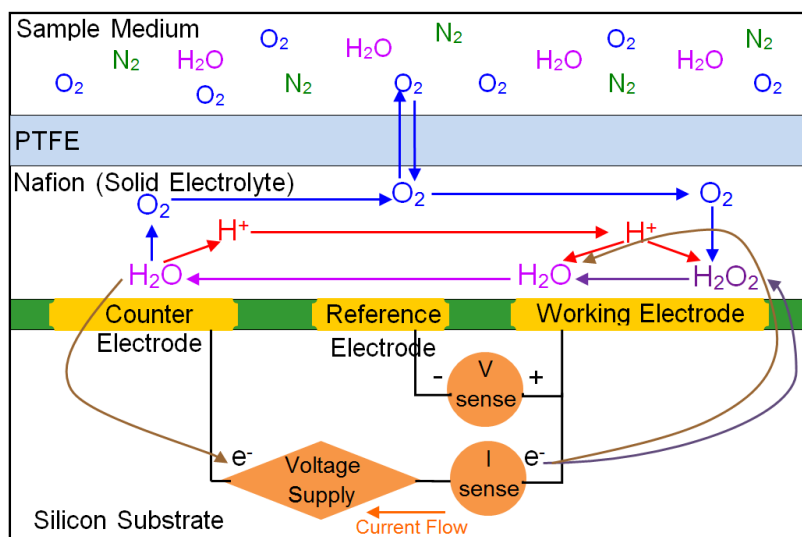
Figure 2.5 Diagram of the reaction mechanism on the sensor [25].

In the three electrodes configuration there is significantly less consumption of the metal electrodes contrary to the two electrodes Clark sensor, which is causing the electrodes to degrade quicker. In the commercial Clark sensors, a shared counter and reference electrode is being used for example Ag/AgCl electrodes (two electrodes configuration). A Potassium Chloride (KCl) solution is being used as an electrolyte because the movements of the K^+ and Cl^- are coordinated, reducing the ionic gradients. The full consumption of the electrodes can be prevented by fabricating large counter electrode in the standard configuration, though it's not possible in the micro dimensions [22].

However in the Ag/AgCl microelectrode, the consumption of the electrodes decreases the life of the sensor to minutes. Hence a practical Clark sensor should not allow for consumption of the electrode's material. Therefore a new design is presented by usage of a solid polymer electrolyte such as Nafion as an ion transport medium and different material and design configuration for the electrodes.

2.4. Electrochemistry of Clark type oxygen sensor

Alessandro Volta at the start of nineteenth century presented the outcomes of his research to the Royal Society of London as a "Voltaic piles" (artificial electrical organ), which was the

first electrochemical cell [30]. Nicholson and Carlisle described the process of using electricity to decompose water to hydrogen and oxygen, which was the first move in the creation of fuel cells [31]. In 1833 Faraday practiced the first quantifiable studies of electrolysis [32]. Since 1950's the topic has progressed extensively in experimental, theoretical and application section and led to the development of microelectrodes application [10].

An electrochemical reaction is the interaction of electrical energy and chemical change. It involves electric charges moving between the interface of electrodes and the electrolyte (or ionic solution). When the electrical current occurs naturally after a chemical reaction, it is called electrochemical reaction such as in a battery or galvanic cell as shown in figure 2.6.a. Otherwise, if it is produced through applying an external electrical energy by an external circuit in order to raise reaction at the electrodes, it is called electrolysis as it can be seen in figure 2.6.b.
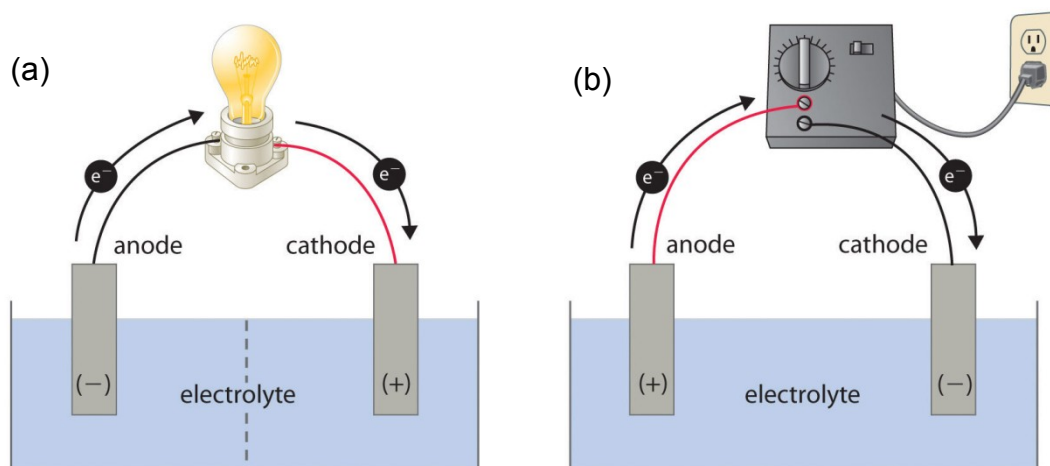
Figure 2.6 (a) Diagram of Galvanic cell, (b) illustration of Electrolytic cell [30].

The redox (oxidation and reduction) reaction involves transfer of electrons from one chemical species to another molecules or atoms in a solution or on the electrode surface until the electroneutrality is attained.

This process is governed by Faraday's law, which states that the total amount of electrical charge passed through the cell is proportional to the amount of chemical change produced and the current generated is called Faradaic current [32].

There are two categories of redox reactions (half-reactions) that are distinguished by the changes in the oxidation state of the element. The compound that loses electrons is said to be oxidized (reduction reaction) and the one that gains electrons is said to be reduced (oxidation process) [33].

If the reactants are in the same phase the reaction is called a homogeneous reaction, while in the heterogeneous reaction, the reactants are in two or more phases. Usually the reactions take place on the solid electrode surface, immersed in the electrolyte solution and are connected through the solution and external electrical circuit. If the electrolyte is different for each electrode, then they can be linked by a salt bridge. The charge transfer process simply can be presented as O for oxidized species and R for reduced species by equation (8) [33].

$$O + ne^- \leftrightarrow R \qquad (8)$$

Where, O obtains n electrons to transform into R. The electrons in the electrode have a maximum energy when distributed around the Fermi level, which is the top of the collection of electron's energy levels at absolute zero temperature.

For a reduction process, the electrons in the electrode must have a minimum energy to transfer from the electrode to the receptor orbital in O. For oxidation, the energy of the electrons of R must be equal to or higher than the electrode's Fermi level in order to be transferred to the electrode [33].

The electrode's material, surface modification or dimensions affects highly the detection capability of the electrochemical oxygen sensor. In the next section the main components of an electrochemical oxygen sensor are defined in more detail.

2.4.1. Electrodes

Electrodes are electrically conductive materials that are in proximity of the electrolyte of the system. They implement the half reaction over an extensive time so the choice of their material is vital. Normally, the electrode is made from a noble metal, such as platinum or gold in order to reduce their corrosion and reactions with the chemicals. All three electrodes can be made of different or same materials to complete the cell reaction depending on the design of the sensor [9].

2.4.1.1. Working Electrode

The electrochemical reaction occurs in the working electrode. It is at the boundary between the WE (working electrode) and the solution that significant electron transfer occurs. Based on the reaction taking place at this electrode, whether it's a reduction or oxidation, it can be stated as cathodic or anodic respectively. Several aspects need to be regarded in material of WE. Ideally it should display fast and repeatable redox reaction with the oxygen upon electron transfer without electrode's surface getting impurities. The electrode that performs in the electrolyte solution should allow for the highest amount of oxygen characterization. The cost of the material, its capability to be shaped into functional geometries, the ease of surface replacement and toxicity are the other factors that should be considered. WE generally have been created from platinum, gold, carbon and mercury. The potential of the WE is controlled with respect to a RE (reference electrode) and the current passes between the WE and the CE (counter electrode) [9].

2.4.1.2. Reference Electrode

The RE is essential to deliver a steady and repeatable potential against the WE, which is the sensing electrode and requires an external driving voltage. The potential of the WE by itself cannot be considered in isolation and it must be compared with another electrode. Since frequent electrochemical reaction occurs on the surface of the WE, its potential does not stay

constant and its performance deteriorates over time. To improve this problem, the RE is presented to act as reference in measuring and controlling the WE's potential and the current doesn't pass through it. It is positioned close to the WE inside the electrolyte and maintains the value of the fixed voltage applied to the WE. The current flows through the WE and the CE while the oxygen particles react at the WE and their magnitude is proportional to the concentration of oxygen [9].

2.4.1.3. Counter electrode

When the CE works as a cathode, the WE operates as an anode and vice versa. The CE's surface area is bigger than that of the WE. The half reaction occurring at the CE should be rapid for not limiting the change at the WE. In a three electrode electrochemical sensor, the CE is utilized for voltammetric analysis or other reactions that involves the flow of electric current. The CE is different from the RE that is recognized to gauge the potential of the WE, and the WE, where the reaction occurs. The CE balances the charge added or removed by the WE and allows the balancing current at the WE to flow. In a two electrode system, where there are WE and RE, the second electrode conducts both functions of the RE and CE in one and it becomes very difficult for the electrode to maintain a continuous potential while passing current to the reactions occurring at the WE. For this reason the CE is introduced and the combination of these three electrodes brands the modern three electrode system. The CE is usually made of electrochemically inert materials such as gold, platinum or carbon [9].

2.4.2. Gas Permeable Membrane (Teflon membrane)

Gas permeable membrane is a hydrophobic film with appropriate porosity to protect and cover the sensor's electrodes and electrolyte, and regulates the amount of gas (preferably oxygen in here) permeating through its pores and approaching the surface of the electrodes. Usually they are produced from thin, low porosity Teflon membranes. They have different porosity and choosing the right pore size permits transmission of appropriate amount of gas

molecules to WE and to filter out unwanted particles. It also prevents the liquid electrolyte from evaporating or leaking as well as mechanically protecting the sensors system [27, 34].

2.4.3. Electrolyte

The electrolyte is a substance that splits into ions in the appropriate ionizing solvents for example water and assists the transport of ionic charges through the electrodes and the sensor reaction to occur.

When a voltage is exerted on the electrodes that are in the electrolyte, the chemical reaction will take place at the cathode using the electrons produced from the anode. As a result a positive charge will grow around the anode and a negative charge develops around the cathode in the electrolyte. At this stage the ions of the electrolyte exert a neutralizing effect on these charges and the reaction will endure. If the electrolyte vaporizes, the sensor's response will decline. Usually the Electrolyte is a solution of salt in water dissociated as a result of thermodynamic reactions. A solid salt such as sodium chloride dissolves into its ionic elements when it's mixed with water, based on the following reaction shown in equation (9 and 10) [27]:

$$2H_2O + 2e^- \rightarrow 2OH^- + H_2 \tag{9}$$

$$2NaCl_{(s)} \rightarrow 2\,Na^+_{(aq)} + Cl_{2(aq)} + 2e^- \tag{10}$$
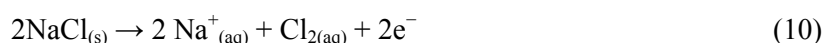
2.4.3.1. Solid Polymer Electrolyte

Solid electrolytes or superionics demonstrate high values of ionic conductivity as a result of the fast diffusion of ionic species through a lattice shaped by the immobile counter ions. The Polymer Electrolyte Membrane (PEM) is a semipermeable membrane generally created from ionomers, they are designed to conduct protons. [35].

Solid polymer electrolyte is different from the liquid and gel electrolyte since the ionic salt is dissolved directly into a high molecular weight polymer and after removing the solvent, the resultant will be the solvent free polymer electrolyte. Typically the polymer is an insulating and relatively high dielectric material such as Polyethylene Oxide (PEO), Poly (Methyl Methacrylate) (PMMA), Polyacrylonitrile (PAN), Polyphosphazenes, Siloxane. The salt has low lattice energy and provides charge transportation. Solid Polymeric Electrolyte (SPE) is generally involved as a Proton exchange membrane (PEM) in the fuel cells fabrication that are predicted to be highly utilized in the transportation industry [36].

2.4.3.1.1. Nafion Membrane

Nafion®117 (DuPont™) is a perfluorinated polysulfonate polyelectrolyte cation exchange membrane and usually it is used as a SPE material. Its general chemical formula is shown in figure 2.7.
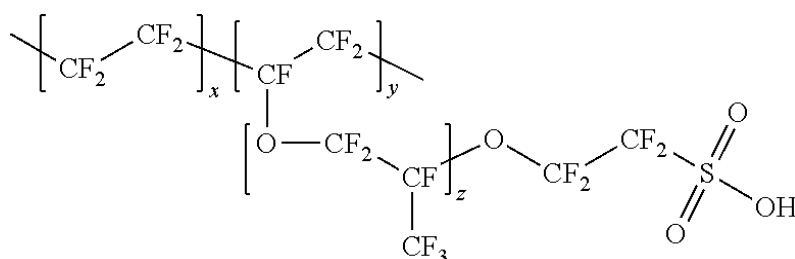
Figure 2.7 Chemical compound of Nafion (Du Pont) is a perfluorinated polysulfonate polyelectrolyte. The values of x, y and z varies from 1 to 13. The sulfonized fluoride group is hydrolysed to form the strongly acidic sulfonic cationic exchange site. The hydrated Nafion membrane provides a highly acidic environment, equivalent to 10wt% H_2SO_4 solution. Nafion 117 is a non-reinforced film based on chemically stabilized perfluorosulfonic acid/PTFE copolymer in the acid (H+) form of 183 micrometers (7.2mil) in thickness, Basic Weight of 360(g/m²) and Conductivity 0.10 min (S/cm), which is selected as the electrolyte for the sensor creation. Hydrated hydrogen ions move across the solid electrolyte membrane by moving from one fixed sulfonic acid group to the nearby one. Nafion membrane was used in macro size

amperometric sensors, as well as being more compatible with integrated microsensor fabrication process than liquid electrolytes [29]. Electrochemical sensors with SPE exhibit advantages over sensors with liquid electrolyte including minimum change in electrolyte concentration and eliminating a liquid electrolyte which leads to a limited life sensor [37] . Nafion has displayed biocompatibility that makes it interesting in the production of biosensors. It was demonstrated to be stable when it's used in the human body or cell culturing. Yet there is considerable research to be done in this area [37, 38].

2.5. Electrical Double Layer
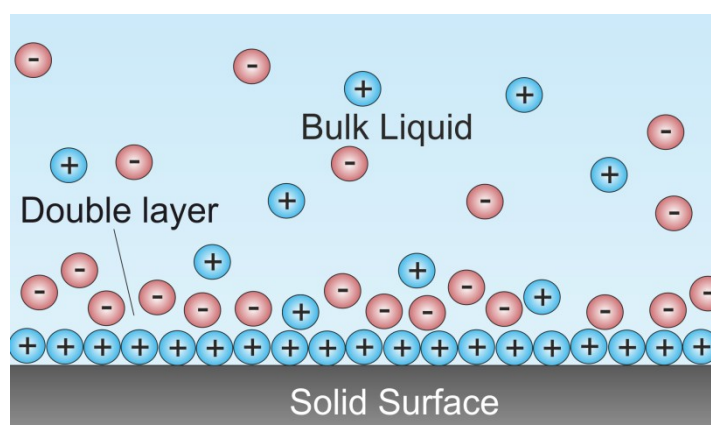
Figure 2.8 Schematic of double layer in a liquid at contact with a negatively-charged solid.

When an electronic conductor is exposed to a solid or liquid electrolyte, a boundary of two parallel layers of charged ions develops between the interfaces of two phases, which is called the electrical Double Layer (DL) as shown in figure 2.8. The first layer consists of negative or positive ions which are adsorbed to the body of conductor as a result of chemical reactions. The diffuse layer or the second layer consists of freely moving ions that is connected loosely to the first layer by the Coulomb force and screening the first layer electrically. The moving ions in the diffuse layer are affected by the thermal motion and electrical reaction [9].

The ions scatter on the boundary in an order depending on the electrode's material, for example its exposed crystallographic surface. Several models of DL have been proposed since 1853, which have evolved by time [9].

The Helmholtz is the first model of DL, which consists of two layers of opposite charge formed at the both sides of the interface in a rigid order, similar to the structure in the parallel plate capacitor. However it does not consider factors such as diffusion of ions in the electrolyte and the possibility of adsorption onto the surface. Gouy and Chapman reflected that the applied potential and electrolyte concentration affect the thickness of the double layer (capacity) where the extremely small ions can go to the proximity of the electrode's surface and move freely in the diffuse layer [39].

Stern united the both abovementioned models and supposed that the double layer was shaped by a rigid layer of ions close to the electrode interface and a diffuse layer spreading into the bulk solution, which is named the outer Helmholtz plane (OHP). Grahame advanced the Stern model and mentioned the existence of specific adsorption, where some ionic or uncharged species which have lost their solvation shell can penetrate the Stern layer. The inner Helmholtz plane (IHP) passes through the centres of these specifically adsorbed ions. Bockris, Devanathan and Müller Model consider the physical behaviour of the solvent in the interfacial region. The dipoles of the solvent molecules such as water near the interface would have a fixed orientation depending to the charge in the electrode. This orientation has big influence on the permittivity of the solvent that varies with field strength. Permittivity is the measure of the resistance that is encountered when forming an electric field in a medium. The permittivity of a medium describes how much electric field (more correctly, flux) is generated per unit charge in that medium [39].

2.6. Transport Process

The electrochemical reaction at the electrode interface in a simple approach consist of mass transport of the electroactive species to the electrode surface then the electron-transfer through the interface and the transport of the product to the solution. The rate of reaction in the electrodes is regulated by the slowest pace in the path. It considers mass transport (transport of reactants or products to or from the electrode surface), electrode kinetics (heterogeneous electron transfer) as shown in the figure 2.9.
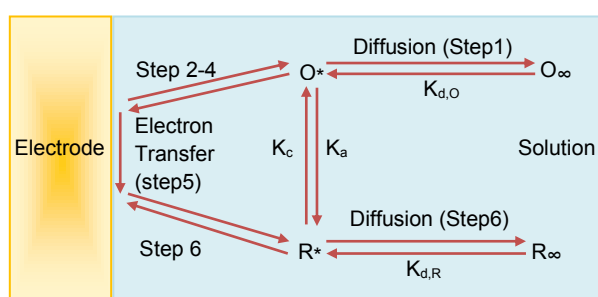
Figure 2.9 Diagram of electron transfer at the surface of the electrode [37].

In the pre equilibrium stage the reactants contact the electrode surface (1) and alter the order in the ionic atmosphere (2), alignment of the solvent dipole (3) and the distance of ligands and the central ion (4). Then electron transfer occurs (5) following by an inverse relaxation stage (6) [39].

In a Nernstian (reversible) reaction, the mass transport is limited and the rate of the electroactive species, v, reaching to the electrodes surface controls the reaction, directed by the equation (11) of flux (J) where the electroactive species is carried to the surface by mass transport for oxidation [39].

$$J(x, t) = -\frac{i}{nFA} \tag{11}$$

Wherein:

- $J(x,t)$ – Flux (mol cm^{-2} s^{-1})

- i – Current (A)

- n – Number of electrons oxidized or reduced

- F – Faraday constant (C/mol)

- A – Area of the electrode (cm^2)

Flux is the number of particles passing through a unit area in a unit of time and can be affected by diffusion, convection and migration. Presence of concentration gradient of electroactive species causes the natural motion of diffusion, which happens for all species. Existence of pumping, gas bubbling or stirring affects the thermal and density gradient in the solution generating the natural convection motion. Passage of charged particles along an electric field causes the migration motion due to presence of dipoles in the species. Nernst-Planck equation defines the overall flux in the electrode by a differential equation as the sum of each effects and when it's reduced to one dimension shown in equation (12) [39]:

$$J(x, t) = \underbrace{- D \frac{\partial C(x,t)}{\partial x}}_{\text{Diffusion}} \underbrace{- \frac{ZFDC_\infty}{RT} \frac{\partial E(x,t)}{\partial x}}_{\text{Migration}} + \underbrace{C(x, t)V(x, t)}_{\text{Convection}} \tag{12}$$

Wherein:

- $J(x, t)$ – Flux (mol cm^{-2} s^{-1})

- D – Diffusion coefficient (cm^2 s^{-1})

- $\frac{\partial C(x,t)}{\partial x}$ – Concentration gradient (at distance x and time t)

- Z – Charge of the electroactive specie

- F – Faraday constant (C/mol)

- C∞ – Concentration of the electroactive specie (mol/cm^3)

- R – Gas constant (8.314 J mol^{-1} K^{-1})

- T – Temperature (K)

- $\frac{\partial E(x,t)}{\partial x}$ – Potential gradient (at distance x and time t)

- V(x, t) – Hydrodynamic velocity.

It becomes complex when all three effects happen together though considering the existence of electrolyte and stagnant solution, the effects of migration and convection can be suppressed respectively and the equation will be reduced to diffusion, demonstrated by equation (13). According to Fick's first law, the electrochemical reaction creates the concentration gradient close to the interface of the electrode inside the electrical DL [39]:

$$J(x,t) = -D\frac{\partial C(x,t)}{\partial x} \tag{13}$$

Merging the equation (13) with the first expression of the flux with current at equation (11) generates the equation (14) for the current for oxidation:

$$i = nFAD\frac{\partial C(x,t)}{\partial x} \tag{14}$$

Fick's second law defines the time dependent diffusional flux as equation (15):
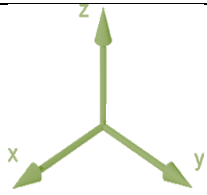
$$\frac{\partial C(x,t)}{\partial t} = D\frac{\partial^2 C(x,t)}{\partial x^2} \tag{15}$$

The general form of Fick's second law considering any coordinate system described as equation (16):
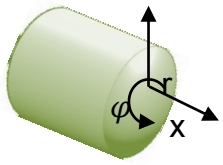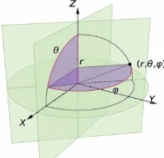
$$\frac{\partial C}{\partial t} = D\nabla^2 C \tag{16}$$

Laplace operator ∇ can be demonstrated at every coordinate system as shown in table 2.1.

Table 2.1 The general form of Fick's second law considering every coordinate system.

Coordinates	Laplace operator	Fick's 2nd law
Cartesian		
	x Axis	
	$\nabla = \dfrac{\partial}{\partial x}$	$\dfrac{\partial C}{\partial t} = D\dfrac{\partial^2 C}{\partial x^2}$
	x,y,z Axis	
	$\nabla = \dfrac{\partial}{\partial x} + \dfrac{\partial}{\partial y} + \dfrac{\partial}{\partial z}$	$\dfrac{\partial C}{\partial t} = D\left(\dfrac{\partial^2 C}{\partial x^2} + \dfrac{\partial^2 C}{\partial y^2} + \dfrac{\partial^2 C}{\partial z^2}\right)$
Cylindrical		

	$$\nabla = \frac{\partial}{\partial r} + \frac{1}{r}\frac{\partial}{\partial \varphi} + \frac{\partial}{\partial x}$$	$$\frac{\partial C}{\partial t} = D\left(\frac{\partial^2 C}{\partial r^2} + \frac{1}{r}\frac{\partial C}{\partial r}\right)$$
Spherical		
	$$\nabla = \frac{\partial}{\partial r} + \frac{1}{r}\frac{\partial}{\partial \theta} + \frac{1}{r\sin\theta}\frac{\partial}{\partial \varphi}$$	$$\frac{\partial C}{\partial t} = D\left(\frac{\partial^2 C}{\partial r^2} + \frac{2}{r}\frac{\partial C}{\partial r}\right)$$

Consequently the concentration and flux can be expressed as a function of time and position in Fick's law as shown in equation (17), where the diffusion limited current can be measured having defined the boundary situations [39]:

$$\frac{\partial C}{\partial t} = D\frac{\partial^2 C(x,t)}{\partial x^2} + D\frac{\partial^2 C(y,t)}{\partial y^2} + D\frac{\partial^2 C(z,t)}{\partial z^2} \tag{17}$$

2.6.1. Diffusion of planar (rectangular) electrodes

Diffusion at rectangular electrodes can be reflected considering boundary conditions listed at table 2.2 considering Fick's second law at Equation (15).

Table 2.2 Boundary conditions for diffusion at planar (rectangular) electrodes.

Boundary conditions	Definition
$t = 0\,s \rightarrow C_0 = C_\infty$	At t=0s without reaction there won't be any change in the concentration gradient.
$t \geq 0\,s \rightarrow \lim_{x\to\infty} C = C_\infty$	Very far from the surface, there won't be difference in the concentration.
$\begin{array}{c} t > 0\,s \\ x = 0 \end{array} \rightarrow C_0 = 0$	At the surface x=0 there is no concentration.

Considering the boundary conditions, the Cottrell equation is acquired which illustrates that as the time increases the diffusion limited current drops as shown in figure 2.10 And equation (18):

$$I_d(t) = \frac{nFAD^{1/2}C_\infty}{(\pi t)^{1/2}}$$

(18)

Wherein:

n – Number of electrons

F – Faraday constant (C/mol)

A – Electrode area (cm^2)

D – Diffusion coefficient (cm^2/s)

C_∞ – Substance Concentration (mol/cm^3)

t – Reaction time (s)
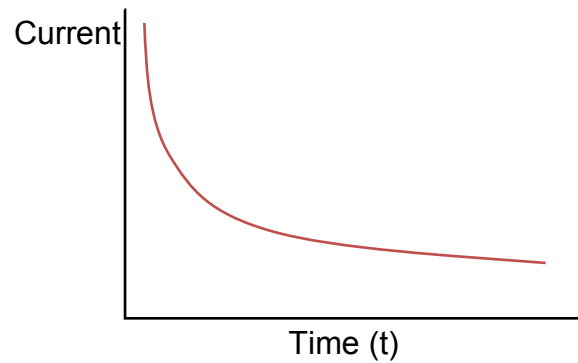
Figure 2.10 Change of current with time according to the Cottrell equation.

2.6.2. Diffusion of spherical electrodes

Fick's second law for a spherical electrode is equation (19) [39]:
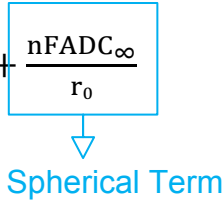
$$\frac{\partial C}{\partial t} = D\left(\frac{\partial^2 C(r,t)}{\partial r^2} + \frac{2}{r}\frac{\partial C(r,t)}{\partial r}\right)$$

(19)

Table 2.3 Boundary conditions for diffusion at spherical electrodes

Boundary conditions	Definition
$t = 0\ s$ $\quad \to C_0 = C_\infty$ $r \geq r_0$	At t=0(s) without reaction there won't be any change in the concentration gradient.
$t \geq 0\ s \to \lim_{r \to \infty} C = C_\infty$	Very far from the surface, there won't be difference in the concentration.
$t > 0\ s$ $\quad \to C_0 = 0$ $r = r_0$	At the surface r=r$_0$ there is no concentration.

The Cottrell equation including a spherical term (radius of electrode), time and boundary conditions as listed on table 2.3 will be equation (20):

$$I_d(t) = nFADC_\infty \left(\frac{1}{(\pi Dt)^{1/2}} + \frac{1}{r^0} \right) = \frac{nFAD^{1/2}C_\infty}{(\pi t)^{1/2}} + \boxed{\frac{nFADC_\infty}{r_0}} \qquad (20)$$

Spherical Term

Diffusion is linear in short times and the second term is negligible compared to the first. Consequently the equation (18) is attained;

$$I_d(t) = \frac{nFAD^{1/2}C_\infty}{(\pi t)^{1/2}} \qquad (18)$$

The full equation should be considered in the case of microelectrodes and short times which complicates the transport process. At macro sized electrodes and in longer times the second term governs (equation (21)). However as a consequence of the convection effects, steady state never attained, contrary to the microelectrodes that the steady state is gained quicker due to the smaller distance and area [39].

$$I_d(t) = \frac{nFADC_\infty}{r_0} \qquad (21)$$

2.6.3. Diffusion of microdisc electrodes

In this case the current is described using the equation (20) for the spherical electrode regardless of the non-uniform flux to the electrode's surface by replacing $r_0 = \frac{\pi a}{4}$, since a is the radius of the microdisc. The equation considering time becomes equation (22) [39]:

$$I_d(t) = \frac{nFAD^{1/2}C_\infty}{(\pi t)^{1/2}} + \frac{4nFADC_\infty}{\pi a} \qquad (22)$$

Diffusion becomes linear in short time same as equation (18), though in the long time becomes equation (23):

$$I_d(t) = \frac{4nFADC_\infty}{\pi a} \tag{23}$$

By substituting area we obtain a formula that is used as a steady state current equation (equation (24)):

$$I_d(t) = 4nFDC_\infty a \tag{24}$$

It is also advantageous to find when the steady state and transient modes become dominant and how they are related with the radius of the electrode. Thus a dimensionless factor (X) has been derived when the steady state dominates the overall current to a specified range such as 10 times more, to measure the lower limit of time.

$$X = \frac{\sqrt{\pi Dt}}{a} \tag{25}$$

Furthermore using the Fick's second law and chronopotentiometry method, the distribution of the electroactive species on the interface can be attained. Normally a steady current is exerted to induce the redox reaction on the electrode's surface and the output potential is measured in time. Table 2.4 shows the concentration variation equation when a concentration gradient imposed on the electrode surface considering time that is achieved formerly employing the Laplace transform and matching boundary conditions applied, excluding the third condition [39].

Table 2.4 The concentration variation when a concentration gradient imposed on the electrode surface.

Time variant	Concentration variation with time
Planar electrode	Planar electrode
$\begin{matrix} t > 0s \\ x = 0 \end{matrix} \rightarrow i = nFAD\left(\dfrac{\partial C(x,t)}{\partial x}\right)_{x=0}$	$C_0 = C_\infty \mathrm{erf}\left[\dfrac{x}{2\,(Dt)^{1/2}}\right]$
Spherical electrode	Spherical electrode
$\begin{matrix} t > 0s \\ r = r_0 \end{matrix} \rightarrow i = nFAD\left(\dfrac{\partial C(r,t)}{\partial r}\right)_{r=r_0}$	$C_0 = C_\infty - \dfrac{r_0}{r}\mathrm{erfc}\left[\dfrac{r - r_0}{2\,(Dt)^{1/2}}\right]$

In a Cottrell experiment the change in concentration with time and distance has been shown in figure 2.11.
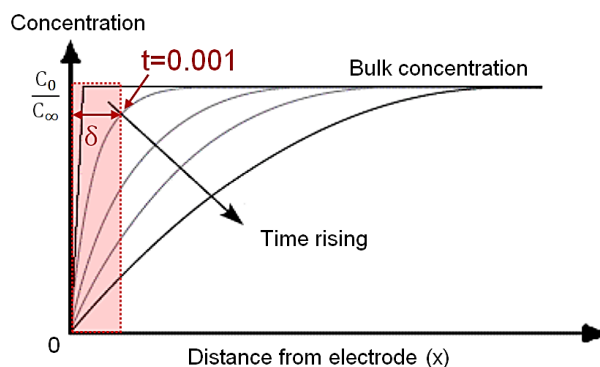
Figure 2.11 Concentration profiles for several times after the start a Cottrell experiment.

The region close to the electrode's surface with concentration gradient is the diffusion layer and its thickness, δ is time dependent as shown in figure 2.10. Nernst expressed an estimative formula for this thickness as equation (26):

$$\frac{\partial C(x, t)}{\partial x} = D \frac{(C_\infty - C_0)}{\delta} \tag{26}$$

After this is applied to Cottrell equation (Equation (15)), the thickness can be calculated by equation (27), verifying that the steady state cannot be acquired in macro sized electrodes in long times.

$$\delta = (\pi D t)^{1/2} \tag{27}$$

2.7. Kinetics of electrode reactions

The heterogeneous electrochemical reaction engages transfer of charges on the electrode's surface and occurs between two species in an electrochemical pair same as the structure of our sensor, usually between the solid electrode (working electrode) and the electrolyte [39].

2.7.1. Heterogeneous electrochemical reactions

Considering the general expression of the current response with concentration gradient (equation (28)) and the one electron reduction process with forward and backward rate constants of k_f and k_b as shown in equation (29):

$$i = nFAD\left(\frac{\partial C(x,t)}{\partial x}\right) \tag{28}$$

$$O + ne^- \underset{K_b}{\overset{K_f}{\rightleftarrows}} R \tag{29}$$

And the net reaction rate of υ:

$$\upsilon = K_f C_O(0,t) - K_b C_R(0,t) \tag{30}$$

Integrating them with the equation (15), the equation will be:

$$i = nFA[K_f C_O(0,t) - K_b C_R(0,t)] \tag{31}$$

The rate constants of K_f and K_b were linked by Butler and Volmer with the reversible formal potential E_f^0, a transfer coefficient of α and a standard rate constant of K_0 [40, 41]. E_f^0 is used as a replacement for E_0 since the measurements are not typically carried out under standard criteria such as unit activity, temperature and pressure. The α is the gradient of the transition-state energy profile and affects the profile of the voltammetric response. Its value ranges from zero to one. Normally in the reversible reactions and for metal electrodes, α is 0.5. The rate of reaction is controlled by the potential of the electrochemical sensor and at a particular potential K_f and K_b is the same, and defined as a heterogeneous rate constant of K_0, wherein at other potentials it can be defined in terms of K_0 as equations (32 and 33):

$$K_b = K_0 \exp\left(\frac{(1-\alpha)nF(E - E_f^0)}{RT}\right) \tag{32}$$

$$K_f = K_0 \exp\left(\frac{-\alpha nF(E - E_f^0)}{RT}\right) \tag{33}$$

At this instant it can be related to current density in which E is the equilibrium potential at equation (34):

$$i = nFAK_0\left[C_O(0,t)\exp\left(\frac{-\alpha nF(E - E_f^0)}{RT}\right) - C_R(0,t)\exp\left(\frac{(1-\alpha)nF(E - E_f^0)}{RT}\right)\right] \tag{34}$$

K_f and K_b are equal at equilibrium so the anode and cathode have equivalent currents, as shown by equation (35):

$$nFAK_0C_O(0,t)\exp\left(\frac{-\alpha nF(E - E_f^0)}{RT}\right) = nFAK_0C_R(0,t)\exp\left(\frac{(1-\alpha)nF(E - E_f^0)}{RT}\right) \tag{35}$$

Equation (35) is the principle connection between the current flow and the applied voltage inside the sensor, which predicts in equilibrium state the net current flow is zero and C_O and C_R become equal. However a stable Faradaic motion can be foreseen as the exchange current i_0 and its linked to k_0 by equation (36):

$$i_0 = nAFK_0C(0,t) \tag{36}$$

And reduce further:

$$i = i_0\left[\exp\left(\frac{-\alpha nF(E - E_f^0)}{RT}\right) - \exp\left(\frac{(1-\alpha)nF(E - E_f^0)}{RT}\right)\right] \tag{37}$$

With equation (37) which is acknowledged as current-overpotential equation, it's likely to study the kinetics of reaction with variation of i_0. With higher amount of i_0, the current change will be higher on the $E-E_0$ and the kinetics reaction will be faster.

Tafel equation (η) has been defined as a limitation to Butler-Volmer formula when applied to high overpotential schemes:

$$\eta = \frac{RT}{\alpha nF}\ln i_0 - \frac{RT}{\alpha nF}\ln i \tag{38}$$

When it's linearized:

$$\eta = a + b \log i \tag{39}$$

This formula presents a Tafel plot, where *b* is known as the 'Tafel slope' and elucidates the mechanism of the reaction. *a* give details about the exchange current density and rate constant. If the Tafel plot is a straight line, it is useful to study the non-reversible and nonequilibrium conditions, which is not possible with Nernst kinetics [39].

2.8. Electrochemical measurement techniques

2.8.1. Cyclic voltammetry

Cyclic voltammetry (CV) is a technique of potentiodynamic and electroanalytical measurement. It studies the electrochemical properties and half-cell activity of an analyte, oxygen in research. It is utilized in many engineering procedures and analytical chemistry and presents information about the analyte, kinetics of heterogeneous reactions, thermodynamics of redox process and adsorptions process while measuring the current as the potential changes. It is necessarily accomplished in a three electrode sensor structure via WE, RE and CE to prevent current pass through the RE and changing its potential by reactions of different species. The current should pass through WE and CE since RE controls the potential passing through the WE as mentioned before.

The Working electrode's potential varies linearly with scan rate υ against time and ends when it gets to a fixed potential value, and then the potential slope of the working electrode is reversed back as shown in figure 2.12. This sequence can occur several times through a single trial until a set cycle number is acquired. The applied potential (volts) to the electrode controlled while the current was being measured (amperes) [39].
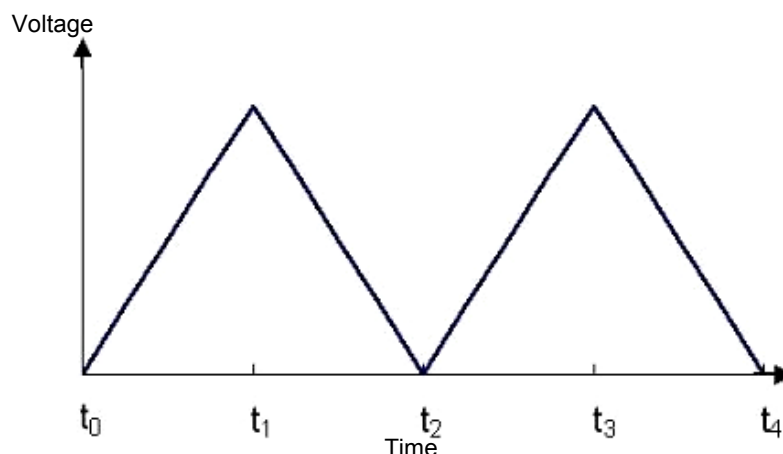
Figure 2.12 WE's potential vs. time variation in cyclic voltammetric experiment.

The $I = f(E)$ is a cyclic voltammogram curve of the reaction, which is the plot of the current versus the applied voltage at the working electrode. The contrary is the amperometry method, which is not very usual. The current is the outcome of redox reactions of the electroactive species in solution (Faradaic current) and the double layer charging (Capacitive current) [39]. Recalling the redox couple (equation (29)), before applying voltage, there is reduced form of R in the electrochemical sensor, while exertion of the voltage with constant scan rate begins the faradaic current rises exponentially caused by the concentration of R on the electrode. The concentration gradient and the current increase as the applied voltage is getting closer to the redox potential, which is positioned at midpoint between the anodic and cathodic peak potentials. Maximum mass transfer of R takes place after passing the redox potential, and then it deteriorates as a result of reduction of R. At that time the potential is directed in the opposite way and the oxidised product O is transformed back into R. In an equilibrium condition or a standard reversible cyclic voltammetry, the heights of the anodic and cathode peak are equal as shown in Figure 2.13. The profile of the curve is determined by the rate of change in the applied potential and the condition of the solution under the test, whether it is stagnant or flowing [39].

35
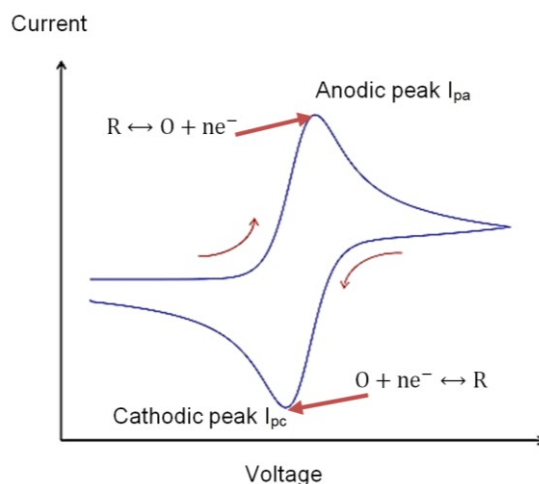
Figure 2.13 cyclic voltammetric behaviour of a macroelectrode for a reversible reaction.

The Randles Sevcik equation determines the applied potential's scan rate relation with the peak current via:

$$i_p = 2.69E5 \; n^{3/2} D^{1/2} C \upsilon^{1/2} A \tag{40}$$

Wherein:

i_{pa} – Anodic peak current (A)

n – Number of electrons

D – Diffusion coefficient ($cm^2 \; s^{-1}$)

C – Bulk concentration ($mol \; cm^{-3}$)

υ – Scan rate ($V \; s^{-1}$)

A – Electrode area (cm^2)

Microelectrodes exhibit an S-shaped CV profile (figure 2.14) since the mass transport is ruled by radial diffusion. As stated earlier in the steady state, a constant current is generated as a limiting or steady-state current [39].
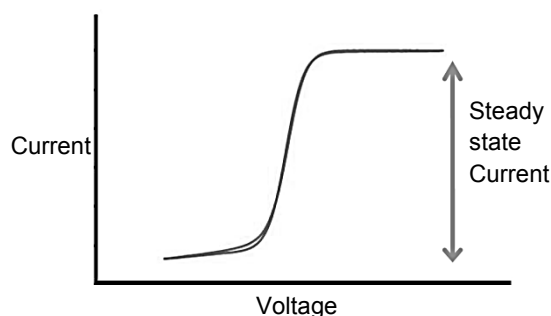
Figure 2.14 Cyclic voltammogram for a microelectrode at a reversible reaction [39].

2.8.2. Chronoamperometry

Chronoamperometry (CA) is an electrochemical method to determine the diffusion limited current of I_d. A controlled Stepped potential is exerted to the working electrode at t=0s in a medium comprised of oxidized or reduced species and it's varied from a point of no electrode reaction to a value that all species arrive to the electrode surface and get involved in the reaction as shown in figure 2.15. The current outcome from the faradaic processes is observed as a function of time.
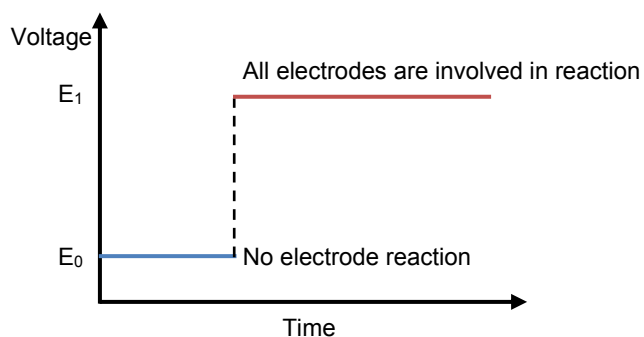
Figure 2.15 Potential step in chronoamperometry to obtain a diffusion-limited current of the electroactive species.

CA also generates high charging currents that exponentially decay with time. The Faradaic current also decays as described in the Cottrell equation with time. However sometimes it is slower than the charging decay for example in sensors with no supporting electrolyte. CA provides a better signal to noise ratio, when it's compared to other amperometric practices and mainly examined on a three electrode sensor as the current is integrated over longer time periods [39].

2.9. Microelectrodes

A microdisc has been used to measure the oxygen in muscle tissue for the first time as a microelectrode in 1940 [42]. The microelectrodes were practically begun to be used in the electrochemical studies in 1980 when Fleischmann and co-workers found that they have qualitative and quantitative advantages. Since then there have been exceptional progress in electrochemical science [43]. Electrochemical techniques had some disadvantages and shortcomings when used with macro sized electrodes, which were improved after introduction of microelectrodes to electroanalysis. Microelectrodes were cost efficient and easily put into practice [9].

There were question on the size of the electrodes so they could be considered as microelectrodes. A general concept is if at least one dimension of an electrode is smaller than the size of its diffusion layer, it could be considered as microelectrode [9]. There were various perceptions on the size of the microelectrodes such as bigger than 50 μm, 25 μm, between 0.1 and 50 μm or between 0.8 and 50 μm. Microelectrodes exist in many shapes and styles for example disc, cylinder, band, ring, sphere, and hemisphere. The key dimension of disc, sphere, cylinder or hemisphere electrodes is their radius and the key dimension of the band, cylinder or ring electrodes is their width. Among them microdisc is the most significant shape and normally created from platinum, gold or carbon isolated in glass or plastic from electric surrounding. Many definition and theories exist in the literature regarding the microelectrodes types and their mathematical relations with the diffusion limited current [35, 39, 44].

The response of the microelectrodes is unlike that of the macro electrodes and due to their minimized interface, they have the advantage of lower detection limit. Capacitive effects and ohmic drops have minimal effect on their response and sometimes they can be utilized even in the lack of the electrolyte [9, 36, 39, 43].

2.9.1. The capacitive current effect

As stated before Faradaic current (I_F) results from the electron transfer in the electrochemical reaction. Though in an electrochemical process when the applied potential varies, the double layer capacitances charges or discharges, triggering the capacitive current (I_C) to rise without any charge transfer as shown in figure 2.16. This is also called the double layer current or non-faradaic current. In this current there is no charge transfer though affects the amassing or elimination of the electrical charge on the electrode and electrolyte's interface. In a steady potential, the capacitive current is zero however if there is any change in the physical environment of the experiment for example in the temperature or the geometries of the electrode, it can change.
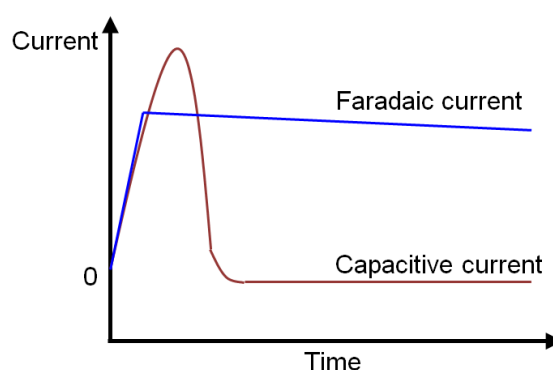
Figure 2.16 The resulting plot current-time (Chronoamperogram) [31].

When a potential scan rate is applied to an RC circuit which is in series, it will have the capacitive current passing through it. A formula for the capacitive current has been presented in the equation (41), where ΔE is the potential step, C is the double layer capacity and t is time. Considering the comparative figure and the formula, the capacitive current decays to zero exponentially compared to the faradaic current and it can be ignored in longer terms [43].

$$I_C(t) = \frac{\Delta E}{R_S} e^{\frac{-t}{RC}} \tag{41}$$

Where R is the resistance.

Microelectrodes are helpful in the range of less than 50 μs and in the investigation of the fast processes, since the I_C is exponentially related to the surface area and can be ignored. As much as the potential scan rate is slower and the electrode's dimension is smaller the current ratio of faradaic current to capacitive current will improve.

2.9.2. The Ohmic drop effect

In the electrochemical process, the electrode has a resistance of R so when the current passes through the electrolyte and electrode, a potential is created that reduces the applied potential to the WE, causing the ohmic drop and has a negative effect on the accuracy of the results. This effect is greater if the flowing current and the resistance of the electrolyte are higher, though it is very low at the microelectrodes due to the minor current flow.

According to the Cottrell equation at short time, if the diffusion in the reaction is linear, the current and eventually the ohmic drop will be in direct proportion to the radius of the microelectrode and both will decrease if the radius gets smaller. But at the steady state at long time (equation (24)), the current is proportional only to the radius of the electrode, which has no effect on the Ohmic drop. To reduce the ohmic drop effect, a high resistivity electrolyte that reduces the current flow through itself, could be chosen, which results in small current being produced and requires utilization of costly and sensitive apparatus [43].

2.10. Review of State of Art in electrochemical oxygen sensor in biological applications

There are three important factors in characterising a sensor; Capability of the sensor to quantitatively measure the test gas (oxygen) in the certain environment (sensitivity), its ability to detect the particular gas without interference of other substances (selectivity) and how fast the changes in signal can be observed by change in the concentration of the gas (response time). Moreover size, power consumption, stability and reversibility are the

important features that affect the sensor's performance. It's important to be able to monitor oxygen within the ambient surroundings, which is essential in the food processing, medical and pharmaceutical industries. The Clark oxygen sensors and aqueous electrochemical cells are best suited for these applications. In this section, some of the recent electrochemical techniques and devices invented so far for the purpose of cellular respiration measurements will be reviewed.

Nga-Chi Yip et al. demonstrated an electrochemical mediator assay by measuring oxygen to evaluate the number of cells and their chemical toxicity for the purpose of monitoring cells metabolism. In this process they compared the catalytic properties of the 2 mM ferrocene carboxylic acid (FcA) and 2 mM ferrocene methanol (FcMeoh) solutions (oxygenated and deoxygenated) separately when interacted with oxygen species. This system is used to detect the oxygen consumption of Escherichia coli DH5-α (E. coli) and the results can be accomplished in minutes. In this experiment the electrochemical cell was made of 3 mm diameter glassy carbon working electrode, Ag/AgCl reference electrode and platinum counter electrode. A data acquisition software and a Gamry 600 potentiostat were used to run the experiments. Cyclic voltammetry (CV) study performed several times to investigate the assay. Before each CV study, the glassy carbon electrode was polished with 50 nm alumina powder for 5 minutes. The CV initiated by applying 0V potential at scan rates from 5 to 2000 mV s^{-1} with a switching potential of 0.6 V and end potential of 0V [45].
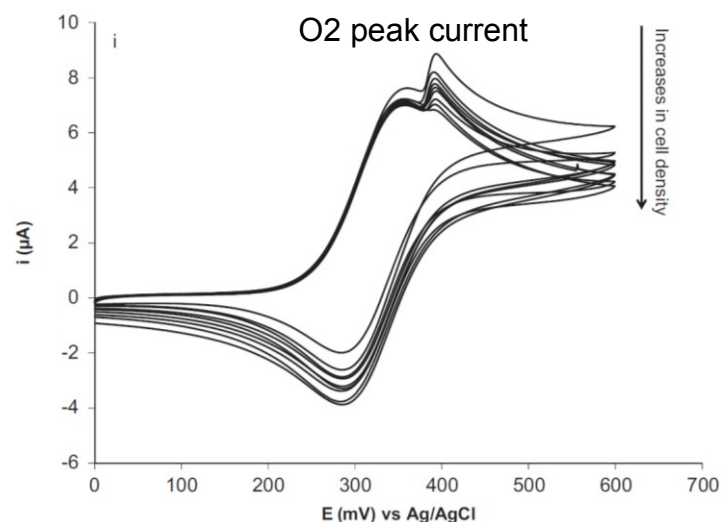
Figure 2.17 Typical CVs obtained for the 2 mM FcA solution containing different E. coli concentration of 0, 0.25, 0.5, 0.75, 1, 1.25, 1.5, 1.75, and 2 Optical density/mL [43].

One of the examples of this assay is shown in figure 2.17, which demonstrates the increase in number of E. coli leads to an increase in oxygen consumption since the E. coli would be constantly consuming oxygen, and hence, a decrease in the electrocatalytic O2 peak current. It also proves the decrease in the electrocatalytic O2 peak current is proportional to the increase in E. coli cell numbers, which is logical [45].

In this assay oxygen consumption per E.coli has been determined by comparison of several CVs, which cannot be trusted since the solution under the test is stagnant and the electrochemical cell itself consumes oxygen during the electrochemical process, there is no flow or stirring in the fluid under the test, resulting in inaccurate results, cellular death and infection could follow during long hours of experiments. Usage of platinum electrode as CE leads to creation of platinum oxide, which makes the system toxic and not fully biocompatible. Polishing the working electrode every single time for 5 minutes and renewing the catalytic solution would make the process time consuming and costly. The chemical content of the FcA and FcMeoh catalytic solutions may interfere with and alter the properties of cells since difference in behaviour observed for FcA and FcMeOH in terms of the position of peak potentials, which is caused by the different functional groups as FcA contains a

carbonyl and FcMeOH a hydroxyl [45]. It's also difficult to carry out this process at places other than biological cell labs and special conditions, it's not portable.

To solve this issue many oxygen sensor devices with different design and structure have been invented. Here we explore some of the most recent inventions and designs to understand the problems and required improvement to create the best possible solution.

Jin-Hwan Lee et al. presented design and application of a Needle-type dissolved oxygen (DO) microelectrode array (MEA) sensors for in situ measurements. The 10mm long sensor probes were fabricated by dynamic etching technique and sharpened to micro meter dimensions and packaged on a PCB carrier as can be seen on figure 2.18. Inside a recess fabricated at the tip of each microelectrode, a gold sensing electrode was used.
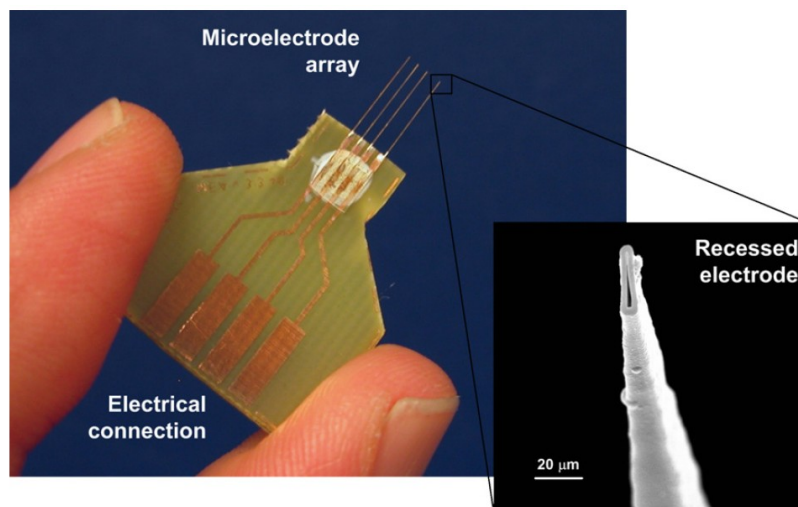
Figure 2.18 Fabricated DO microelectrode array sensor is packed on a PCB carrier and a scanning electron micrograph (SEM) of the recessed electrode [46].

Performance of these sensors was characterized by measuring the oxygen concentration of saline solutions with an Ag/AgCl reference electrode. The DO MEA displayed a quick 15 s linear response in the 0–21% O2 (0–9 mg/L) range (figure 2.19). The sensor was used for evaluation of DO micro profiles in a multi-species aerobic bacterial film. It was able to

penetrate samples to measure DO and the time for 90% response was typically less than 20 s [46].
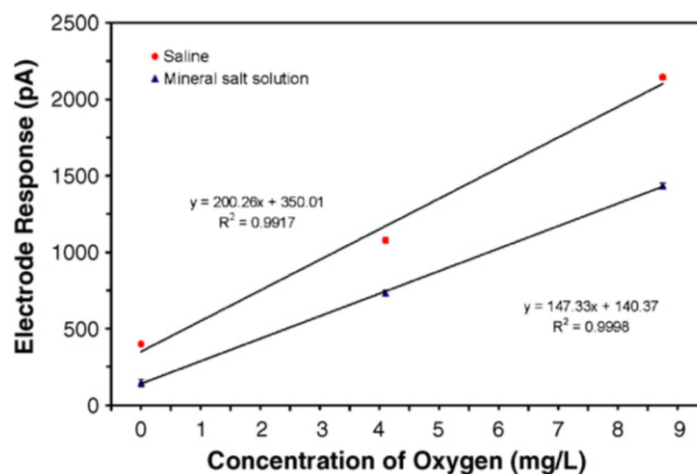
Figure 2.19 Calibration curves for the recessed DO microelectrodes array against saline (0.85% NaCl solution) and a mineral salt solution [46].

Although the recessed structure with inner cathode improved sensitivity and stability of the DO microelectrode, the fabrication process was very lengthy. Its fabrication sequence consisted of: 1) form glass probes by dicing; 2) taper probes in HF-based etchant; 3) use meniscus etching to sharpen probes; 4) deposit Au conductive layer; 5) use silver epoxy to establish electrical connections; 6) coat microelectrodes with Parylene insulating layer and recess tips by beveling and etching. These steps were generally very difficult to manufacture, necessitated trained people to use, and must be applied in a laboratory under firmly controlled circumstances. Additionally, because of the minor signals involved, the sensors were subject to electrical interference and need to be used inside a well-grounded Faraday cage. This sensor required a separate reference electrode to perform the electrochemical reaction and was not integrated in one sensor. The time consuming, costly fabrication process of this sensor and brittle nature of the probes doesn't guarantee a long shelf time and multiple usages during the extended period of time.

More recently, Ching Wu's and Yasukawa's group have presented the Fabrication of a miniature Clark oxygen sensor combined with microstructure, which consisted of a glass substrate with a three electrode configuration, connected by a groove, and a PDMS container, and covered with a PDMS oxygen permeable membrane as shown in figure 2.20. O2 plasma bonding method was used to assemble the substrates.
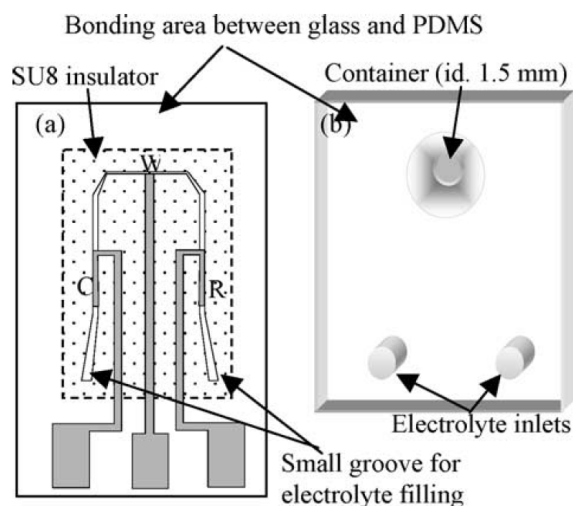
Figure 2.20 The arrangement of a miniature sensor. It's made up of (a) a glass substrate with a groove made by SU8 photoresist and (b) a container substrate with an oxygen-permeable membrane. W, C and R are the working, counter and reference electrode, respectively [6].

It was used for measurement of the adhering cells respiration. Alginate sol electrolyte was used. The sensor had the response time of 13.4 s, linearity with a correlation coefficient of 0.993, and lifetime of at least 60 h. One of the advantages of this sensor is its fast response to a change in oxygen concentration (90% response time, 6.8 s), which is useful to monitor the kinetics of oxygen variation in biological samples. The response of the sensor is due to the Usage of the thin membrane for oxygen permeation (7μm) and the vicinity of the measuring container to the detection electrode. Figure 2.21 demonstrates the calibration curve for the oxygen sensor. The experiment has been carried out in a 10mM PBS solution (pH 7.0) by adding Na2SO3 and applied voltage of −0.7V in 0–7 ppm (0–7 mg/L) range [6].
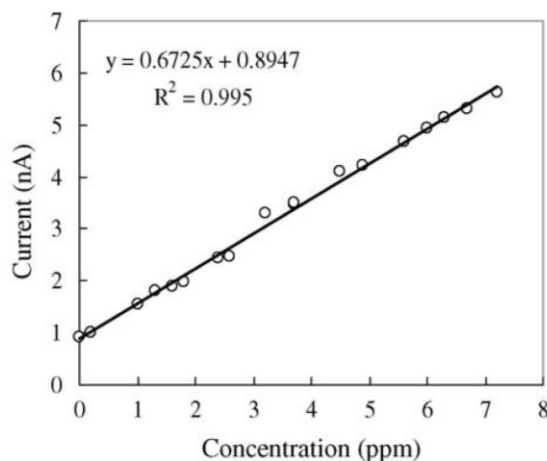
Figure 2.21 Calibration curve for the oxygen sensor. The trial was conducted in a 10mM PBS solution (pH 7.0) by adding Na2SO3. Applied voltage: −0.7V [6].

This work has found to be effective in the measurement of the cellular respiration; however usage of PDMS container and oxygen permeable membrane makes it difficult to keep the same properties stable in the long term. Prior to each experiment the device needs to be fabricated fresh, which is time consuming and expensive considering the materials being used. Additionally, if the attachment between the PDMS and the glass material doesn't yield a good sealing, the external PBS will pour into the groove and affect the pH value of the electrolyte. Extended operation of the working electrode at certain voltages for example −0.4V caused it to become transparent and damaged it seriously, which was revealed in a microscopy observation at 33 hour [6].

Jungil Park's group at Korea University, Seoul have published their work in the development of the array type oxygen sensors. Their research focuses on the fabrication and use of 2 X 3 array oxygen sensor for measuring cellular respiration level [3, 17, 47]. This oxygen sensor array was able to measure the cellular respiration level in a solution containing cells simultaneously from various samples. The oxygen sensor comprised of Clark-type sensors of 2 x 3 array type on the substrate as demonstrated in figure 2.22.
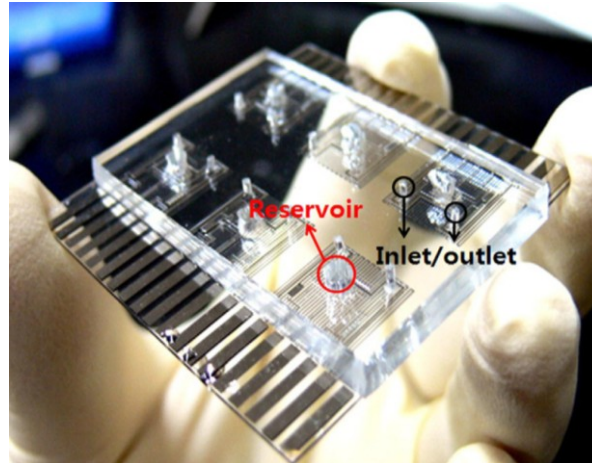
Figure 2.22 The fabricated array reservoir-type oxygen sensor [3].

18μm PDMS was used as a permeable membrane of the Clark-type sensor. Having 90% response time of about 10 sec from full oxygen (air-saturated) state to zero-oxygen state (figure 2.23(a) and (b)), it was reported to present linearity correlation coefficient of 0.997.
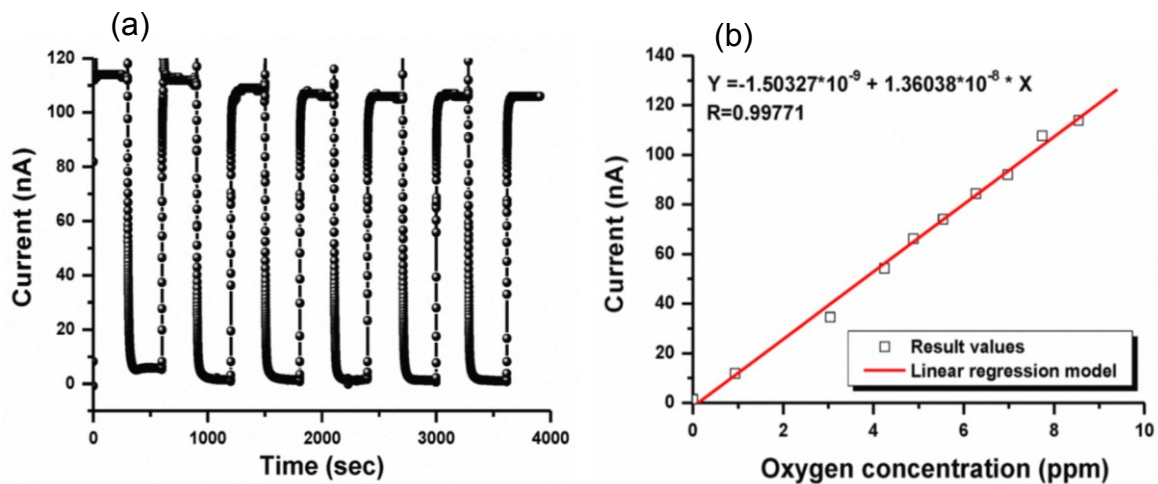
Figure 2.23 (a) Reproducibility of the fabricated Clark-type sensor. (b) Linearity curve of the fabricated Clark-type sensor [17].

However in order to attain reproducible results it was necessary to maintain supply of liquid electrolyte constantly. For such devices, using liquid electrolyte created challenges of high maintenance.

In 1999 Jayashri Gopalakrishna and his co-workers developed one of the first oxygen sensors that utilized a solid electrolyte instead of liquid electrolyte and investigated the Performance of Solid Polymer Electrolyte (SPE) based Oxygen Sensor without External Humidification.

The sensor's working, reference and counter electrodes were made of porous C/Pt based, Gas Diffusion Electrodes (GDE). The functionality of the sensor is tested without external humidification of the test gases. Basic diagram of the sensing system is shown in figure 2.24. To attain internal humidification of the Nafion membrane, the oxygen reduction principle and back diffusion of water, is used. The sensor responds to oxygen concentrations from 10 ppm to 20% as shown in figure 2.25.
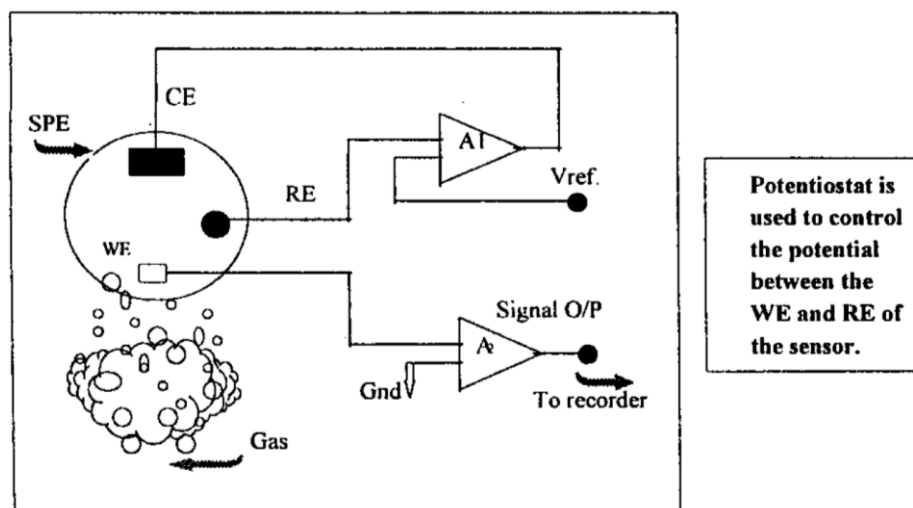
Figure 2.24 Basic diagram of the sensing system [48]
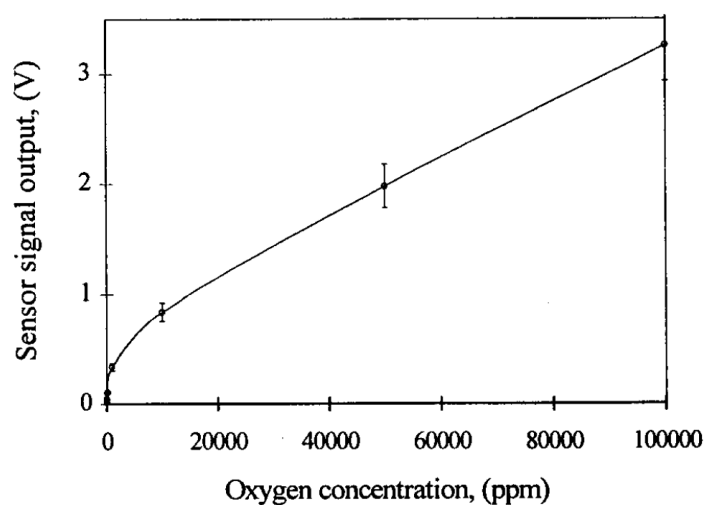
Figure 2.25 Calibration curve of the sensor [48].

The proper cleaning of a Nafion membrane was essential to the successful sensor performance.

The oxidation reaction at counter electrode yields water. This water evaporates and dehydrates the membrane. By using Teflon bonded platinum as the counter electrode, membrane dehydration can be avoided. Additionally the hydrophobic nature of Teflon helps the Nafion membrane to sustain water and membrane dehydration can be prevented by the back diffusion of water and internal humidification of membrane. In dry gas measurements the sensor output signal was 35% lower than the humidified sensor output signal.

In this study, the maintenance free operation of the sensor is reached and removed the need of gas humidification system [48].

Glen W. McLaughlin and his colleagues have pioneered in the development of solid-state dissolved oxygen sensor test matrix having deposited solid-state proton conductive matrix (PCM) as solid electrolyte on a silicon wafer substrate and encapsulated in a bio-inert polytetrafluoroethelene (PTFE) film. Four different working electrode diameters: 10 μm, 20 μm, 40 μm, and 80 μm are arrayed. Figure 2.26 shows the Pictorial depiction and single element cross-section of the dissolved gas sensor test matrix.
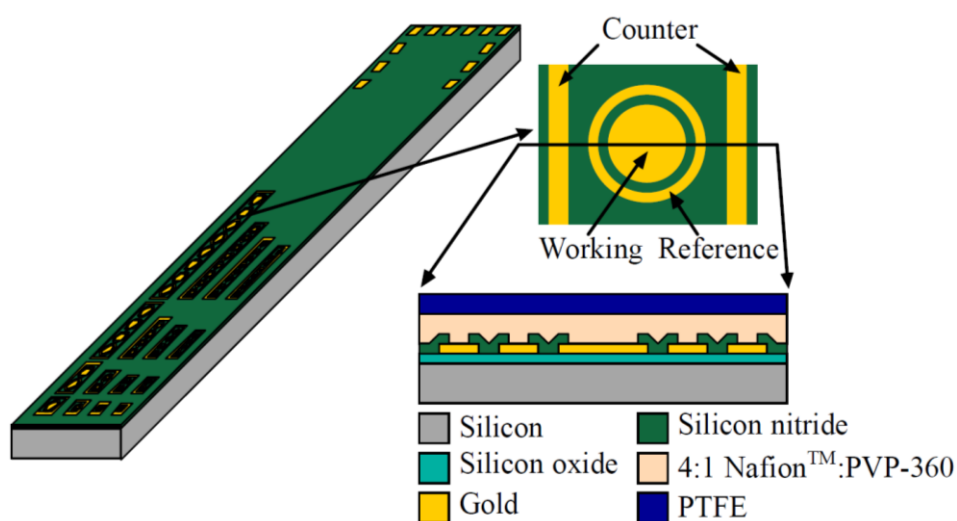
Figure 2.26 Pictorial depiction and single element cross-section of the dissolved gas sensor test matrix [5].

49

In this sensor the number of elements arranged in each set also differs in four stages: 1, 2, 4, and 8. Therefore, each column of the matrix have the same working electrode diameter, while each row has arrays of the same number of electrode elements.

It was reported, through cyclic voltammetry (CV) and voltage step (VS) measurements, the device displayed a linear response with respect to dissolved oxygen concentration over a range of 0 – 300 mmHg with a response time constant of 0.51 s (±0.087 s). CV measurements results for the electrode sets are shown in figure 2.27 [49].
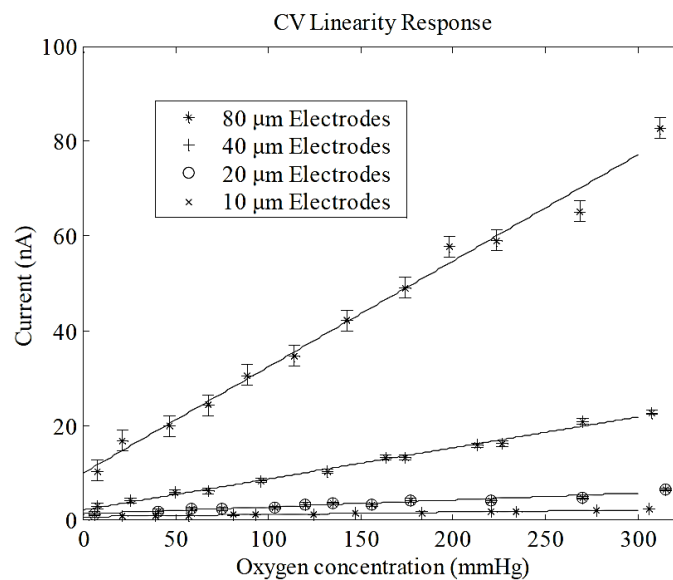
Figure 2.27 CV calibration measurement of 10 μm, 20 μm, 40 μm, and 80 μm working electrode diameter, 8 electrode array sets.

In this sensor, unlike standard Clark cell configurations, there is no net consumption of either electrode. This sensor performed more accuracy and sensitivity with respect to changes caused by cellular respiration [5]. However the electrodes were fabricated using micro fabrication techniques, which is a time consuming and expensive process and was difficult to incorporate it into a sealed packaging due to its significant reduction in robustness after fabrication process.

In 1998, H. Camon and his colleagues presented their work about an oxygen sensor that is a miniaturized hersch battery. This electrochemical cell was made of two micromachined silicon wafers containing two electrodes: a gold working electrode that is deposited by an evaporation process and the counter electrode made of lead obtained by electrochemical deposition process. They were immersed in a liquid electrolyte and separated by a porous membrane from the solution to be tested. Cross sectional and top view of the oxygen sensor is shown in figure 2.28.
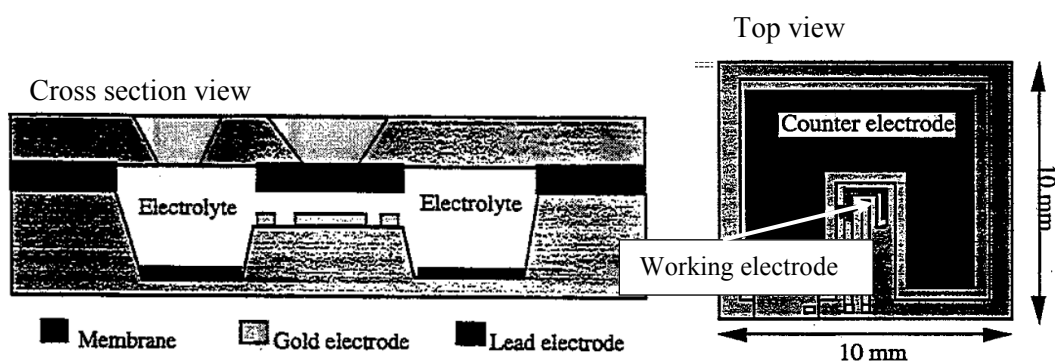
Figure 2.28 Cross sectional and top view of the oxygen sensor [50].
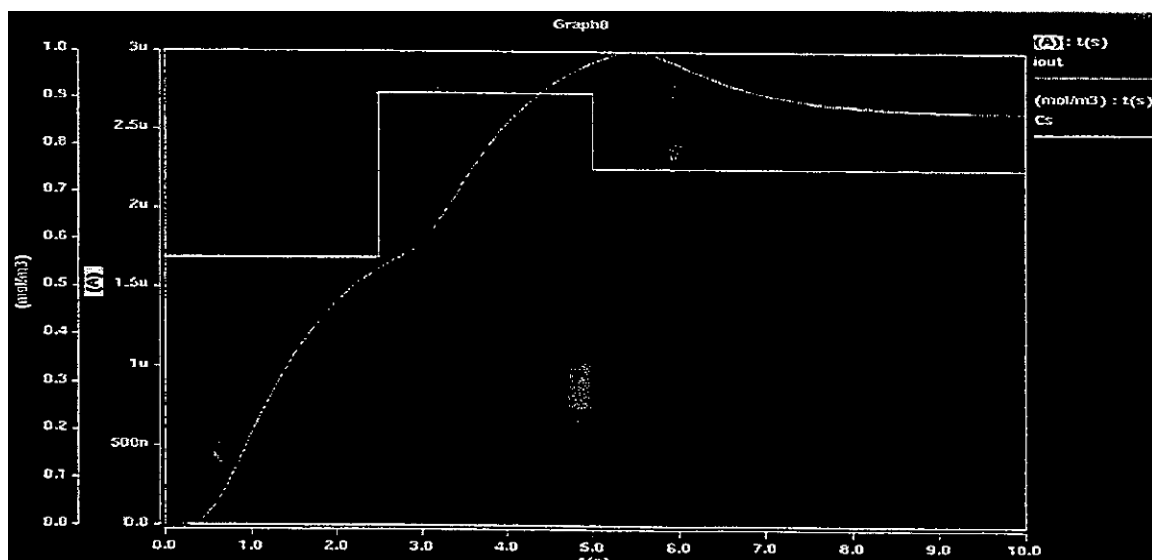
Figure 2.29 Response of the output current when oxygen concentration varies by implementing on a SABER simulator [50].

To validate the oxygen sensor model, they have implemented the schematic of the sensor control circuit in SABER simulator. Figure 2.29 presents the behaviour of this model when oxygen concentration varies [50].

In this experiment other than a simulation, a real experiment has not taken place and doesn't represent the real response and sensitivity of the sensor to the changes of the oxygen concentration. Silicon wafer usage in this sensor reduces the robustness and shelf life and has high risk of leakage of the liquid electrolyte to the sample under test, which will interfere with the reliability of the results. This device will increase the cost and labour by requiring constant humidification of the device by using liquid electrolyte. However this work can be used as an example for future work in the area of simulation and modelling the electrochemical oxygen sensor as a first step.

Most of the works presented in this section showed good response and sensitivity toward changes of oxygen concentration such as the electrochemical mediator assay demonstrated by Nga-Chi Yip et al. and the Needle-type dissolved oxygen sensor presented by Jin-Hwan Lee and his group. The electrochemical mediator assay demonstrated by Nga-Chi Yip et al. was a good example of a test showing the necessity of monitoring cellular respiration, which leads to the design and development of more compact and sensitive oxygen sensors that ease the process of cellular respiration. The Needle-type dissolved oxygen sensor presented by Jin-Hwan Lee was a packaged sensor on a PCB having micro needle probes and used a separate reference electrode. This sensor needed to be placed in a faraday cage to eliminate the outside signal interferences and proved that there is more potential to miniaturization and optimization of electrochemical oxygen sensors. Ching Wu's and Yasukawa's group and Jungil Park's group at Korea University have published their work in the development of the oxygen sensors. They presented a miniature Clark oxygen sensor combined with microstructure, a PDMS container, and a PDMS oxygen permeable membrane. Their design was a more compact device presenting effective measurements in cellular respiration changes. However the unstirred solution of the cell chamber that caused stagnation in long term, requirements of electrolyte rehydration and usage of materials such as PDMS decreased

the shelf life and increased the price. Jayashri Gopalakrishna and his co-workers developed an oxygen sensor that used a solid electrolyte instead of liquid electrolyte which made it possible to use an electrochemical oxygen sensor without the need of maintenance and external humidification. This method made it conceivable to have miniaturized oxygen sensors without needing electrolyte rehydration and as a result to have a more integrated sensor. Glen W. McLaughlin and his colleagues developed a solid-state dissolved oxygen sensor test matrix having deposited PCM as solid electrolyte on a silicon wafer substrate and encapsulated in a bio-inert PTFE film. This sensor showed effective accuracy and sensitivity to changes caused by cellular respiration. However usage of expensive and time consuming fabrication techniques was a disadvantage in developing this sensor, and brittle nature of the silicon wafer after fabrication course made it difficult to incorporate this sensor into a sealed integrated packaging.

Due to problems associated with the aforementioned sensors, a design has been proposed that is being made from a material with good mechanical properties such as PCB and Nafion membrane as a solid electrolyte to reduce cost and time being consumed for maintenance of rehydrating the sensor.

2.11.   Summary

In this chapter overview of biosensor and different types of oxygen sensors has been presented. Fundamentals of electrochemistry and the Clark type oxygen sensor have been reviewed. Electrochemical measurement techniques such as cyclic voltammetry and chronoamperometry have been explained. Summary of microelectrodes behaviour in the electrochemical reaction is also given. State of art in the field of electrochemically working oxygen sensors for the purpose of cell culturing was presented.

3. Design of Oxygen Sensor

55

56

57

59

62

63

65

67

69

73

75

76
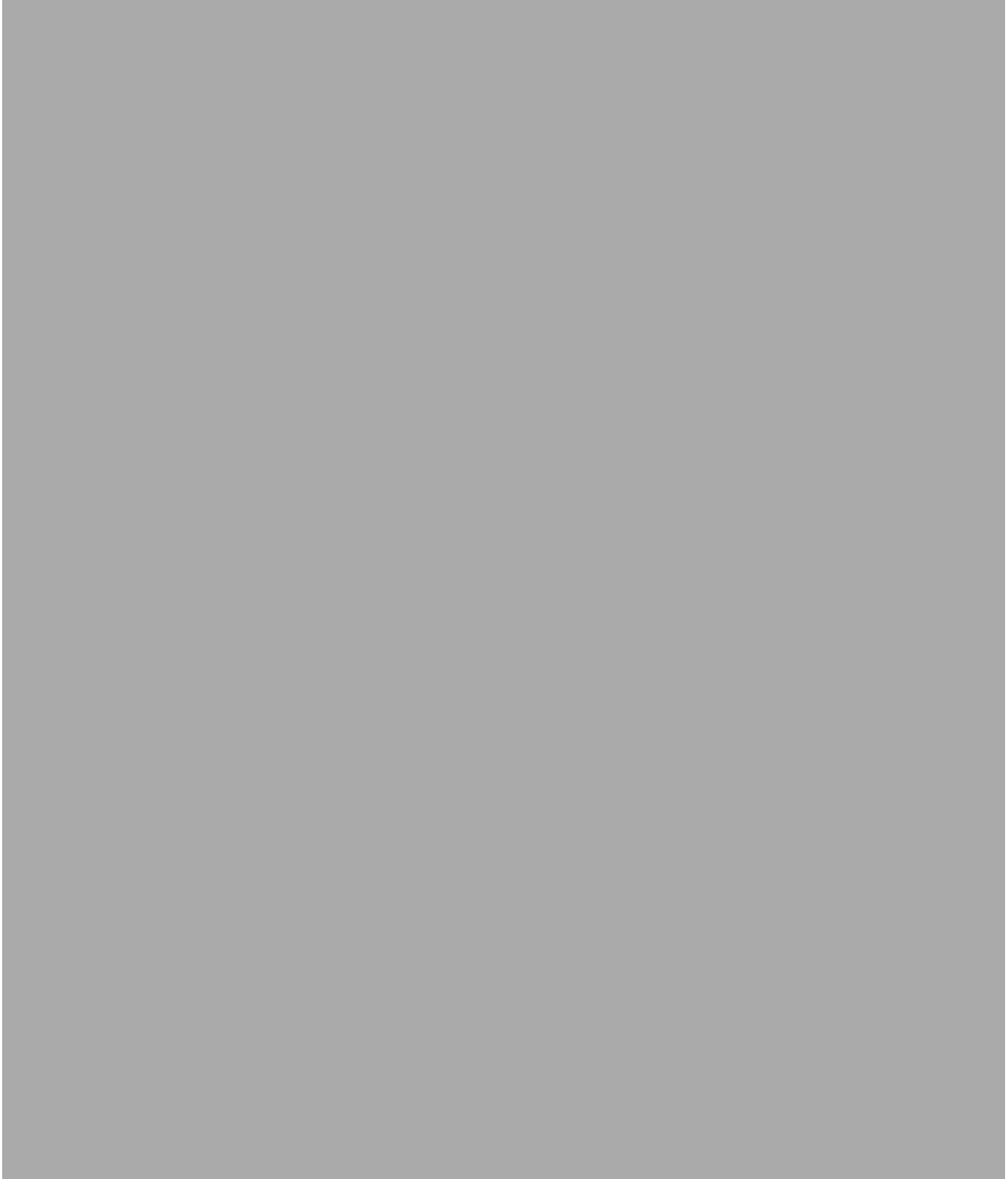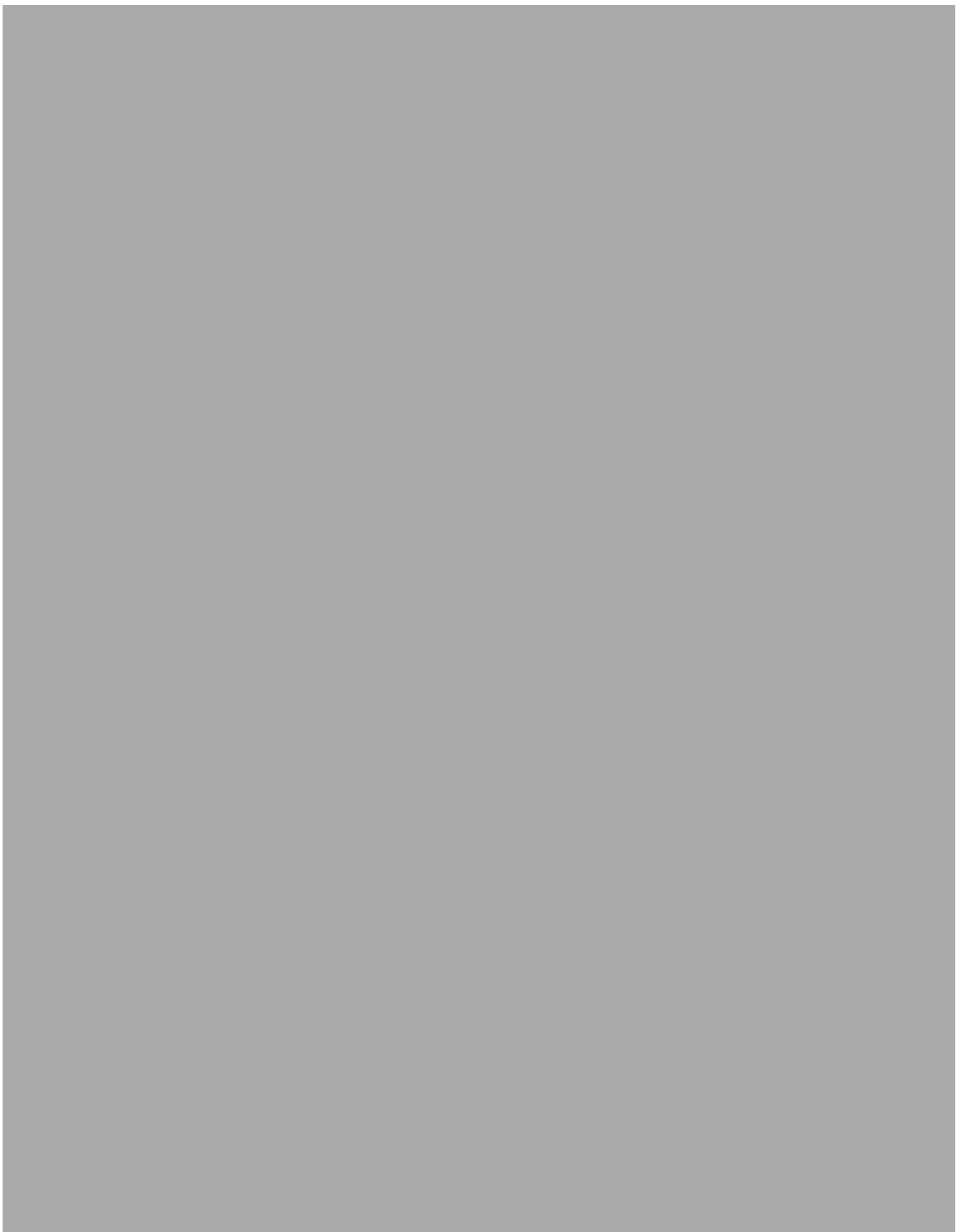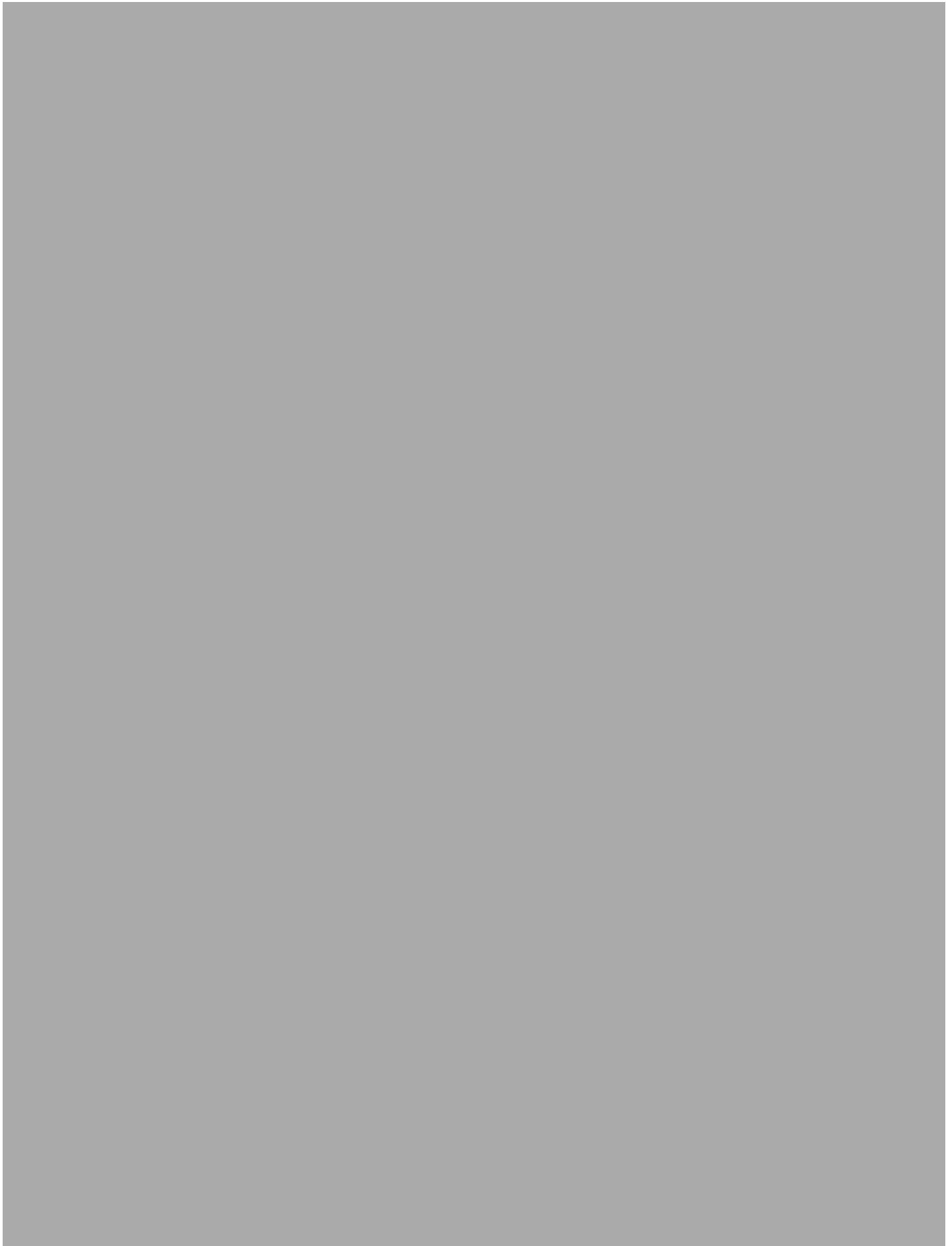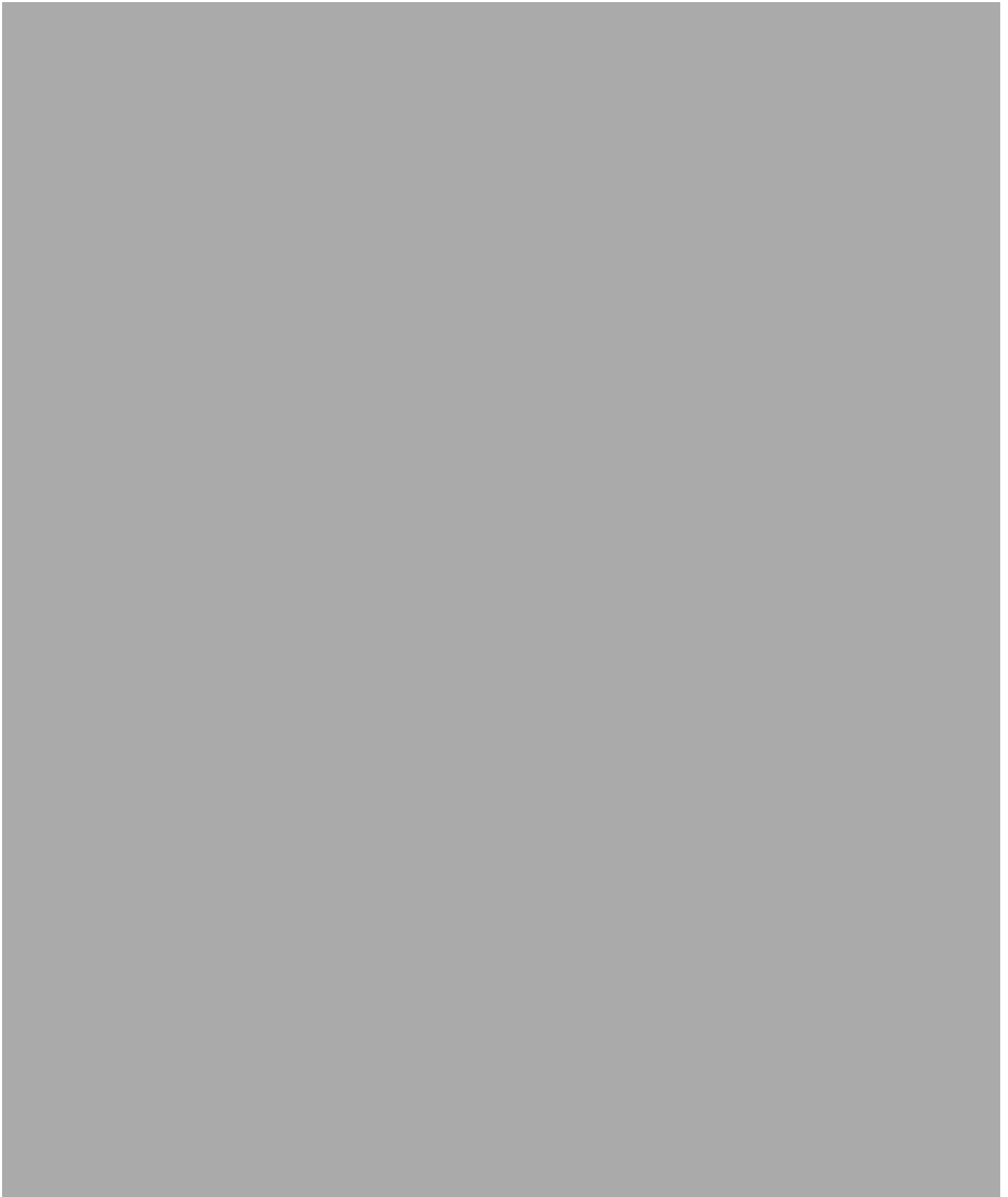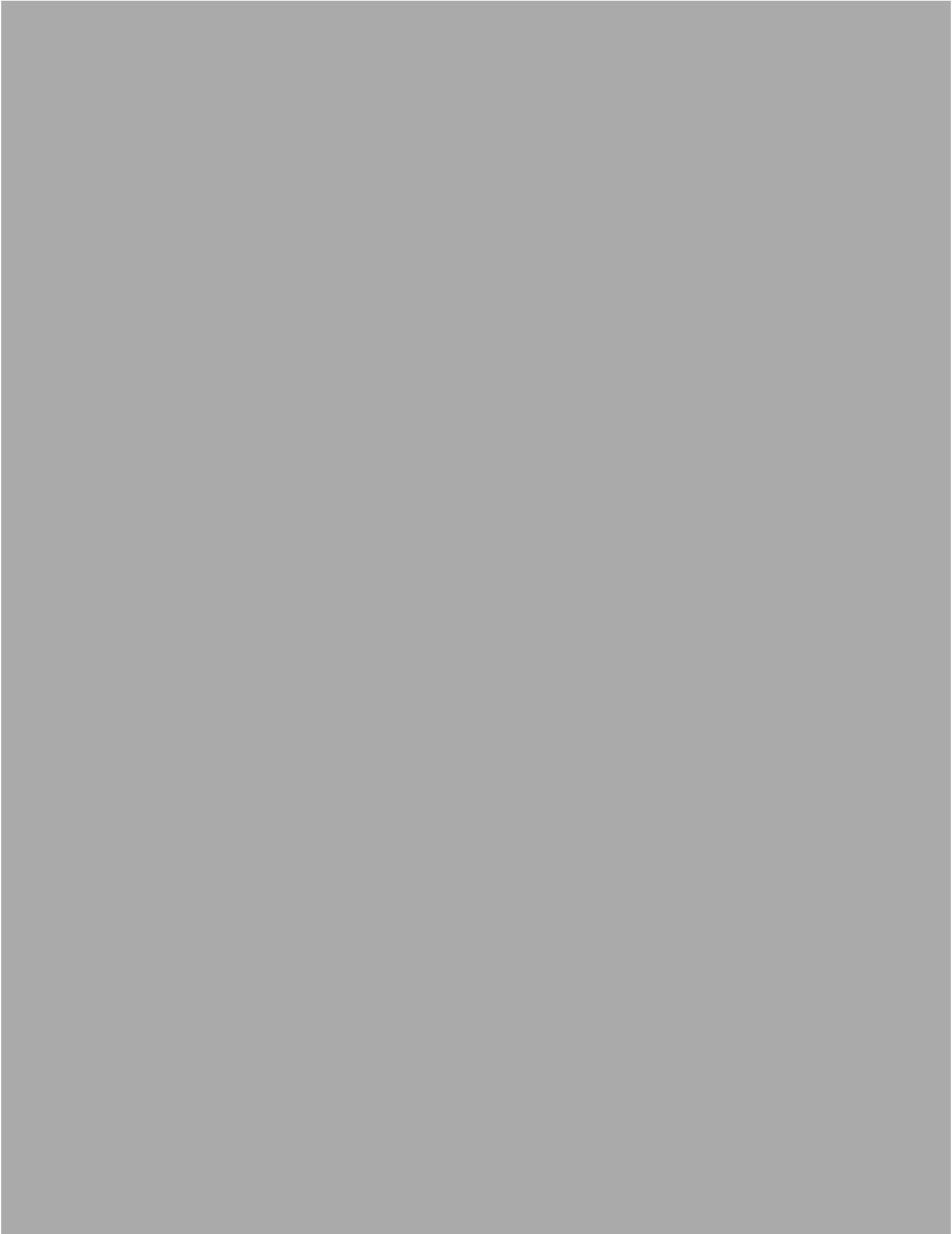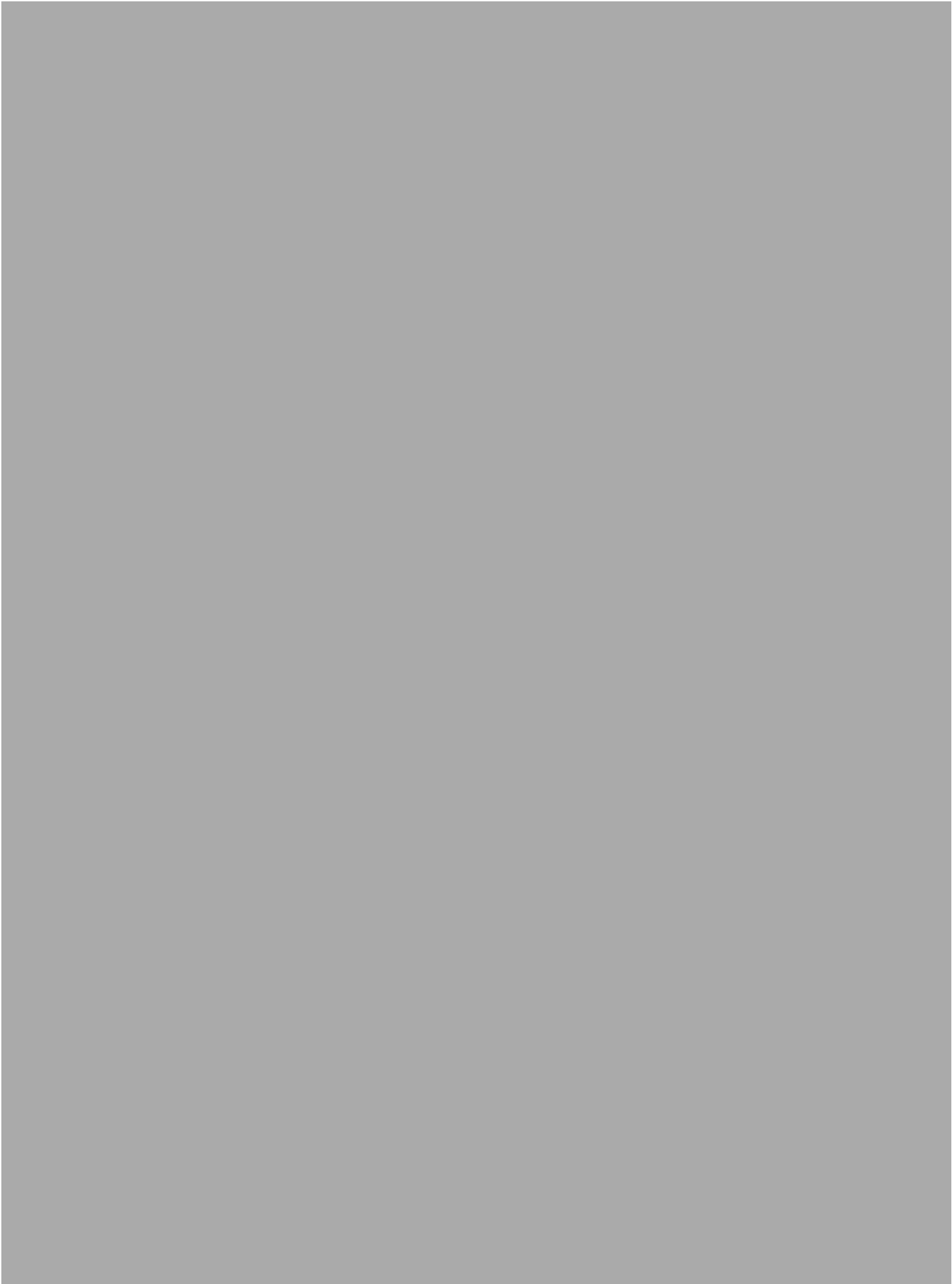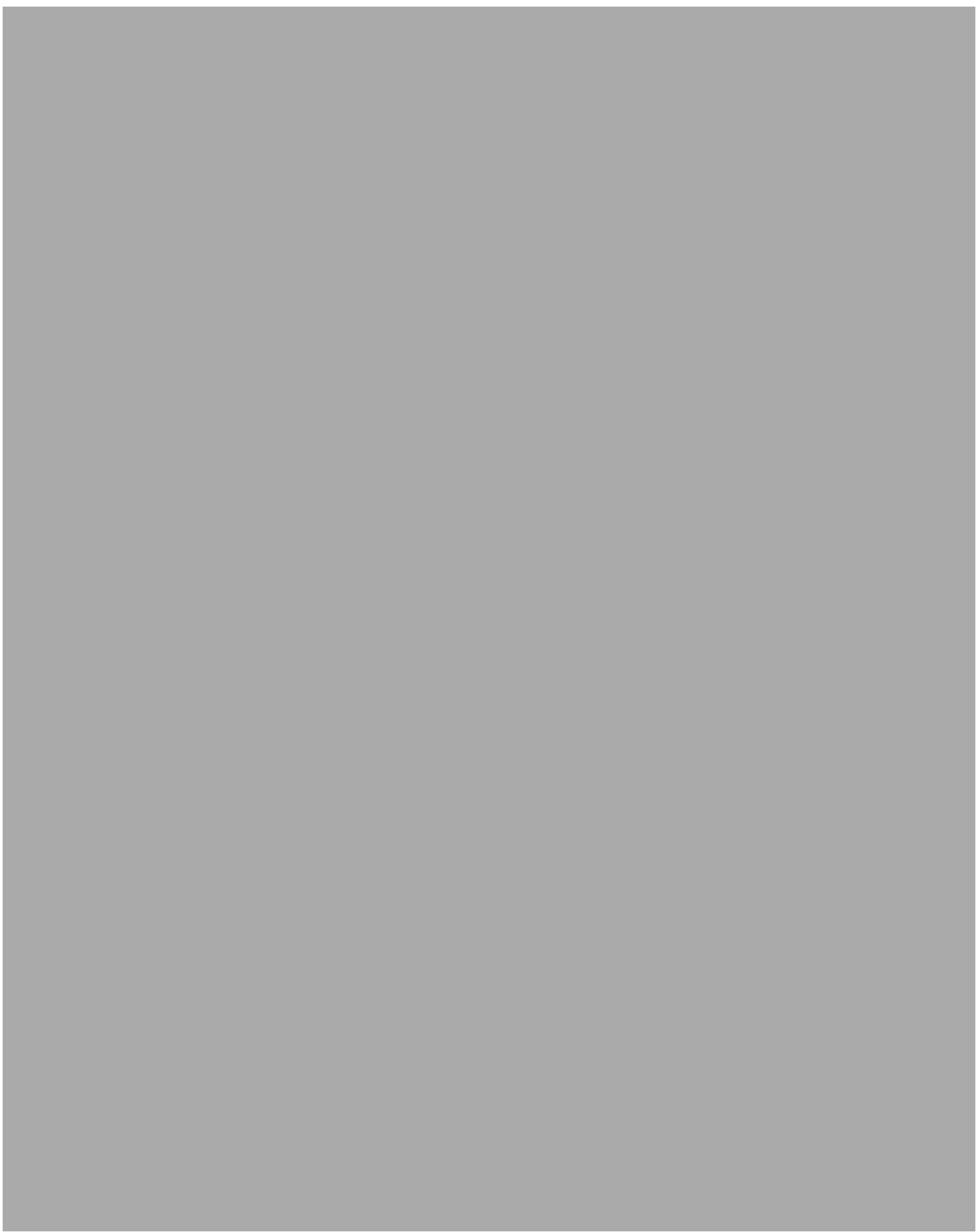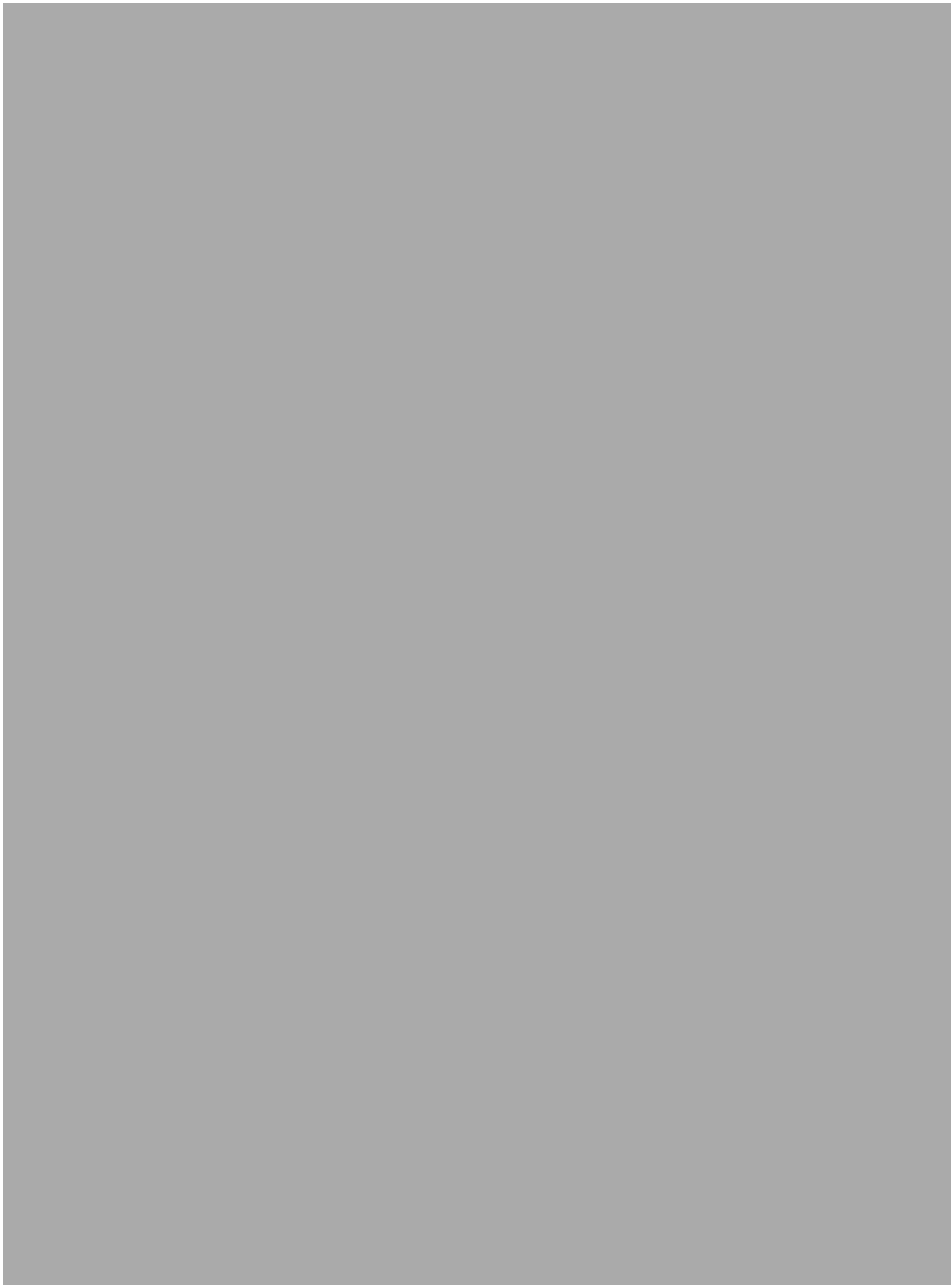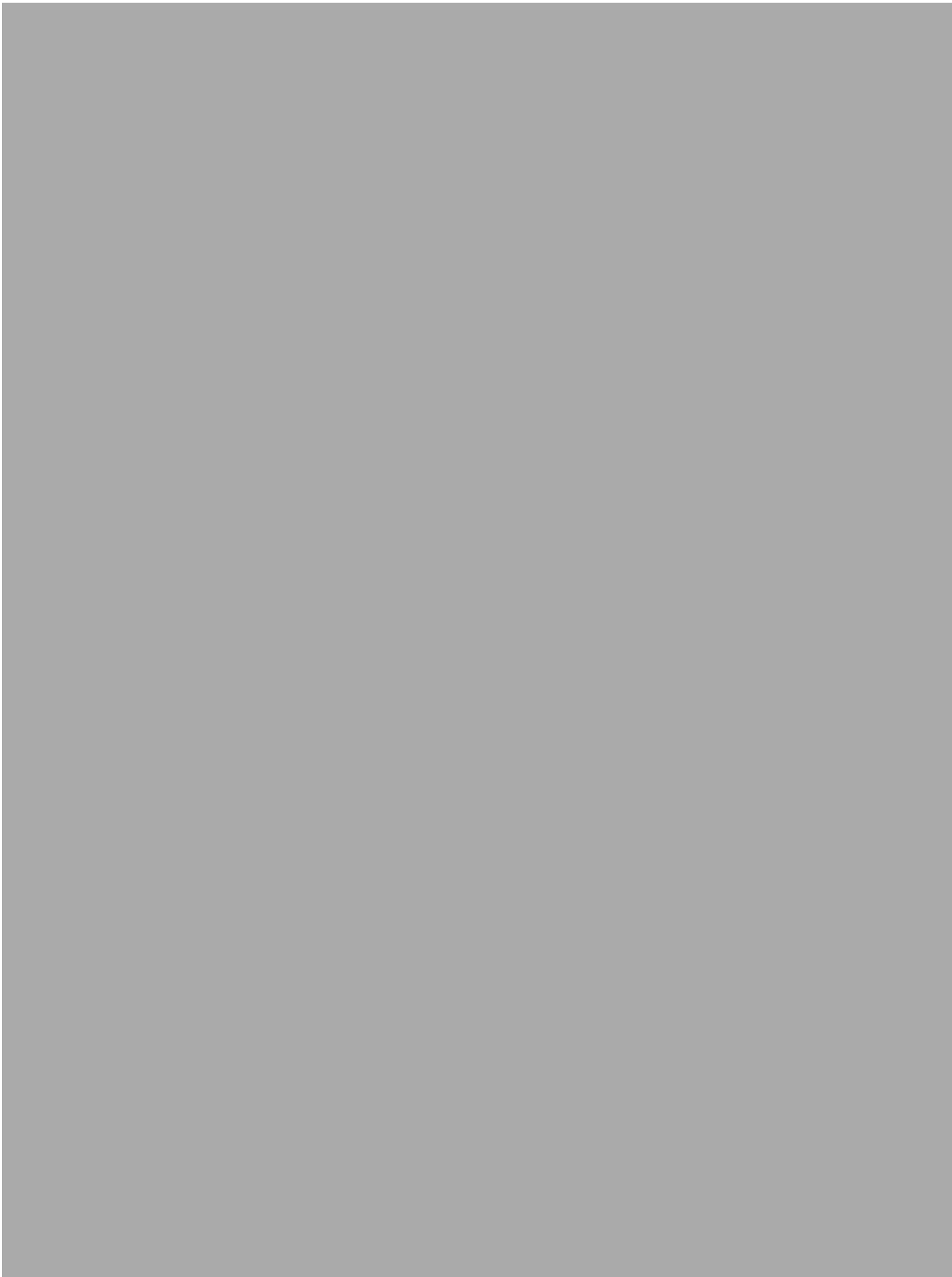
4. Materials and Fabrication

4.1. Introduction

In this chapter material preparation and fabrication processes for different parts of the oxygen sensor including the sensor's electrodes, control circuit and cell culturing platform will be described.

An introduction to different materials used in electrode design will be given, as well as materials used for the cell culturing platform and different fabrication processes such as PCB fabrication, Laser micromachining and 3D printing.

4.2. Materials and Fabrication

Material selection and fabrication process is a step in the process of creating any physical object. In this context, the main goal of material selection and fabrication process is to minimize cost while meeting product performance goals. Logical selection of the best fabrication method and material for a given application begins with properties and costs of candidate materials and process.

4.2.1. PCB Oxygen sensor

Printed circuit boards (PCB) is used in every electronic product. Printing circuits with PCBs is cheaper and faster than other wiring procedures such as wire wrap and point-to-point construction, as components are mounted and wired with one single part (with requirement for additional design to lay out the circuit). Also, operator wiring errors are eliminated.

A PCB mechanically and electrically links electronic components such as conductive pads (in this case micro disks and ring electrodes), tracks and other features etched from copper sheets that are laminated onto a non-conductive substrate. PCBs can be single sided (one copper

layer), double sided (two copper layers) or multi-layer (outer and inner layers). Conductive features on different layers are connected with plated-through holes called vias.

4.2.1.1. Materials for the sensor's electrodes

PCBs are mainly produced from FR-4 glass epoxy. It is an insulating substrate, and since low currents are being measured during the experiments, it will be important to insulate the sensor. The choice of the material for the electrodes is very important since they implement the half reaction over extended times. To reduce cost and to maintain the simplicity of the design, all three electrodes are fabricated from the same conductive material to complete the electrochemical reaction.

Electrode reactions take place at the electrodes thus its material should be chosen considering the redox behaviour of the oxygen, its potential window, electrical conductivity, mechanical properties, surface reproducibility, cost, availability and toxicity. Among the range of different material, the most popular are noble metals (platinum, gold, silver), glassy carbon and mercury [54].

Glassy carbon is mainly used in the study of supercapacitors and known as current collectors and they are more desirable than graphite because of their high density and low porosity which produces smooth surfaces after polishing and consequently minimised double layer current effect. However it is very expensive and not suitable for commercial development. It is very brittle, and difficult to prepare into a desirable electrode shape. The resistance of glassy carbon is not minor and it disturbs high power performance [55].

Electrodes have also been made from mercury since it has a smooth and uncontaminated surface free from any adsorbed analyte or impurity. The self-renewing electrode does not need to be cleaned or polished like a solid electrode. However, due to its toxicity and constantly changing surface area, mercury is gradually being substituted by environmental

friendly solid electrode materials. Mercury electrodes are not suitable for monitoring oxidisable compounds because of their anodic limit potential range. Therefore, solid electrodes with extended anodic potential windows have drawn significant attention [54].

Among the extensive choice of noble metals, platinum and gold are mostly used. They have good electron-transfer kinetics, high conductivity (low background currents) and large anodic potential range.

In this work, copper is etched from PCB as the electrodes. In a double layer PCB, a thin layer of copper foil is coated to both sides of an FR4 sheet and circuitry interconnections are etched into copper layers. Copper other than being a good electrical conductor, is easily manufactured and shaped into the desired features and can produce a mirror-like surface finish [54].

One of the disadvantages of copper is its proneness to corrosion such as oxidation at relatively normal temperatures, which reduces its shelf life [54]. To solve this problem, a thin layer of Electroless nickel and immersion gold plating on the copper electrodes is considered. Also problem of high resistivity can be overcome by using gold-coated copper electrodes [55].

Electroless nickel immersion gold (ENIG) is a type of surface plating used for printed circuit boards. It comprises of electroless nickel plating covered with a thin layer of immersion gold, which protects the nickel from oxidation. ENIG creates an even layer on copper pads for good solderability and improved resistance to corrosion and wear while preserving electrical conductivity. Nickel acts as a diffusion barrier for copper while the thin immersion gold layer over nickel protects the Nickel from oxidation [56].

4.2.1.2.   Fabrication of PCB sensors

In this section, the manufacturing process of a double layer circuit board has been explained in order to etch the electrodes of the oxygen sensor. A double layer PCB of 1.55 mm

thickness, and copper thickness of 35 microns with Nickel/Gold (4-7 μm Ni/0.05-0.1 μm Au) surface finish is chosen for this design. FR4 (glass-reinforced epoxy laminate) is the base material for the double layer PCB. FR4 is a composite material consisting of a woven fibreglass cloth and an epoxy resin binder which is pressed together with copper foil and is flame resistant. The base material is cleaned and the photosensitive laminate is applied, next an image from a photo instrument is transferred through exposure and the potential conductive pattern is generated. The following three production steps all take place in one system. In the first step the layout generated by the exposure process is developed by means of a chemical process and the unexposed parts of the laminate are removed. In the next step the unprotected copper is etched away to create the conductive parts that was imaged. Finally the polymerized photo laminate is removed. These three steps are called developing, etching and resist stripping as shown in Figure 4.1. Before next process is carried out, an automated optical inspection takes place.
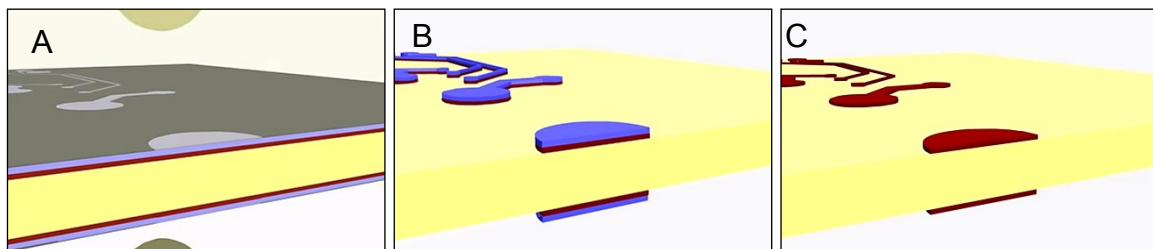
Figure 4.1 A. Covering the base material with photoresist to create circuit structures, covering the conductor pattern using the negative process. B. Developing the exposed material, removing the copper not covered by the photoresist. C. Removing the photo-laminate used as etching mask.

Once these steps have been completed, holes are drilled. The next step after the drilling is the through hole plating process. In this process the holes are cleaned, activated and given a thin copper coating to create a vertical electrical connection between the conductive layers. The outer layers are then processed, initially laminate is applied. In the photopositive method, the areas that are not needed for the PCB layout are exposed; the aim is to expose the areas that will subsequently be plated. In the following step the unexposed laminate is removed, then

the exposed copper areas, the copper coating is plated up and the final copper thickness is attained. A layer of tin is applied to protect the copper layer for the next three processes. These steps are shown in Figure 4.2.
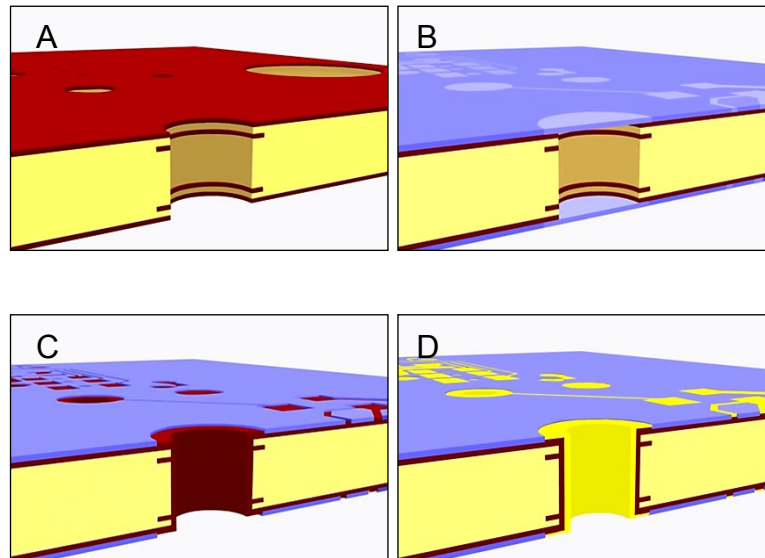
Figure 4.2 A. Drilling of holes, metallisation of the entire circuit board including the inside of the borehole with a thin copper layer. B. Covering with photoresist to create the circuit structures, Applying and exposing the film. C. Developing the exposed material, reinforcing the circuit structures to their final thickness with an additional copper layer. D. Covering with a Tin layer as an etching mask.

The next stage is photoresist stripping, in which the polymerized photoresist is removed, and then the areas that are not covered with tin are removed in an alkaline etching process, finally the protective tin coating is removed. At this point the circuit board is already electronically functional. Now the protective and finishing processes are accomplished. The first step of these finishing processes is to apply a photo sensitive layer of solder resist; this protects the PCB against corrosion and mechanical damage and during soldering. It prevents solder from being applied to the areas covered with solder resist on the PCB. It also improves the electrical properties and dielectric strength. Same as the previous photo processes the desired surfaces are protected against exposure, in the subsequent development process the solderable area, pads and the component holes are uncovered. Then surface finish is applied, which is the electroless nickel immersion gold. Temporary solder resists or protective tapes can be

applied depending on the requirements of the solder processes, one of the last steps is application of the desired annotation via screen printing. The final mechanical processing ensures that the PCB gets its final shape, which is done by milling as shown in Figure 4.3. At the end further electrical, optical and dimensional inspections of the PCB are carried out. The explained procedure is carried out at Wurth Electronics Company, which is a leading manufacturer of PCB and Inductive components.
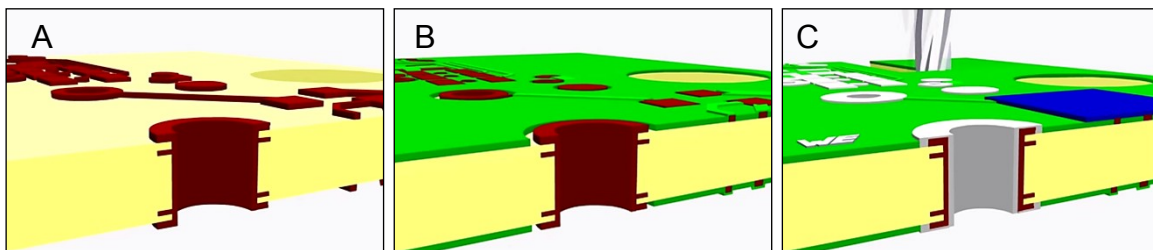
Figure 4.3 A. Removing the photoresist and the copper not covered by the Tin resist, removing the metal resist. B. Applying a photo-sensitive solder-stop layer, Applying and exposing the film, developing the material. C. Applying a solder able surface e.g. chemical nickel-gold, covering the solder mask lacquer, Labelling with screen printing, milling the end profile.

Figure 4.4 shows the oxygen sensors fabricated by the above-mentioned method; they are illustrating the final shape of the sensor from A to E shown on Table 3.3 of chapter three. Images are taken with Alicona microscope.
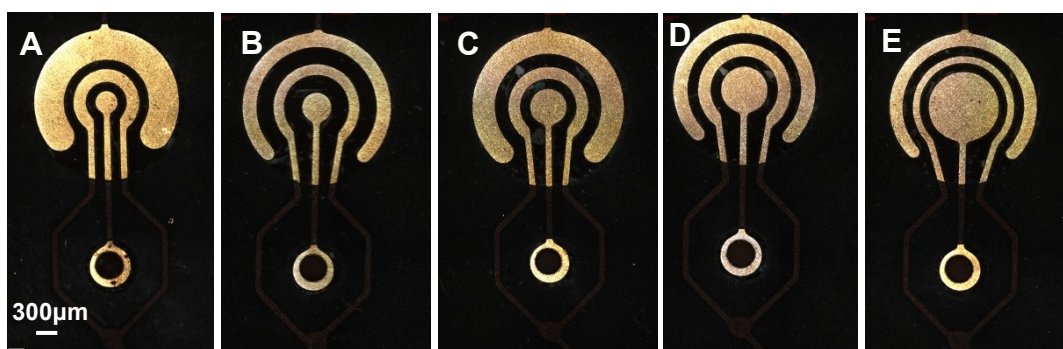
Figure 4.4 Oxygen sensors fabricated by PCB fabrication method and with ENIG coating. Sensors shown from A to E in this figure coincide with dimension shown on Table 3.3 of chapter three.

Würth Elektronik specifies a standard tolerance of +0.10/-0.05 mm for the pad used on the PCB.

The actual deviation from the design of the delivered units was less than 0.01mm, measured with the Alicona microscope.

4.2.1.2.1. Laser micromachining of PCB sensors

It was not possible to fabricate the sensor mentioned in the Table 3.3 from F to J with the PCB fabrication method described for sensor A to E due to their small dimensions being in the range of 20 μm to 100 μm. For this reason Laser micromachining technique was used further to machine the electrodes on the PCB. The repeatability of the laser machine is +/- 0.75 μm, with accuracy per axis of +/- 2μm. Measured deviation from design was about 2μm for the 20 μm pad, which was the highest deviation measured.
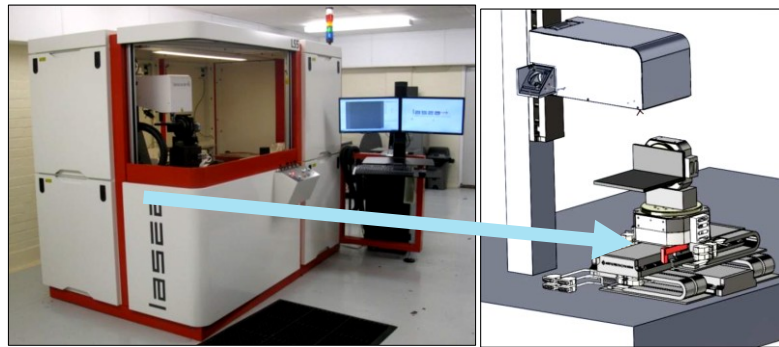
Figure 4.5 Reconfigurable Lasea Multi-Axis Laser Micro Machining platform.

In this method the base copper pad, which is ENIG coated and created by the PCB manufacturing method, is further machined with Lasea Multi-Axis Laser Micro Machining device (Figure 4.5) to achieve dimension down to 20 μm. This process carried out using facilities located at Laser Micro Processing (LMP) Group of University of Birmingham, School of Mechanical Engineering.
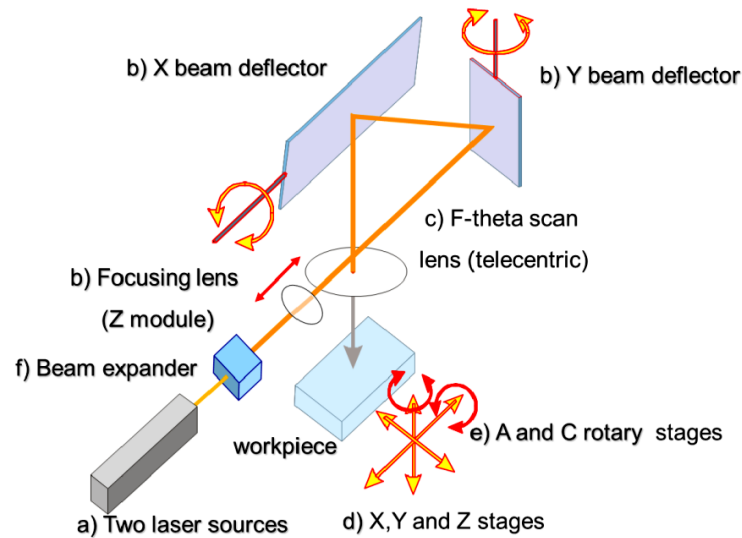
Figure 4.6 Main component technologies of the laser micro machining platform.

The laser micro processing platform is a hybrid system that integrates a novel beam delivery system and a multi axis setup for recognizing the relative beam-workpiece movements in performing structuring, polishing and texturing of free form surfaces. It has a reconfigurable laser micro machining platform that integrates 3 optical axes and 5 mechanical axes as shown in Figure 4.6. In specific, the platform combines innovatively the capabilities:

a) Two laser sources; a Satsuma femtosecond laser (5W) and a MOPA-based Yb fibre laser (50W), to realise different and at the same time complementary laser spot characteristics.

b) Optical axes, X & Y beam deflectors and a Z module, for beam spatial modulation.

c) Focusing F-theta telecentric lenses for machining different field sizes with their corresponding beam spot diameters.

d) XYZ mechanical axes (stages) to machine surfaces with dimensions bigger than the scan field.

e) Rotary axes (stages) to change the incident direction of the beam for machining free form surfaces and axisymmetric workpieces.

f) Integrated high resolution camera and confocal microscope for automated process setting and a beam expander to condition the beam diameter to the requirements of any specific processing task [57].

Table 4.1 Specifications of the laser sources used for the surface machining of sensors E to J of Table 3.3.

Ultrafast Ytterbium-based laser:	Satsuma
Nominal wavelength	1030 nm
Beam quality	$M^2 < 1.3$
Pulse duration	350 fs
Average power	5 W
Pulse energy	$< 10\ \mu J$
Repetition rate	0 - 2 MHz

Table 4.1 illustrates the specifications used to machine the surface of sensor F to J of table 3.3. Graphical structure of the features to be machined was designed by Solidworks software and transformed to a DXF file format and imported to the control software of the device for multi axis machining process. Figure 4.7 shows Sensors F to J of Table 3.3 after laser machining.
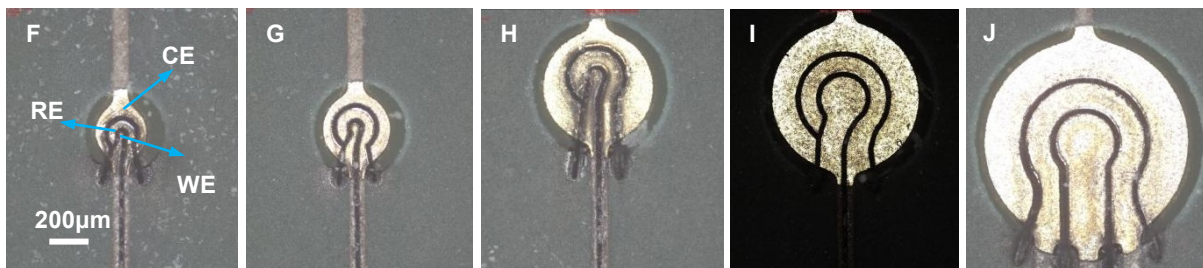
Figure 4.7 Oxygen sensors fabricated by PCB fabrication method with further laser micromachining. Sensors shown from F to J in this figure coincide with dimension shown on Table 3.3 of chapter three.

4.2.1.2.2.   Alicona Microscope

Images shown in Figure 4.4 and Figure 4.7 are captured by Alicona G4 InfiniteFocus (IF) system microscope (Figure 4.8) for conducting high resolution 3D surface measurements. This procedure performed using facilities located at LMP Group of University of Birmingham, School of Mechanical Engineering.

Figure 4.8 Alicona G4 InfiniteFocus (IF) system.

This system uses Focusvariation sensor that comprises a special optic, a white LED which emits modulated light and a vertical axis with a linear encoder with high resolution. This encoder provides accurately z-positions with 10 nm resolution. The limited depth of the optic focus is used to measure the specimen topography. Throughout the measurement the distance between objective and specimen is altered, so the depth of focus of the objective is moved on the specimen surface topography. The variation of focus in every point is measured and produces 3D dataset color information. The principle of operation for Alicona G4 IF system is shown in Figure 4.9 [57].

The specimen is illuminated by modulated light. This light is transferred through the optic and focused through a beam splitter onto the specimen. Coaxial illumination is produced. The light is reflected by the specimen and projected on to the digital sensor in the precision optic. As the distance between the specimen and objective is varied the change of sharpness is measured. The correct interaction between modulated light and continuous vertical

movement of the sensor are essential for the quality of the measurement. For every position on the object the sharp regions are measured. The variation of the sharpness values is used for the measurement of the 3D-position [57].

1. Sensor
2. Optic
3. White Light
4. Semi transparent mirror
5. Objective
6. Specimen
7. Vertical scanning
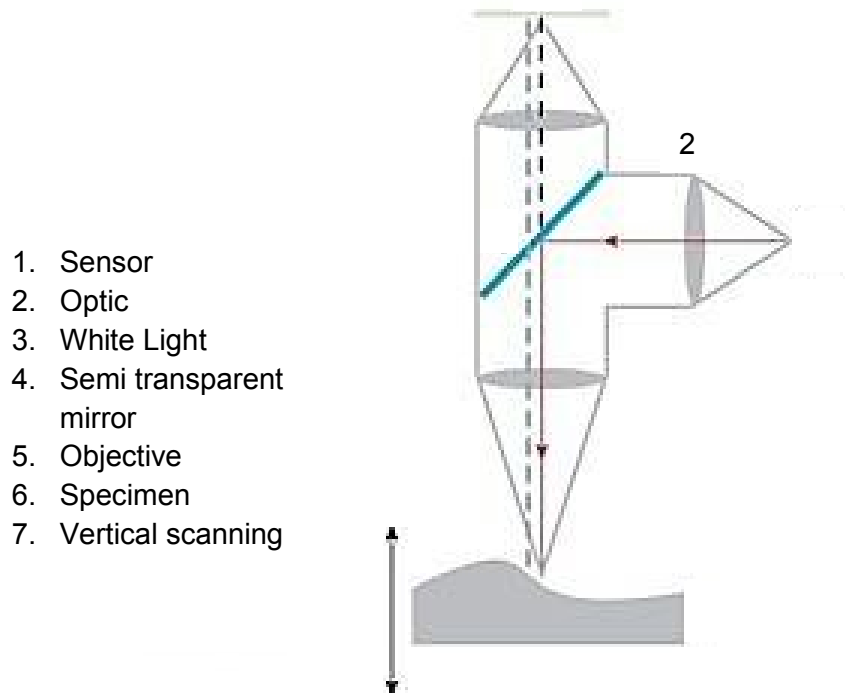
Figure 4.9 Principal of operation for Alicona G4 InfiniteFocus system [57].

3D image of sensor J from Figure 4.7 that was taken with Alicona G4 IF system is demonstrated in Figure 4.10.
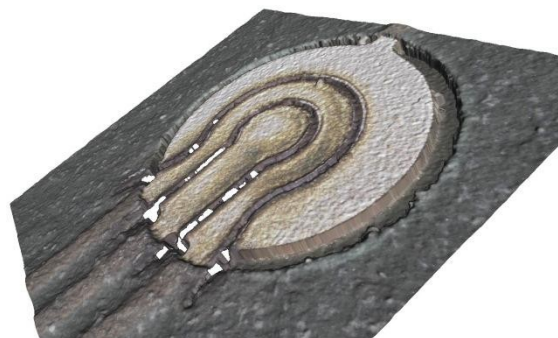
Figure 4.10 3D image of sensor J shown at Figure 4.7 produced using Alicona InfiniteFocus system.

4.2.2. Control circuit fabrication

The layout of the PCB for control circuit board was designed using Diptrace as a double layer circuit board and was shown in Figure 3.10 of section 3.3.3. Then it was printed as a mirrored

printout on to an opaque film to produce a contact print (black tracks) to use with photo positive laminate (pre – coated). This was exposed using a UV source for about 160 to 180 seconds, the resulting artwork on the laminate was developed using an alkali developer. Then washed and dried in an oven at 60 to 70ºC then etched using Ferric Chloride. The exact time for etching is dependent on both concentration of the etchant and the temperature. The resulting board as shown in Figure 4.11 had the tracks coated in the etching resistant paint, this is then removed using a suitable solvent (Acetone). The board was then drilled using Tungsten Carbide drills. The dust removed carefully (Vacuum) then the board sprayed with flux to prevent oxidation of the bare copper prior to assembly of the electronic components on to the board which was then soldered and tested and proven to work.
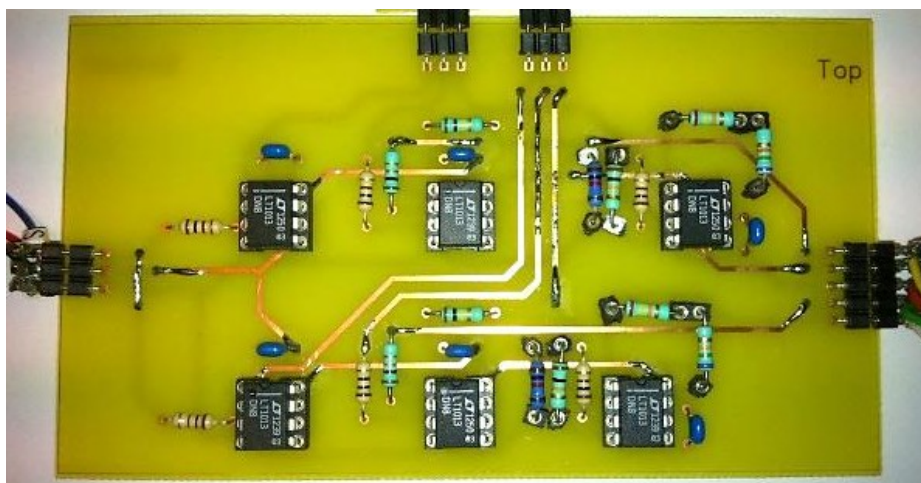
Figure 4.11 Fabricated control circuit board.

4.2.3. Cell culturing platform fabrication

A cell culturing platform is going to be used in the cellular respiration measurement experiments, so it needs to have a solid structure, non-brittle and easy to disassemble and drill holes and attach fluidic channels to them while incorporating interior channels inside the platform. The Eden250™ 3D Printing System provides the perfect way to manufacture this part in the desired shape [7]. One of the materials being used in this printer is Objet Bio-Compatible material MED610™, which is supplied in sealed, ready-to-load cartridges [7].

More information is given below about the Eden250™ 3D Printing System, MED610 and reviews about cell culturing methods and biocompatible surface enhancements.

4.2.3.1. Material for cell culturing platform

At this point a biomaterial with appropriate biochemical and mechanical characteristics is required to display high bio conformity for the purpose of cell culturing. Among the existing three dimensionally printable materials the choice is limited due to their low chemical or biological compatibility. MED610 is a biocompatible material available for 3D printing and due to its mechanical robustness can be exploited as a material for the cell culturing platform. Objet Bio-Compatible MED610™ is a rigid material featuring dimensional stability and colourless transparency. This material is desirable for applications requiring prolonged skin contact of over 30 days and short term mucosal-membrane contact of up to 24 hours. But there is no report available regarding its biocompatible properties for the cell culturing applications in the literature. However it has 5 medical approvals including Cytotoxicity, Genotoxicity, Delayed Type Hypersensitivity, Irritation and USP Plastic Class VI and can be used on all Objet Eden printers. It is also been produced under the ISO 13485:2003 certification that ensures, every batch of the material goes under bio-compatibility conformity testing, before it is packaged. These standards endorse bio-compatibility of MED610 for the purpose of cell culturing [58].

4.2.3.2. Fabrication (cell culturing platform)

Solid object 3D printing can creates prototypes having several faces of features and covering large area in one round of printing up to 480 cm^2 and a height up to 26 cm.

However limited resolution and minimal surface roughness, which it leaves on the surface after printing, are of the major drawbacks of this printer. Even though the resolution of the printer has been stated to be 42μm, 84μm and 16μ in X, Y and Z directions respectively, it is

not possible to fabricate channels having diameter less than 250 μm using this printer [58]. However considering the dimensions of the cell culturing platform designed in chapter 3, it is sufficient to use this method to manufacture the part without needing dimensions smaller than 250 μm.

The device prints the structure of platform in layer by layer techniques by selectively applying droplets of light curable material (MED610) in three dimensions without any requirements for mask, alignment, timed exposure or development. The CAD file of the platform which was designed by Solidworks is converted into a STL file format and transferred to the 3D printer.

4.2.3.2.1. Surface treatment of cell culturing chamber

The scope of this device is to measure effectively the respiration rate of the cultured cells. Cells are not cultured at this stage of project; however methods of appropriate cell culturing and surface modification for making the surface of the chamber more compatible with cells are investigated and suggested.

Surface modifications are done to enhance their hydrophilic properties, cell adhesion and growth. Existing biomaterials for cell culturing are mainly plastics but some types of plastics have a hydrophobic surface, which makes it difficult for cells to attach and grow. Extensive research has been done in this area on different materials.

Parylene-C is known for having the maximum level of biocompatibility for polymers labelled by the United States Pharmacopeia as a Class IV polymer, making it acceptable for long-term implantation. It has already been used in a set of biomedical devices such as cardiovascular implants, wireless neural interfaces, and catheters. This material retains many desirable assets such as chemical inertness and resistance to biological degradation in medical application. A thin film is created when coating the considered surface, using chemical vapour deposition method [59-61]. It is desirable to use this material in medical devices, due to its advantages in

its deposition process, which offers excellent adhesion, a solvent-free environment, and high accuracy and control over film thickness, highly resistant to hydrolytic degradation and stable in a biological environment [60-63].

This sort of coating is ideal for the cell culturing platform however it has not been possible to actually coat any of them with this material because of not having access to the system. The following section describes the work has been done to prove the validity of this type of coating and that it is a good way of improving the cell culturing platform.

Tracy Y. Chang and her group have demonstrated an experiment, which compares the surface properties and cell and protein compatibility of eight biomaterials used in bio-mems application. These materials are glass, polystyrene, Parylene-C, plasma-treated Parylene-C, fibronectin-coated Parylene-C, PDMS, plasma-treated PDMS, fibronectin-coated PDMS [60].

In their experiment, the surface hydrophobicity and roughness of Parylene-C has been measured and its results been compared to those of tissue culture-treated polystyrene, poly (dimethylsiloxane) (PDMS), and glass. Parylene-C and PDMS have also been treated with air plasma and their surfaces been coated with fibronectin to show that it is possible to modify the surface properties of Parylene-C with biochemical treatments. Table 4.2 shows the contact angle measurements on static drops of water on substrates utilizing a contact angle measurement system (Phoenix 300 plus, SEO) to provide information about hydrophobicity of the surfaces. Whatever the contact angle is higher the surface is more hydrophobic.

Table 4.2 Contact angle measurements. a) Measurements made immediately after PDMS was treated in oxygen plasma. b) Measurements made after 40 min following treatment in oxygen plasma. c) No significant change observed in measurements made immediately after and following 40 min after plasma treatment [60].

substrates	contact angle (deg)		
	untreated	plasma-treated	fibronectin-coated
glass	36.3 ± 2.6		
polystyrene	79.1 ± 5.9		
PDMS	105.9 ± 4.5	9.9 ± 1.1[a]	99.0 ± 6.7
		73.7 ± 3[b]	
parylene-C	97.2 ± 4.2	4.4 ± 2.4[c]	105.0 ± 10.4

Both of the Parylene-C and PDMS became hydrophilic after plasma treatment but only Parylene-C substrate kept its hydrophilic properties over time and also it exhibited higher degree of nano scale surface roughness (>20 nm) than the other substrates.

Table 4.3 Surface Roughness Measurements [60].

substrate	roughness (nm)
glass	1.6 ± 0.6
polystyrene	1.2 ± 0.2
parylene-C	19.3 ± 6.3
plasma-treated parylene-C	19.3 ± 5.4
fibronectin-coated parylene-C	29.0 ± 11.5
PDMS	2.2 ± 0.6
plasma-treated PDMS	0.4 ± 0.1
fibronectin-coated PDMS	3.2 ± 0.6

Surface roughness values were evaluated with atomic force microscopy (AFM) (Q-Scope 250, Quesant Instrument Corporation) using noncontact mode with a cantilever tip (NCS 16, Quesant). Areas of 50 μm × 50 μm were randomly chosen on the substrates to scan. It can be observed from the Table 4.3 that Parylene-C, plasma treated parylene-C and fibronectin coated parylene-C has highest surface roughness, which means they can produce more surface for cells to attach and cells elongate better in the direction of roughness. This roughness is because of the irregularities in the deposition process of parylene-C with usage of vapour deposition process, which were further increased with fibronectin molecules adsorbed onto the surface.

The level of protein adsorption of bovine serum albumin (BSA) and immunoglobulin G (IgG) proteins on these eight surfaces were evaluated. In general parylene-C had high BSA and IgG

adsorption, whereas surface treatments on parylene-C reduced level of adsorption of these proteins.

Also the degree of cell adhesion and distribution of two mammalian cell types, NIH-3T3 fibroblasts and AML-12 hepatocytes has been investigated on these substrates, and it was detected that adhesion of both cell types to surface-treated parylene-C were comparable to standard tissue culture polystyrene. NIH-3T3 cells didn't adhere to the plain parylene-C and PDMS but surface treatment increased the attachment of these cells to these surfaces. The same behaviour occurred at the adhesion of AML-12 to the same surfaces.

Shape factor measurements were carried out and indicates whatever it is closer to 1(dimensionless), the cells are rounder and it means that they have not elongated well and less adhesive, but whatever its closer to zero it means they are taller and thinner and elongated on the surface and in the direction of the roughness well. The NIH-3T3 spread well on fibronectin-coated parylene-C and PDMS in contrast to the other substrates. Shape factor was not a satisfactory measurement for AML-12 cells proliferation on the surfaces because of their non-axial distribution.

Both cell types did not attach to plain PDMS and parylene-C, and they remained in rounder shapes and simply rinsed away and were considerably less adhesive than tissue culture polystyrene and glass. There wasn't a significant change between the adhesiveness of both types of cells to both plasma treated and fibronectin coated surface. Surface treated parylene-C stayed hydrophilic and more favourable for cell adhesion, even though the surface of the plain parylene-C was quite rough (>20 nm) and hydrophobic, so it was more suitable than both surface treated and plain PDMS, which their induced hydrophilicity decreased and cells did not attach onto them.

Parylene-C coating is biocompatible, pinhole-free, conformable, and are great barriers against diffusion of humidity and gases as well as being chemically inactive and unaffected by acids and bases, and creating excellent device protection against attacks from corrosion, bacteria and fungi. It is possible to improve surface adhesiveness after Parylene-C coating by surface modification methods of plasma treatment and fibronectin coating.

4.2.3.2.2. Cell culturing method

As mentioned in previous section, the methods of cell culturing have not been carried out in this research. After consultation with researchers at School of Biosciences at University of Birmingham, several adherent cell populations such as fibroblast, Caco-2 cells are proposed for culturing. However, the presence of surface treatments is necessary on the chamber. Depending on the cell type used, these surface treatment materials could be fibronectin, collagen or matrigel.the following information describes the key features of cell culturing that would need to be considered when this process takes place

There are different Sterilization methods depending on the material of the cell culturing platform. In this case, the material would not stand the heating and pressure in an autoclave, though a brief time (a few hours) under UV light lamp which can also be combined with some immersion in ethanol afterwards would be sufficient. It's recommended to put the chamber in a hood and let the UV lamp on for the typical time to sterilize the place, then immerse it in absolute ethanol for 10 minutes and let it dry in a sterile Petri dish.

In the typical cell culturing procedures when cells are maintained in incubators, media (cell culturing fluid) has to provide with signalling molecules (calf serum), minerals and elements (salts), carbon source (sugars) and protection from contamination (antibiotics). These are necessary for growing the cells to a high number and keeping them for long time. However,

for brief experiments (after growth) e.g. a few hours (3-6) media can be substituted with media such as HBSS with fewer substances (therefore less probability for interferences).
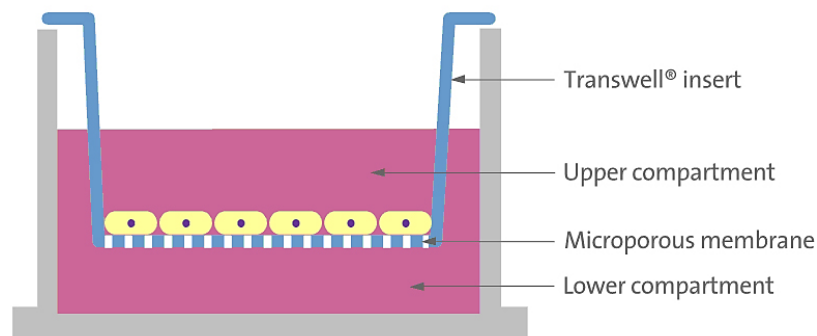
Figure 4.12 Schematic of a Transwell.

In an alternative method cells also can be cultured in transwells, which it can be later transferred to the cell culturing chamber. Transwell is a membrane containing chamber that goes in a well as can be seen in Figure 4.12. These are accessible to any cell culturing laboratory and it's possible to culture adherent cells on them (with appropriate dimension) and then transfer to chamber. However with this method modification to the shape of the cell culturing chamber will be necessary considering the inlet and outlet pipes position. Typical dimension of Transwells will match the ones of cell culturing wells and is shown in Table 4.4 along with information about their average cell yield.

Table 4.4 Typical dimension of cell culturing wells and their average cell yield volume.

Corning Multiple Well Plates	Well Diameter (Bottom - mm)	Single Well Only			
		Approx. Growth Area (cm^2)	Average Cell Yield	Total Well Volume (mL)	Working Volume (mL)
6 well	34.8	9.5	9.5×10^5	16.8	1.9 – 2.9
12 well	22.1	3.8	3.8×10^5	6.9	0.76 – 1.14
24 well	15.6	1.9	1.9×10^5	3.4	0.38 – 0.57
48 well	11.0	0.95	9.5×10^4	1.6	0.19 – 0.285

4.2.4. Integration of oxygen sensor and cell culturing platform

At this stage the PCB oxygen sensor, cell culturing platform (and the control circuit) that are fabricated (Figure 4.13) can be assembled together and be prepared for experimentation and testing of the sensors. Prior to assembly, Nafion membrane is applied to the PCB sensor. A thin laminated PTFE oxygen permeable membrane is applied on top of the Nafion prior to the experiment, to limit diffusion of other species.
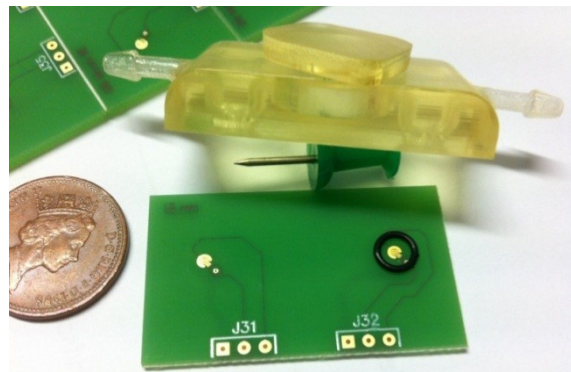
Figure 4.13 PCB oxygen sensor and cell culturing platform after fabrication.

After placing the O' rings to seal the cell culturing platform to the PCB, two platforms are fastened and tightened to each other with four screws as shown in Figure 4.14. O' rings seal the sensors from the outside environment and from each other.
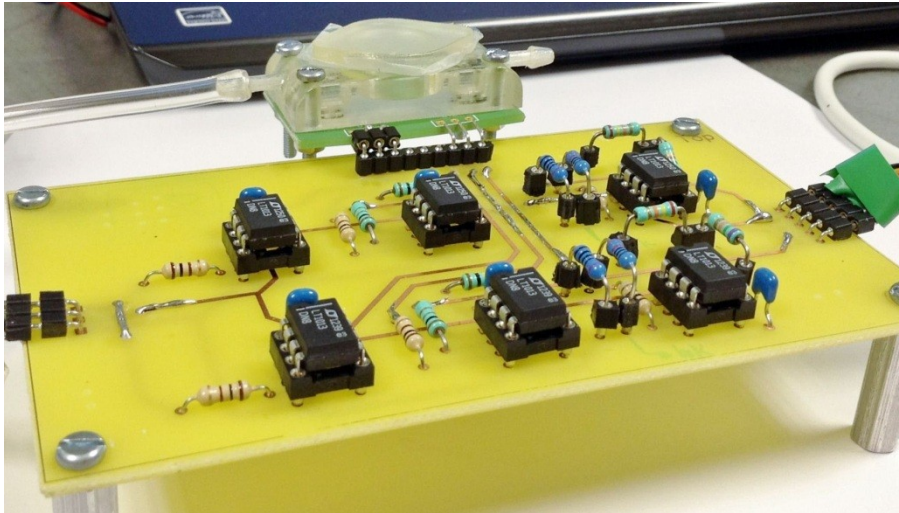
Figure 4.14 Integrated PCB oxygen sensor, cell culturing platform and control circuit.

4.2.4.1.   Nafion membrane application

Nafion 117 membrane was used as a solid electrolyte with 183 μm thickness and 360 (g/m2) basis weights. First, a small area of the membrane (5mm x 5mm for each oxygen sensor) was cleaned by immersing in 60ºC deionised water for one hour, which is a standard operation to ensure a good adhesion between the electrodes and Nafion membrane, then dried with nitrogen gas and left in room temperature in a container for 24 hours. The membrane was then ready for hot pressing. Membrane was hot pressed to the top of the electrodes on the printed circuit board in the oven for 2 hours at 120ºC, which were found to be the optimum duration and temperature for higher sensitivity and faster response time in the sensor. The PCB sensor was cleaned with deionised water and ethanol before hot pressing. Nafion membrane after being hot pressed onto the PCB is shown in Figure 4.15.
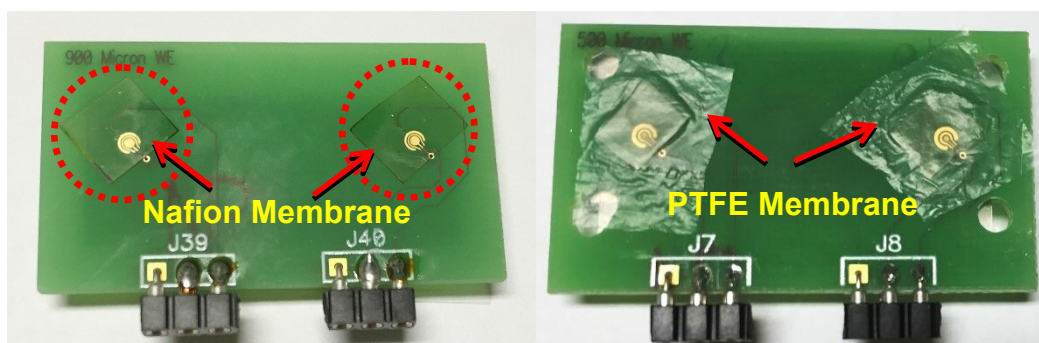
Figure 4.15 Nafion and PTFE membranes after being hot pressed onto the PCB

4.3.Summary

In this chapter fabrication of the PCB oxygen sensor, cell culturing platform has been described. Material choices were explained and their important properties are introduced, further their appropriate manufacturing methods are shown. Oxygen sensors were fabricated using PCB fabrication method and laser Micromachining process were applied to reach smaller dimensions using Lasea laser machining station. Control circuit were fabricated using PCB manufacturing methods and electronic parts were soldered. Material choice of MED610 and fabrication method utilizing Eden 250 3D printer of the cell culturing platform also explained and further methods of surface enhancement and cell culturing were suggested. In final stage device integration was explained and images of the final assembled device illustrated.

5. Tests and Results

5.1. Introduction

In this chapter, the characterisation of the fabricated oxygen sensor is described. It was tested by liquid and gas medium and the experimental setups are demonstrated. Cyclic voltammetry and voltage step measurements are evaluated. The sensitivity, linearity and reproducibility of the sensor are examined and investigated. In this experiment sensor A to F of Table 3.3 of section 3.2.2 are tested, sensors G to J due to problems with Laser machining process were not machined as desired, the depth of laser beam machining were not sufficient to separate the three electrodes from each other and prevented the electrodes to function as a three-electrode sensor, however this problem can be overcome by changing the parameters of laser machining in future. Out of five sensors that were laser machined only sensor F with WE diameter of 20 μm was found to be functional.

As described in section 3.3 the control circuit is measuring the resultant current as a voltage output and to transfer this to current the shunt resistors and the gain of the Op-Amp should be considered. I_Sense gives sensitivity of 1 V/μA or 1 mV/nA. If this sensitivity needed to be changed it is possible to adjust either the local gain of the Op-Amps or the shunt sensing resistors.

5.2. Technical problems associated with the PCB oxygen sensor with solid electrolyte membrane

Nafion membrane is a flexible polymeric membrane, and the formation of a well-defined attachment between the electrode structure on the PCB and the membrane has found to be difficult. In the process of hot pressing there was a need for an intermediate layer to prevent

Nafion membrane getting attached and stuck to the pressing surfaces. For this reason a plastic film that is being peeled off from a double sided Cleanroom adhesive tape is used as a non-sticky surface between the Nafion membrane on the PCB and the hot pressing surfaces.

Figure 5.1 PCB sensors prepared for hot pressing.

The PCB and Nafion membrane are hot pressed between two aluminium plates and clamped by metallic paper clips as illustrated in Figure 5.1. This found to be sufficient since too much pressure would damage the PCB chips at high temperatures. Even though that it has been tried to process the hot pressing as identical condition as possible, there were problems associated with the attachment of the Nafion membranes. Sometimes they did not stick and fell off and sometimes they stick very well. Or even when they stick very well, while taking measurements, two identical set of sensors on the same PCB chip showed different response at the same testing conditions.

The output current lowered when the sensor was exposed extensively in the gas stream due to an increase in the resistance of the membrane (and dehydrated state of membrane) and decreased the reaction rate (current density). This problem was the reason in which higher voltage were applied to WE of the sensors.

The liquid state experiments were conducted while the syringe pump was pumping the water with stabilized dissolved oxygen concentration through the sensor and the commercial

oxygen meter probe was measuring the dissolved oxygen concentration of the fluid that was being pumped. Even though only one parameter was changing (such as applied voltage to WE or Oxygen concentration) and the other parameters kept fixed, there was a sinusoidal wave noise, affecting the measurements. This problem reduced significantly by removing the oxygen probe from the beaker (containing the water sample) after the dissolved oxygen was stabilized and placing the measurement instrumentation inside a tin box (Figure 5.2). However wasn't removed completely.

Figure 5.2 Measurement instrumentation inside a tin box.

After many tests were taken cell culturing platform became brittle and showed signs of leakage and its sealing became weaker. A new cell culturing chip was designed and produced with stronger sealing and improved features and deeper chamber to allow easier cell culturing process as shown in Figure 5.3.

Figure 5.3 New cell culturing chip with improved features.

5.3. Gas state measurement

In this experiment, the sensor is exposed to different concentration of gas and its results are evaluated.

5.3.1. Experimental setup

A diagram of the experiment setup is shown in the Figure 5.4. In order to get test points for testing the sensor, air is blended with Nitrogen. Air is pumped with an aquarium pump and mixed with 99.9999% purity Nitrogen gas and directed to a portable gas analyser provided by Super Systems Europe Company. The ratio of oxygen is regulated using flow meters down to 0%, 5%, 10%, 15% and 20% (maximum oxygen concentration in the ambient air) and verified using the gas analyser as an existing commercial sensor to allow a more accurate assessment to be carried out. The output gas from the gas analyser is directed and flows into the PCB oxygen sensor platform while the percentage of the oxygen is being monitored using the gas analyser. Electrochemical measurements of the PCB oxygen sensor are conducted using a computerized measurement system comprising of a laboratory power supply and a computer equipped with Data acquisition unit (DAQFactory Express and LabJack). All tests are done in room temperature of 22ºC.
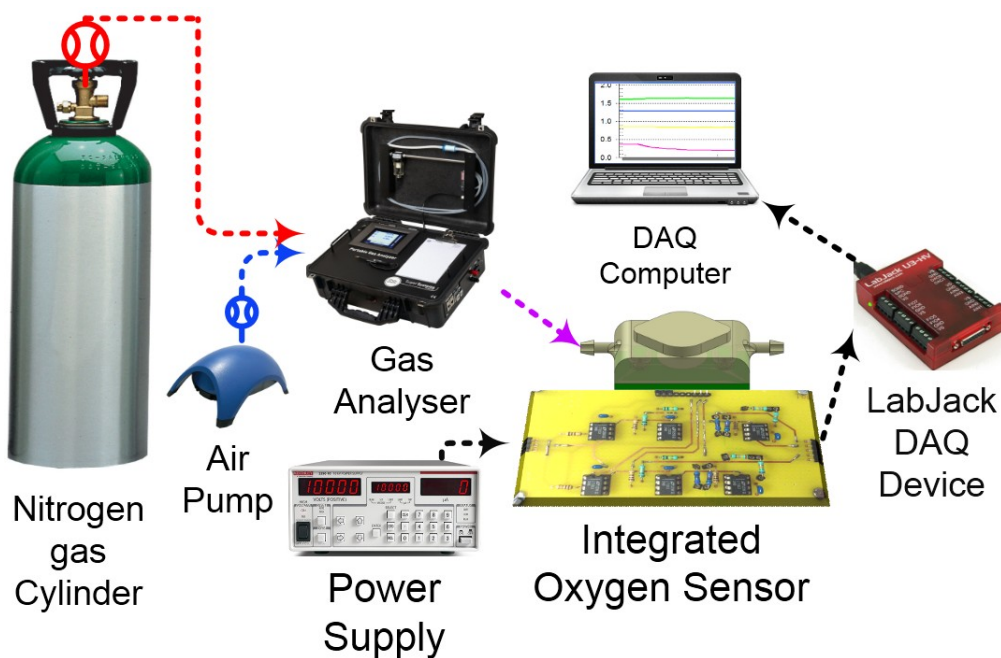
Figure 5.4 Diagram of the experiment setup.

Before each recording the sensor is subjected to a potential scanning for several cycles until a stable, reproducible scan is observed. For each sensor the data were obtained by steady state measurement at applied potential from 0.0 to 2.5V. Figure 5.5 shows the image from the experimental setup and instrumentation system.
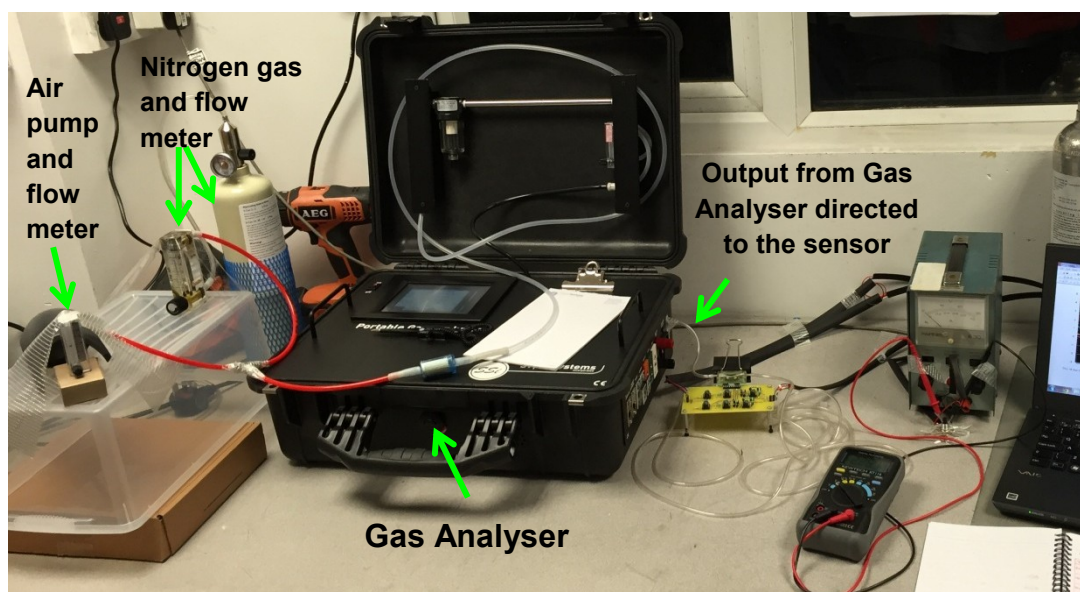
Figure 5.5 Experimental setup and instrumentation system.

5.3.2. Sensor characterization

Measurements of the six electrode set (sensors A to F) were made to determine the performance of the sensor using cyclic voltammetry (CV) and chronoamperometric methods. CV is done to determine the bias points of the device and to verify that no other competing reactions exists at the certain bias point. Chronoamperometric measurement is used to determine the dynamic behaviour of the device.

5.3.3. Cyclic voltammetry

Cyclic voltammetry of sensors A to F were made over a voltage range of 0 to 3V applied to the WE at a step increment of 100 mV/s, starting at 0V bias, and current from the WE to CE is plotted versus the applied voltage. The output current is generated by the oxygen reduction reaction at the WE. This experiment is done while sensor was exposed to fresh air (20% oxygen). The maximum voltage that was possible to supply the Op-amp was 5V. However 4V is considered to be the maximum voltage supplied to the circuit to prevent damaging the Op-amps.

Therefore after the set potential is reached (0-3 V interval, 100 mV/s step increaments), WE potential is ramped in the opposite direction to return to its initial point as shown in Figure 5.6. This process can be repeated as many times as desired.
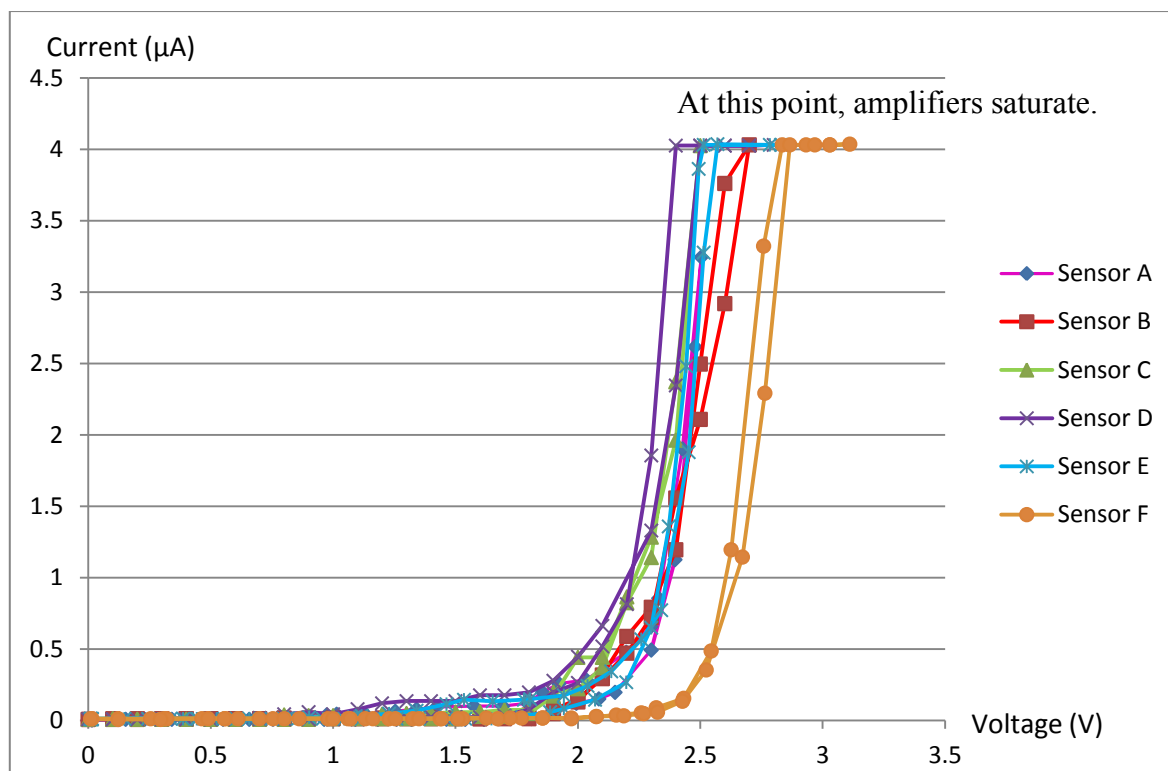
Figure 5.6 CV measurements of six sensors with WE diameter ranging from 20μm to 900μm.The measured current by the control circuit, increased by increasing the voltage.

In Figure 5.6 the maximum voltage that was applied was from 0 to 3V, the point where the amplifiers saturate is shown in figure 5.6, each sensor presented consistent response while increasing the voltage and decreasing it in the opposite direction. Also the response of the sensor depending on their WE size was different, sensor F having WE diameter of 20μm showed lower current response at lower bias voltages compared to other sensors. At low bias voltage, the reaction at the WE is in kinetic control region and the current is dependant strongly to the applied voltage. At bigger bias points the oxygen transport to WE goes into the diffusion limited region, which is independent of the applied voltage. Kinetic control range of this reaction is from bias level of 0V to 1.6. Since the sensors are exposed to air and there is no change of oxygen concentration it can be seen that diffusion control region ranges from 1.6V to 2.25V. These bias points are chosen to make linearity measurement of the electrodes and to allow determining the maximum level of oxygen concentration within in the

diffusion limited region. After this region, the current can be seen to increase quickly by the applied potential and is not related to the oxygen concentration.

5.3.4. Voltage step measurement (chronoamperometry)

Figure 5.7 shows the response time of each sensor after voltage is applied by increment of 100 mV in 1 second intervals. The range of applied voltage is varied from 0 to 4V. The measurements were performed 0.5 second after introducing the voltage and as the sensor were placed in room atmospheric condition (20% oxygen). It can be observed that the IV characteristic of the sensors can be considered to be linear.
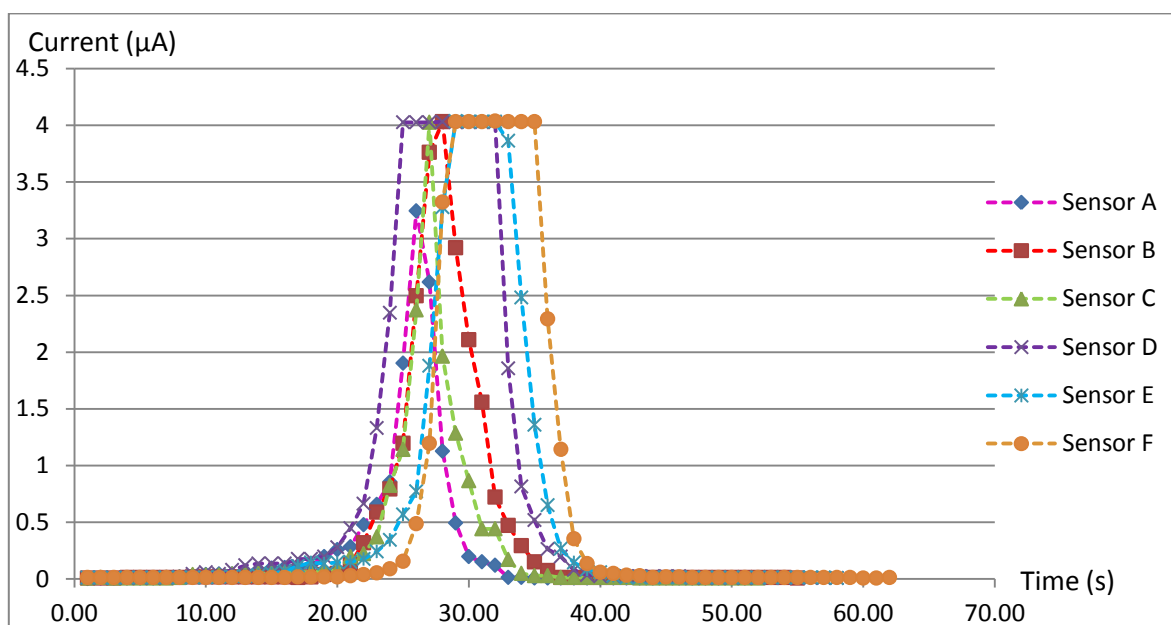
Figure 5.7 Step response plot of sensor A to F.

5.3.5. Sensor performance

Figure 5.8 to 5.11 shows the linearity of the step response measurements of the 6 sensor set with working electrode of 20 μm, 300 μm, 400 μm, 500 μm, 600 μm and 900 μm between bias voltages of 1.6V to 2.25V. The results are taken separately for each bias voltage of 1.6V, 1.8V, 2V and 2.25V. The graphs show that the current/oxygen concentration has a linear relationship as anticipated.
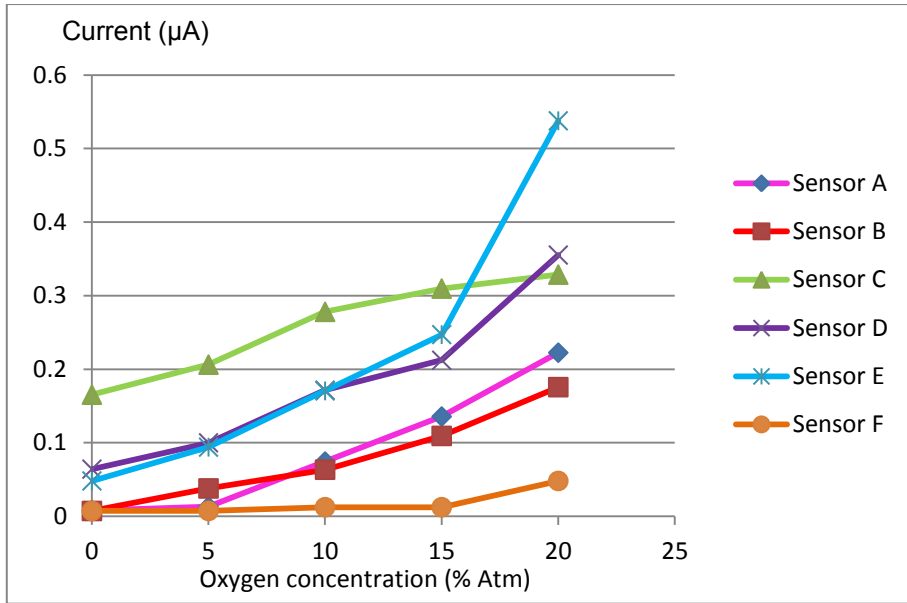
Figure 5.8 Step linearity response at 2.25V.
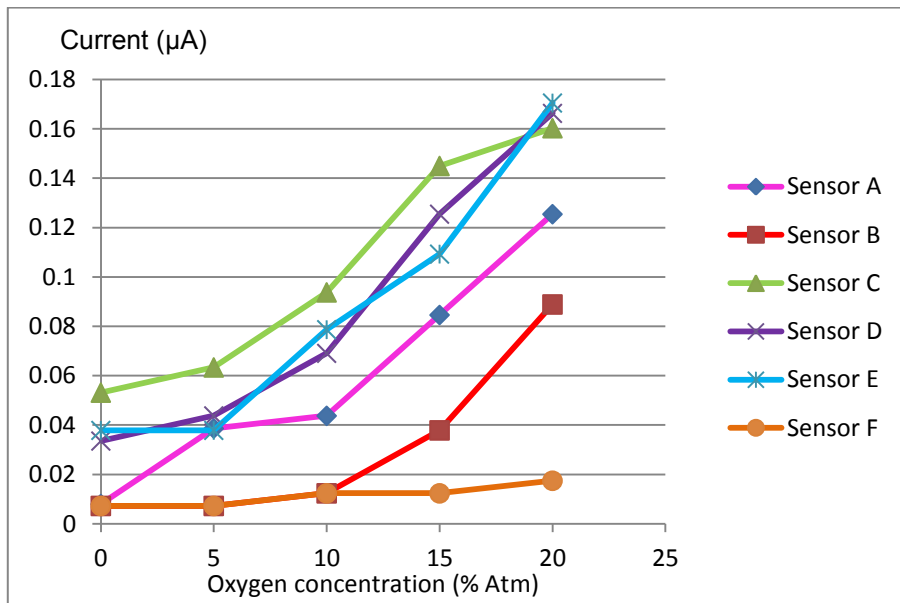
Figure 5.9 Step linearity response at 2V.
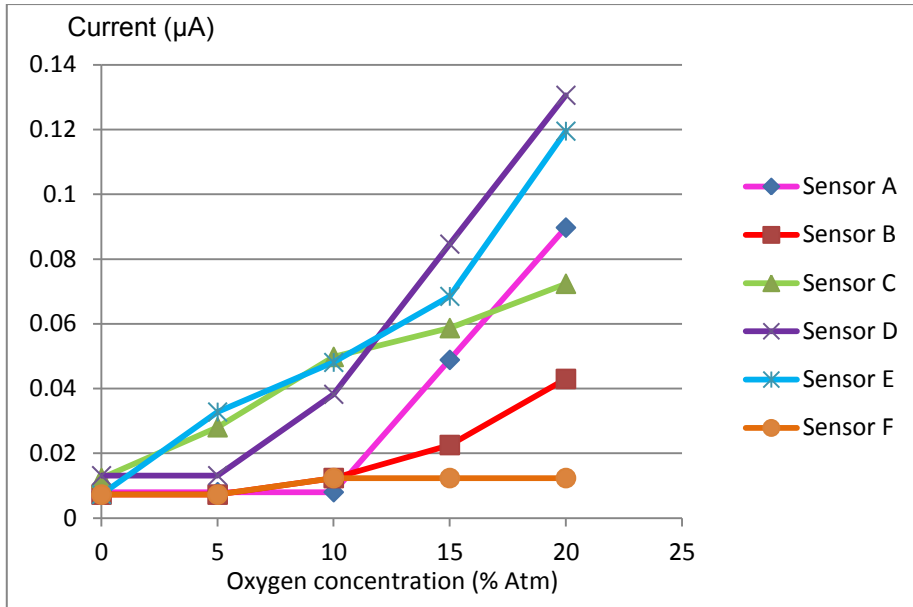
Figure 5.10 Step linearity response at 1.8V.
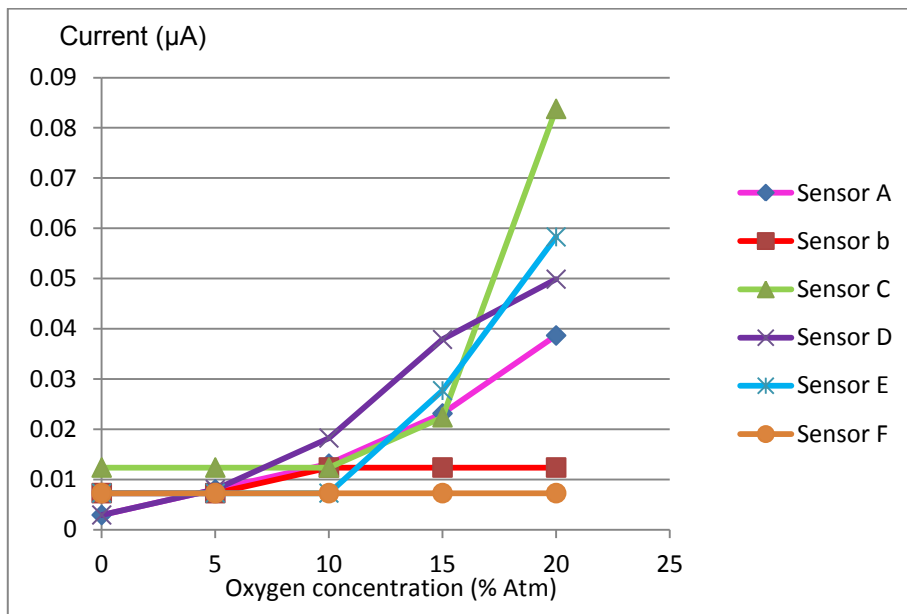
Figure 5.11 Step linearity response at 1.6V.

The offset currents at the zero oxygen concentration level are mainly caused for two reasons: 1) the capacitive current effect and 2) Solid polymer electrolyte Nafion membrane's resistance. The capacitive current effect is caused by the sensor capacitance due to the constant sweep rate of the measurement ($I = CdV/dt$). The resistance of the Nafion membrane also increases proportionally as the area of the electrodes becomes bigger. These two aspects contribute to create bigger offset currents for electrodes with bigger dimension.

Figure 5.12 shows CV linearity measurement of the sensor with 20 μm diameter of WE when exposed to oxygen concentration of 0 to 20%. The current response of the sensor between bias voltages of 1.6V to 2.25V was below the measurement capabilities of the instrumentation. For that reason its linearity was measured when voltage up to 3.8V was applied to its WE. As it can be seen it shows consistent linearity as the oxygen concentration increased.
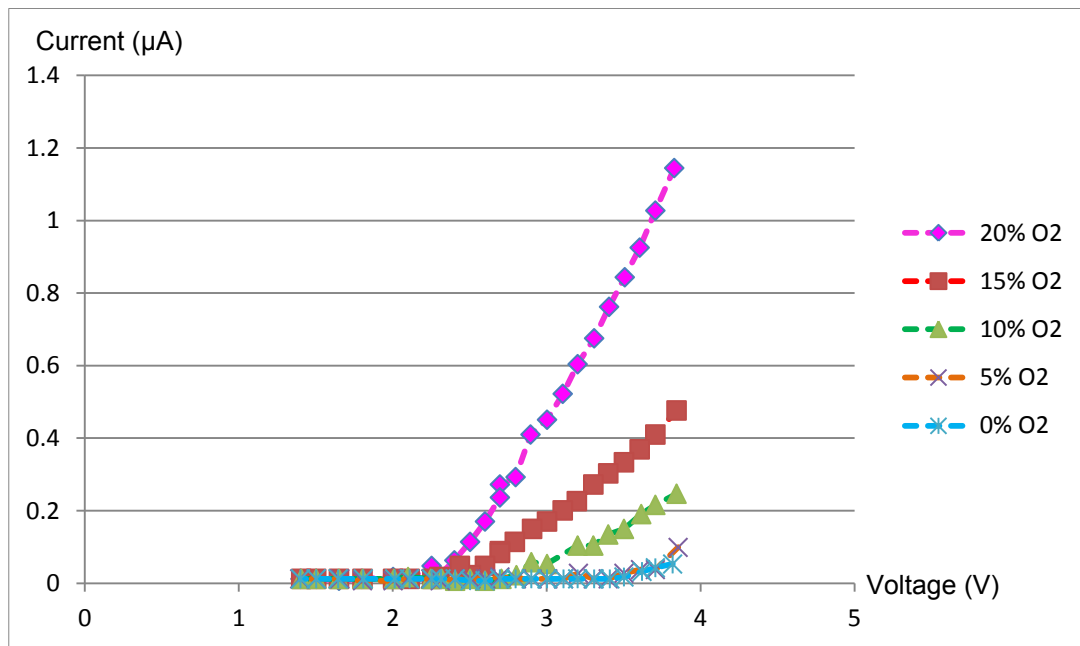
Figure 5.12 CV linearity response of the sensor with 20 μm diameter of WE.
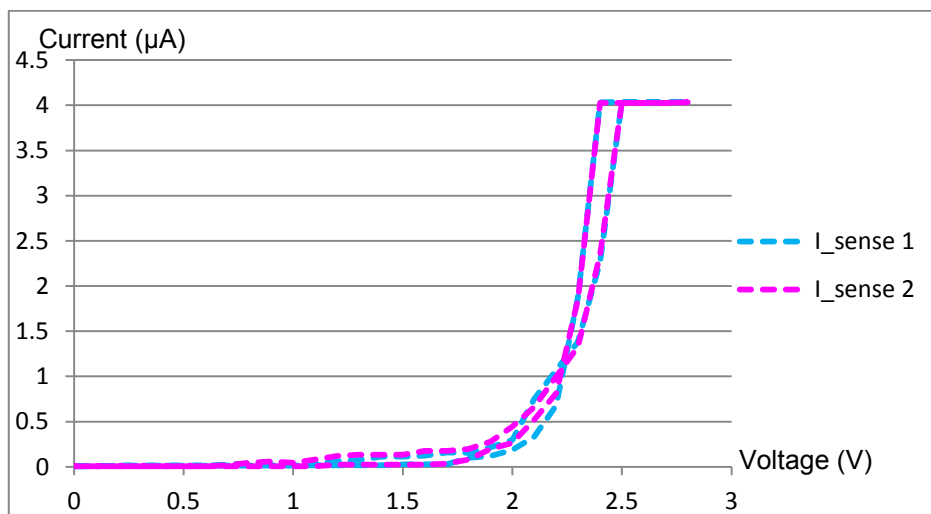
Figure 5.13 CV linearity response of two electrode's set at individual PCB sensor chip.

109

Figure 5.13 shows the CV performance of two identical set of electrodes with 600 μm diameter of WE on the same PCB sensor chip. It was measured at the same time by the control circuit having ability to measure two sensor's performance. Two sensors show consistent linearity. This size is shown randomly and the other sensors perform in the same way. The small nonconformity between their responses is due to the electronic parts that were used in the control circuit such as resistors with different percentage of precision. In the next page the data on the effect of exposure to a gas stream with different concentration of oxygen at different bias voltages are shown.

Applied at 2.25 V	Gas O2%	Sensor A	Sensor B	Sensor C	Sensor D	Sensor E	Sensor F
	20	0.2224709	0.1755983	0.3286283	0.3552284	0.5377693	0.04807335
	15	0.135668	0.1092853	0.3096383	0.2122588	0.2470123	0.01236635
	10	0.07439526	0.06337634	0.2780223	0.1714104	0.1704973	0.01236635
	5	0.01312256	0.03787135	0.2062043	0.09992555	0.09398234	0.007265354
	0	0.008016503	0.007265354	0.1653963	0.06418314	0.04807335	0.007265354
Applied at 2.1 V	Gas O2%	Sensor A	Sensor B	Sensor C	Sensor D	Sensor E	Sensor F
	20	0.1254558	0.08888134	0.1602953	0.1663043	0.1704973	0.01746735
	15	0.08460737	0.03787135	0.1449923	0.1254558	0.1092853	0.01236635
	10	0.04375891	0.01236635	0.09378034	0.06907708	0.07867934	0.01236635
	5	0.03865285	0.007265354	0.06337634	0.04375891	0.03787135	0.007265354
	0	0.008016503	0.007265354	0.05317434	0.03354679	0.03787135	0.007265354
Applied at 2 V	Gas O2%	Sensor A	Sensor B	Sensor C	Sensor D	Sensor E	Sensor F
	20	0.08971343	0.04297235	0.07236635	0.1305619	0.1194873	0.01236635
	15	0.04886497	0.02256835	0.05867934	0.08460737	0.06847734	0.01236635
	10	0.008016503	0.01236635	0.0497903	0.03822862	0.04807335	0.01236635
	5	0.008016503	0.007265354	0.02807335	0.01312256	0.03277035	0.007265354
	0	0.008016503	0.007265354	0.01236635	0.01312256	0.007265354	0.007265354
Applied at 1.8 V	Gas O2%	Sensor A	Sensor B	Sensor C	Sensor D	Sensor E	Sensor F
	20	0.03865285	0.01236635	0.08378034	0.04986497	0.05827534	0.007265354
	15	0.02312256	0.01236635	0.02236635	0.03786497	0.02766935	0.007265354
	10	0.01312256	0.01236635	0.01236635	0.01822862	0.007265354	0.007265354
	5	0.008016503	0.007265354	0.01236635	0.008016503	0.007265354	0.007265354
	0	0.002910445	0.007265354	0.01236635	0.002910445	0.007265354	0.007265354

Applied at 1.65 V	Gas O2%	Sensor A	Sensor B	Sensor C	Sensor D	Sensor E	Sensor F
	20	0.01312256	0.007265354	0.007265354	0.02333468	0.01236635	0.007265354
	15	0.008016503	0.007265354	0.007265354	0.008016503	0.01236635	0.007265354
	10	0.008016503	0.01236635	0.007265354	0.01312256	0.007265354	0.007265354
	5	0.008016503	0.01236635	0.007265354	0.008016503	0.007265354	0.007265354
	0	0.008016503	0.007265354	0.007265354	0.002910445	0.007265354	0.007265354
Applied at 1.5 V	Gas O2%	Sensor A	Sensor B	Sensor C	Sensor D	Sensor E	Sensor F
	20	0.008016503	0.007265354	0.007265354	0.01822862	0.01746735	0.007265354
	15	0.008016503	0.007265354	0.007265354	0.008016503	0.01236635	0.007265354
	10	0.008016503	0.007265354	0.007265354	0.008016503	0.007265354	0.007265354
	5	0.008016503	0.007265354	0.007265354	0.008016503	0.007265354	0.007265354
	0	0.002910445	0.007265354	0.007265354	0.002910445	0.007265354	0.007265354
Applied at 1.4 V	Gas O2%	Sensor A	Sensor B	Sensor C	Sensor D	Sensor E	Sensor F
	20	0.008016503	0.007265354	0.007265354	0.01312256	0.02256835	0.007265354
	15	0.008016503	0.007265354	0.007265354	0.002910445	0.01236635	0.007265354
	10	0.008016503	0.007265354	0.007265354	0.008016503	0.007265354	0.007265354
	5	0.002910445	0.007265354	0.007265354	0.008016503	0.007265354	0.007265354
	0	0.002910445	0.007265354	0.007265354	0.002910445	0.007265354	0.007265354

5.4. Liquid state measurement

At this stage, the sensor is tested with different concentration of dissolved oxygen in water and its results are investigated.

5.4.1. Experimental setup

Diagram of the experiment setup with liquid medium is shown in the Figure 5.14. The condition is almost the same as the gas state measurements; however instead of using gas analyser, a dissolved oxygen meter probe is used to verify the percentage of the dissolved oxygen in water. In order to get test points for testing the sensor, air is blended with Nitrogen. Air is pumped with an aquarium pump and mixed with 99.9999% purity Nitrogen gas and the gas mixture was fed and bubbled into a glass beaker containing water where the dissolved oxygen is being monitored by a commercial dissolved oxygen meter probe provided by the School of Chemical Engineering of University of Birmingham. The ratio of oxygen is regulated inside the water using flow meters down to 0%, 25%, 50%, 75% and 100% and verified using the oxygen meter probe as an existing commercial sensor to achieve accurate evaluation. Then the liquid is directed and pumped through the PCB oxygen sensor platform by a syringe pump with flow rate of 5 ml/min. The measurements are conducted using the same computerized measurement system equipped with Data acquisition unit (DAQFactory Express and LabJack) and room temperature of 22°C.
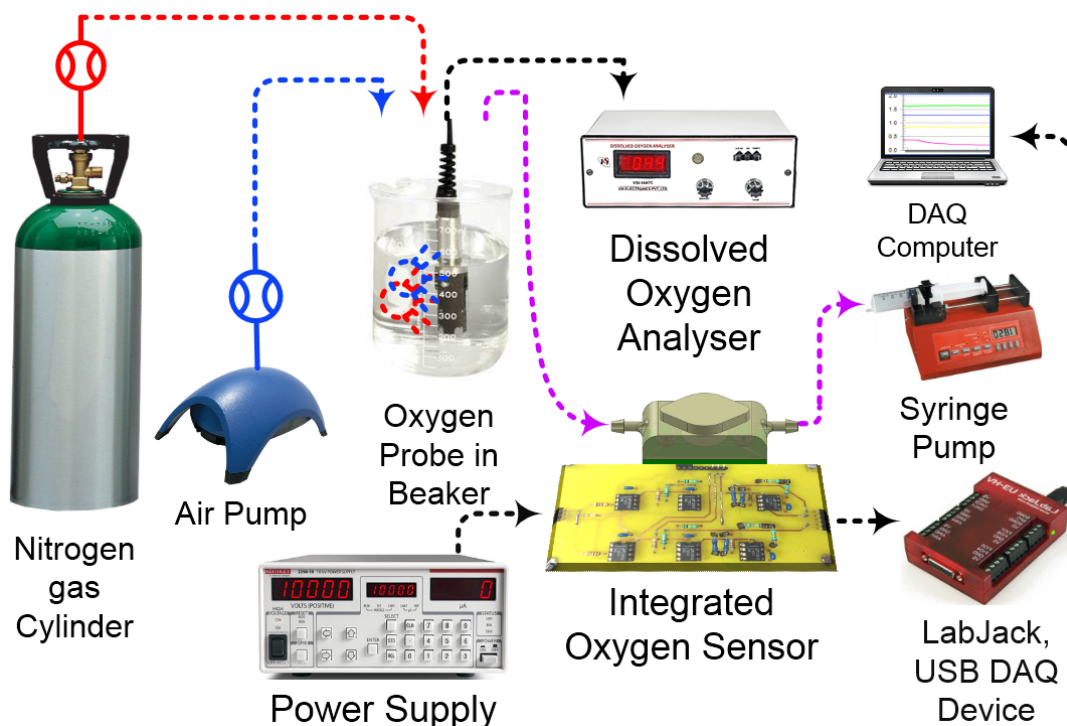
Figure 5.14 Diagram of liquid state experimental setup.

Each sensor is subjected to a potential scanning for several cycles to achieve a stable, reproducible scan prior to testing. And the data were attained by steady state measurement at applied potential from 0.0 to 2.5V. Figure 5.15 shows an image from the experimental setup for liquid state measurements.
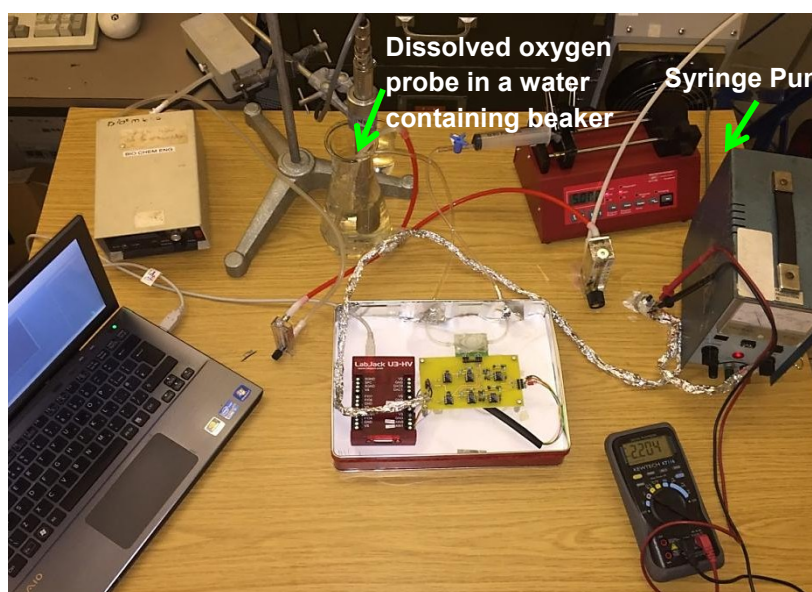
Figure 5.15 Experimental setup and instrumentation system for liquid state measurements.

5.4.2. Sensor performance

Figure 5.16 to 5.20 shows the linearity of the step response measurements of the 6 sensor set with working electrode of 20 μm, 300 μm, 400 μm, 500 μm, 600 μm and 900 μm between bias voltages of 1.6V to 2.5V. The results are taken separately for each bias voltage of 1.6V, 1.8V, 2V, 2.25V and 2.5V. The graphs show that the current/oxygen concentration has a linear relationship as expected, however sensors C and E with Diameter of WE being 500 μm and 900μm has found to be more sensitive to the change of dissolved oxygen in water.

The offset currents at the zero oxygen concentration level are produced by: 1) the capacitive current effect and 2) Solid polymer electrolyte Nafion membrane's resistance as explained before.
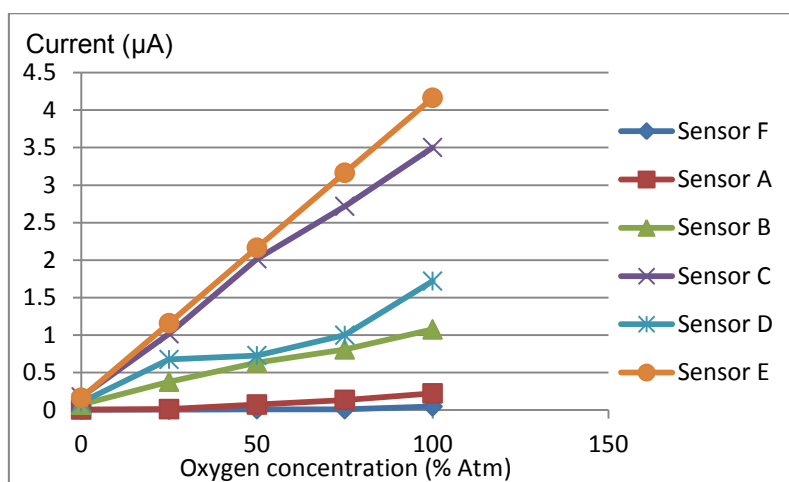
Figure 5.16 Step linearity response at 2.5V.
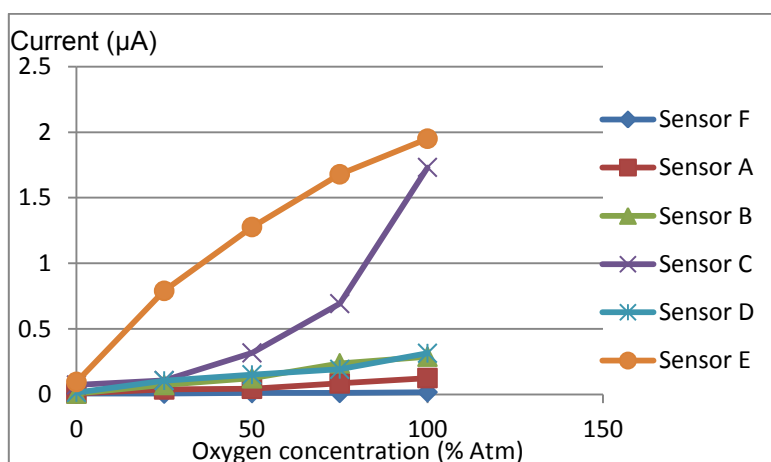
Figure 5.17 Step linearity response at 2.25V.
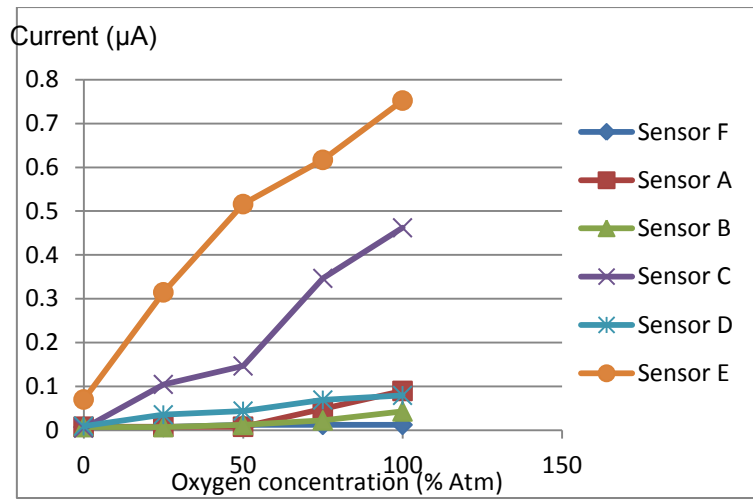
Figure 5.18 Step linearity response at 2V.
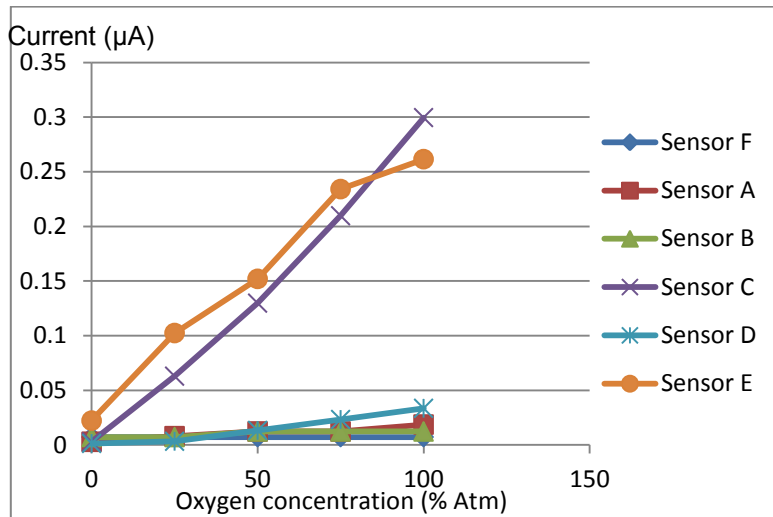
Figure 5.19 Step linearity response at 1.8V.
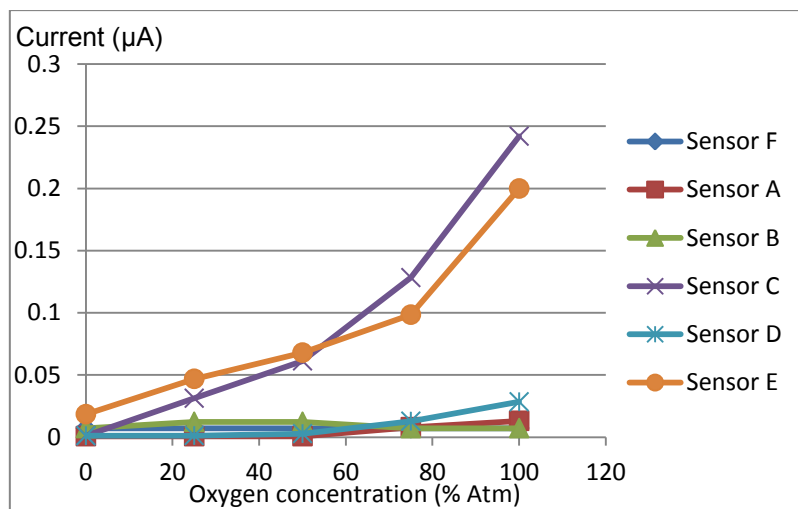
Figure 5.20 Step linearity response at 1.6V.

5.5. Summary

In this chapter tests and measurements were conducted to investigate the functionality of the PCB made oxygen sensor integrated with the 3D printed cell culturing platform. A series of experiments were designed to identify the appropriate design features (size of the electrodes). Six set of sensors with different WE diameter were tested in gas and liquid state and exposed to different concentration of oxygen in liquid and gas. Experimental setup for gas and liquid state measurements were demonstrated. The results of CV and step linearity measurements were shown to be consistent with the size of the electrodes. The sensors have shown sufficient electrocatalytical activity (high output current density). The current was proportional to the oxygen concentration under diffusion controlled region. Information provided in this chapter could be used to further improve the functionally of the sensor. The size of the WE could be used to determine the desired response from the device and by improving the adhesion of Nafion membrane, technique for constructing optimized oxygen sensors can be attained.

6. Conclusion

In this research an integrated oxygen sensor with cell culturing platform that is capable of monitoring the cellular respiration of the cultured cells was designed and developed, which is suitable for mass production and to be used in pharmaceutical industries. The prototype is the first micro electrochemical oxygen sensor built using high precision printed circuit board technology that incorporates Nafion 117 membrane as a solid electrolyte. The integration of a 3D printed cell culturing sample chamber with this sensor is an original innovation. A miniaturized Clark type oxygen sensor as a cellular respiration monitoring device has several advantages including robustness and advanced fabrication techniques allow easy production of optimal microelectrode features like pads and tracks with gold coating and strong connectivity on its surface.

The electrochemical oxygen sensor's configuration designed using microelectrodes and the theory of its design was explained. Overview about the background theories and fundamental of the electrochemical oxygen sensors was given. The state of the art and the most recent studies in this field were explored and a new idea considering the previous studies was developed. A three electrode sensor configuration is chosen and to prevent current passing through the reference electrode, the counter electrode is introduced, which balances the charge added or removed by the working electrode and allows the balancing current at the working electrode to flow. Usage of microelectrodes improved some of the disadvantages and shortcomings of macro sized electrodes when electrochemical techniques were applied. Additionally they were cost efficient and easily put into practice. Due to their minimized interface, they are capable of lower detection limit. Capacitive effects and Ohmic drops (iR) have minimal effect on their response. The sensor and its electrodes were made on the PCB.

Since low currents are being measured during the experiments, it will be important to insulate the sensor and PCBs are insulating substrate, made from FR-4 glass epoxy. Electrodes implement the half reaction over extended times so its material type is important. To reduce cost and to maintain the simplicity of the design, all three electrodes are fabricated from the same conductive material to complete the electrochemical reaction. Copper is etched from PCB as the electrodes. Copper is prone to corrosion such as oxidation at relatively normal temperatures, which reduces its shelf life to solve this issue, a thin layer of Electroless nickel and immersion gold plating on the copper electrodes is considered.

The electronic control circuit board is designed and developed to control the electrochemical oxygen sensor and record data during the measurements, which was an aanalogue circuitry to condition the low level signals to a point where they can be measured using Data Acquisition (DAQ) modules such as LabJack. The LT spice simulation was performed to show the functionality of this circuit.

A cell culturing platform prototype is developed utilizing a 3D printing device and a material choice of MED610, having complex features inside the chip with the potential for cells to grow and adhere to its chamber. Using 3D printing technology provided the freedom of designing complex shape and features contrary to the conventional silicon wafer manufacture techniques. The cell culturing platform was designed that its critical features coincide with the design of the oxygen sensor on the PCB. The oxygen respiration of cells in the cell culturing chamber was modelled using Finite Element Analysis software COMSOL, which is a solver and Simulation software package for various physics and engineering applications, especially coupled phenomena, or multiphysics. Further methods of surface enhancement and cell culturing were suggested.

Experiments were designed and carried out and the functionality of the sensors was verified. Six set of sensors with different WE diameter were tested in gas and liquid state and exposed

to different concentration of oxygen in liquid and gas. The results of CV and step linearity measurements were presented to be consistent with the size of the electrodes. The current was proportional to the oxygen concentration under diffusion controlled region.

Current medical oxygen sensors are encapsulated aqueous based devices. Despite being large, they have inconsistent performance and limited shelf lives. The use of aqueous based electrolytes reduces their shelf life. Microfabrication methods while improving device consistency and reducing the size, they increase the cost and reduce the robustness of the sensor while being incorporated in cell culturing platforms.

Instead of electrolyte solution, a solid polymer electrolyte membrane, Nafion membrane was used, which removed requirement for extra humidification and extended shelf life. The prototype successfully detected the changes in the current affected by oxygen concentration, in the 0-5 μAmp range, having response time of less than 5 seconds. When exposed to different gas concentration, the sensor was more consistent in function than the time when exposed to liquid sample.

6.1. Suggestions for Future Work

It is possible to improve further the functionally of the sensor by finding an appropriate condition for Nafion membrane application during the hot pressing. As presented in section 5.4, Nafion membrane hot pressed between two aluminium plates, clamped between metal clips. It has been tried to do the measurement with the sensors that were Nafion coated successfully and in similar condition in the aspect of Nafion adhesion. However there was not an identical pressure all over the surface of the PCB considering the two identical sensors on the same chip or two different chips from each other, which was anticipated while comparing the results that were different, however they are not presented here. It will be ideal to design a

system which could be capable of hot pressing these chips with Nafion membrane in an equal condition.

It is important to test the sensor with the living cells, so in the next stage to improve this sensor, it is suggested to culture cells on the cell culturing platform after surface treatments, and test the functionality of the sensor with living organisms.

The sensors with different electrodes size and diameter were fabricated and tested separately. For each sensor, a separate experiment has been carried out. It has been tried to create similar testing conditions for each sensor, though it's likely that sometimes the stages of experiment were not exactly the same. To solve this issue, it's suggested to design a new set of sensors with different sizes that are located on the same PCB (like an array) and be tested at the same time and log its data on the same device (requiring a Labjack device with more ports of connection). In this way, it's easier to analyse and compare the different sized sensor to each other and have a better understanding.

In this project the design of the sensor's electrodes are inspired by the existing previous miniature electrochemical sensors and in a way to minimize the cost and fabrication time by miniaturization. As a future work it is recommended to explore mathematical rationalization and simulation to justify and predict the sensor's reaction before manufacturing. In this way, it's possible to optimize the design.

References

1. Wilson, G.S., *Bioelectrochemistry*. 2002, New York: Wiley.
2. Clark, L.C., *Electrochemical device for chemical analysis*. 1956.
3. Park, J., et al., *A reservoir-type oxygen sensor with 2×3 array for measuring cellular respiration levels.* Sensors and Actuators B: Chemical, 2013. **176**: p. 913-920.
4. Lee, Y.J. and J.Y. Park, *A Highly Miniaturized Dissolved Oxygen Sensor Using a Nanoporous Platinum Electrode Electroplated on Silicon.* Journal of Korean physical society, 2011. **58**: p. 1505-1510.

5. McLaughlin, G.W., et al., *Microfabricated solid-state dissolved oxygen sensor.* Sensors and Actuators B 83, 2002: p. 138-148.
6. Wu, C.-C., et al., *Fabrication of miniature Clark oxygen sensor integrated with microstructure.* Sensors and Actuators B: Chemical, 2005. **110**(2): p. 342-349.
7. Cheneler, D., et al., *Printed circuit board as a MEMS platform for focused ion beam technology.* Microelectronic Engineering, 2011. **88**(1): p. 121-126.
8. Chien, S., *Metabolic Management.* In: Madame Curie Bioscience Database, 2000. **Landes Bioscience**.
9. Wang, J., *Analytical Electrochemistry*. Second Edition ed. 2000, New York: Wiley-VCH Publishers.
10. Dixon, B.M., J.P. Lowry, and R.D. O'Neill, *Characterization in vitro and in vivo of the oxygen dependence of an enzyme/polymer biosensor for monitoring brain glucose.* Journal of Neuroscience Methods, 2002. **119**(2): p. 135-142.
11. Bănică, F.-G., *Chemical Sensors and Biosensors: Fundamentals and Applications*. 2012, Chichester, UK: John Wiley & Sons, Ltd.
12. Cavalcanti A, S.B., Zhang M, Kretly LC (2008). "Nanorobot Hardware Architecture for Medical Defense" (PDF). Sensors 8 (5): 2932–2958. doi:10.3390/s8052932, *Nanorobot Hardware Architecture for Medical Defense.* Sensors 2008: p. 2932–2958.
13. Sassolas A, B.L.J., Leca-Bouvier B.D (2011) Immobilization Strategies to Develop and E.B.B.A. 489-571, *Immobilization Strategies to Develop Enzymatic Biosensors Biotechnology Advances.* 2011: p. 489-571.

14. Nambiar, S. and J.T.W. Yeow, *Conductive polymer-based sensors for biomedical applications.* Biosensors and Bioelectronics, 2011. **26**(5): p. 1825-1832.
15. LC Jr CLARK and C. LYONS, *Electrode systems for continuous monitoring in cardiovascular surgery.* 1960. **102**: p. 29-45.
16. Thevenot, D.R., et al., *Electrochemical biosensors: recommended definitions and classification, Pure Appl.* Vol. 7. 1999: Biosens Bioelectron. .
17. Park, J., et al., *2 X 3 Array Oxygen Sensor for Measuring Cellular Respiration Level*, in *4th IEEE International Conference on Nano/Micro Engineered and Molecular Systems*. 2009: Shenzhen, China.
18. Biran, I. and D.R. Walt, *Chapter 1 - Optrode-Based Fiber Optic Biosensors (Bio-Optrode)*, in *Optical Biosensors Present and Future* F.S. Ligler and C.A.R. Taitt, Editors. 2004, Elsevier Science: Amsterdam. p. 5-16.

19. Enews, I.T.A.I. *Dissolved Oxygen Analyzers*. 2010; Available from: http://www.instrument.org/2014home/index.html.
20. Permyakov, E.A., *Luminescent Spectroscopy of Proteins*. 1992 CRC Press

21. Lanz, M., D. Schürch, and G. Calzaferri, *Photocatalytic oxidation of water to O2 on AgCl-coated electrodes.* Journal of Photochemistry and Photobiology A: Chemistry, 1999. **120**(2): p. 105-117.

22. Bisen, P.S. and A. Sharma, *Introduction to Instrumentation in Life Sciences*. 26 Sep 2012, CRC Press. p. 53.

23. Arora, P., et al., *Biosensors as innovative tools for the detection of food borne pathogens.* Biosensors and Bioelectronics, 2011. **28**(1): p. 1-12.

24. Kuila, T., et al., *Recent Advances in Graphene-Based Biosensors, Biosensors and Bioelectronics.* Biosensors and Bioelectronics, 2011. **26**: p. 4637– 4648.

25. McLaughlin, G.W., *Microfluidic and biosensor applications of fluoropolymer films*, in *Departement of Electrical Engineering*. 2001, Stanford University: Stanford, California.

26. Cunningham, B., *[Illinois] ECE 416 Electrochemical Sensors*. 2013.

27. Clark, L.C., *Monitor and Control of Blood and Tissue Oxygen Tension,” Transactions of the American Society of Artificial Internal Organs.* Transactions of the American Society of Artificial Internal Organs 1956. **2**: p. 144-156.

28. Alberty, R.A. and R.J. Silbey, *Physical Chemistry Second Edition*. 1996, New York: John Wiley & Sons, Inc.

29. Maruyama, J., M. Inaba, and Z. Ogumi. *Rotating ring-disk electrode study on the cathodic oxygen reduction at Nafion®-coated gold electrodes*. Journal of Electroanalytical Chemistry 1998; Available from: http://www.sciencedirect.com/science/article/pii/S0022072898003623.

30. Network, I.G.H. *Milestones:Volta's Electrical Battery Invention, 1799.* 18 October 2015]; Available from: http://www.ieeeghn.org/.

31. Chemistry, R.S.o. *Enterprise and electrolysis*. Chemistry World 2003 25 September 2015].

32. Ehl, G. and A. Ihde, *Faraday's Electrochemical Laws and the Determination of Equivalent Weights.* Journal of Chemical Education, 1954. **31**: p. 226–232.

33. Aguiar, F.A.S., *Characterisation of electrode microarrays produced photolithographically and with thiol self-assembled monolayers on gold electrodes*, in *Department of Chemistry*. 2009, Durham University: Durham, United Kingdom.

34. Kovacs, G.T.A., *Micromachined Transducers Source book*. 1998, New York: NY: McGraw-Hill.

35. West, A.R., *Solid Electrolytes.* Berichte der Bunsengesellschaft für physikalische Chemie, 1989. **93**(11): p. 1235-1241.

36. Smitha, B., S. Sridhar, and A.A. Khan, *Solid polymer electrolyte membranes for fuel cell applications—a review.* Journal of Membrane Science, 2005. **259**(1–2): p. 10-26.

37. Heitner-Wirguin, C., *Recent advances in perfluorinated ionomer membranes: structure, properties and applications.* Journal of Membrane Science, 1996. **120**(1): p. 1-33.

38. Chen, D., et al., *PVDF-Nafion nanomembranes coated microneedles for in vivo transcutaneous implantable glucose sensing.* Biosensors and Bioelectronics, 2015. **74**: p. 1047-1052.

39. Brett, C.M.A. and A.M.O. Brett, *Electrochemistry: principles, methods, and applications*. 1993, Oxford Oxford science publications.

40. Erdey-Gruz, T. and M. Volmer, *Z. Physik. Chem.* 1930. **150A**: p. 203 – 213.

41. Butler, J.A.V., *Transactions of the Faraday Society*. 1924. **19**: p. 729 – 733.

42. Glasstone, S., *The Electrochemistry of solution*. second edition ed. 1937, London: Methuen.

43. Inczedy, J., T. Lengyel, and A.M. Ure, *Compendium of Analytical Nomenclature*. The Orange Book. Vol. Definitive rules 1997. 1998, Oxford: Blackwell Science.

44. Pletcher, D., *Microelectrodes: Theory and Applications*, ed. I. Montenegro, M. A. Queirós, and J.L. Daschbach. 1991.

45. Yip, N.-C., et al., *Real-time electrocatalytic sensing of cellular respiration.* Biosensors and Bioelectronics, 2014. **57**: p. 303-309.

46. Lee, J.-H., et al., *Needle-type dissolved oxygen microelectrode array sensors for in situ measurements.* Sensors and Actuators B: Chemical, 2007. **128**(1): p. 179-185.

47. Park, J., et al., *Array type dissolved oxygen sensor and measurement system for simultaneous measurement of cellular respiration level.* Transducers, 2009.

48. Gopalakrishna, J., W. Wlodarski, and P. Iles, *Performance of Solid Polymer Electrolyte based Oxygen Sensor without External Humidification.* IEEE, 1999.

49. McLaughlin, G.W., et al., *Solid-state Dissolved Oxygen Sensor Test Matrix Using a Pulsed-plasma Deposited PTFE Film*, in *The 11th International Conference on Solid-State Sensors and Actuators*. 2001: Munich, Germany.

50. H. Camon, et al. *From Layout to System Simulation: An Example of an Oxygen Sensor*. in *The 1998 International Conference on Modeling and Simulation of Microsystems*. 1998.

51. C.M. Bautista-Rodriguez, et al., *Effect of a Rigid Gas Diffusion Media Applied as Distributor of Reagents in a PEMFC in Operation, Part I: Dry Gases.* International Journal of Electrochemical Science, 2009. **13**.

52. M. Brischwein, D. Grundl, and W. X. Zhang, *Finite Element Modelling of Microphysiometry on Cellular Specimen*, in *World congress on medical physics and biomedical engineering*. 2009: Munich, Germany. p. 30-33.

53. A. R. Oller, et al. *Growth of mammalian cells at high oxygen concentrations*.

54. I. J. Langmuir, J. Am. Chem. Soc., 1917. **39** p. 1848 – 1906.

55. Laurent, J.Y., *Development of micro fuel cell by using microelectronic process for next generation of portable equipment*, in *3rd European PEFC Forum*. 2005: Atomic Energy Commision - DTEN.

56. G. Milad and M. Orduz. *Surface Finishes in a Lead Free World*. 2 December 2015].

57. The Advanced Manufacturing Technology Centre, U.o.B. *Lasea Multi-Axis Laser Micro Machining Centre* [cited 2015 5 December]; Available from: http://www.birmingham.ac.uk/facilities/advanced-manufacturing/index.aspx.

58. [cited 2012 27th August].

59. A . Sharma, et al., *Long term in vitro function stability and recording longevity of fully integrated wireless neural interfaces based on the Utah Slant Electrode Array.* Neural Eng. , 2011.

60. T.Y. Chang, et al., *Cell and protein compatibility of Parylene-C surfaces.* Langmuir, 2007. **23**: p. 11718–11725.

61. E. Meng, P.Y. Li, and Y.C.J. Tai, *Plasma removal of Parylene-C.* Micromech. Microeng., 2008: p. 180.

62. J. Lahann, *Vapor-based polymer coatings for potential biomedical applications.* Polym. Int., 2006. **55**: p. 1361–1370.

63. J.B. Fortin and T.M. Lu, *A model for the chemical vapor deposition of poly (para-xylylene) (Parylene) thin films.* Chem. Mater., 2002. **14**: p. 1945–1949.